Study upon the possible influence of animal burrows on the failure of the levee of San Matteo along the Secchia river.

Modelling of groundwater flow with precipitation and water level changes and mechanism of collapse of the Secchia Failure with particular attention to burrows geometry and their influence to the stability of the dike (19th January 2014, San Matteo, Modena, Italy).

Maria Luisa Taccari
Student number: 4326482
MSc Thesis Civil Engineering
Geo-Engineering Section
Civil Engineering and Geosciences - TU Delft

MSc Thesis Committee:
Prof. dr. Jommi, C.
Prof. dr. ir. Jonkman, S.N.
Ir. van der Meij, R.
Dr. ir. Schweckendiek, T.

Title

Study upon the possible influence of animal burrows on the failure of the levee of San Matteo along the Secchia river.

Project	Pages
-	138

Keywords

Dike failure; Secchia river; animal burrowing; groundwater flow; macro-stability; internal erosion; badger setts; unsaturated zone

Date	Author	Commitee	Organization
13 July 2015	Maria Luisa Taccari	Prof. dr. Jommi, C.	TU Delft
		Prof. dr. ir. Jonkman, S.N.	TU Delft
		Ir. van der Meij, R.	Deltares
		Dr. ir. Schweckendiek, T	TU Delft

13 July 2015

Acknowledgments

This work was performed as a part of the MSc program of the Civil Engineering Faculty - Geo-Engineering track, TU Delft, The Netherlands and was carried out at the research institute Deltares from December 2014 to July 2015.

First of all, I would like to acknowledge the members of assessment committee, who provided valuable feedback and support during the meetings and all the graduation process. I owe special words of many thanks to ir. Van der Meij – my daily supervisor – for his constant guidance during the project: his precious support has helped me not only for my work but also for a personal growth within a professional environment. The pleasant atmosphere that I found in Deltares has given me support during all the stages of my research, through the courtesy and knowledge transfer of the colleagues, the availability of facilities, the attendance of courses and workshops, the support of the field visit to Italy. For this reason, I particularly thank dr.ir. M. Sule – head of the Dike Safety Department (DKS) – for giving me this possibility.
I then owe special thanks to the dr.ir. S. Orlandini and prof. dr. ir. G. Gottardi, for their welcome and guidance during my Italian stay, dr. A. Byrne for his suggestions about badger setts and to dr. V. Galavi for his support in using PLAXIS.

Finally, I would like to keep a great thanks to my family for their great support, encouragement and motivation despite the distance.

Maria Luisa Taccari

TU Delft, July 2015

13 July 2015

13 July 2015

Abstract

Animal burrowing can be a main cause of initiation thereby be a cause of breaching of flood defences. However, little guidance and literature is available on this subject. This Master Thesis investigates the contribution of badgers, porcupines and foxes to the failure of the levee of San Matteo (Modena, Italy) on 19th January 2014.

Firstly, the study is initiated with literature research on the Investigative Evaluation Report ("*Relazione tecnico-scientifica sulle cause del collasso dell'argine del fiume Secchia avvenuto il giorno 19 gennaio 2014 presso la frazione San Matteo*") which analyses the breach and presents data that will be used in the following analyses. Second, the thesis investigates the properties, geometry and distribution of animal burrows, in order to draw networks for the analyses. Finally, the literature review focuses on possible failure mechanisms caused by animal burrowing and historical cases.

The assumed method evaluates first the influence of animal burrows on the water pressures in the embankment during rainfall and a high water tide. The influence of the burrowing is assessed through a transient FEM flow analysis. Starting from the documented entrances situated in the vadose zone, different scenarios for the internal distribution of tunnels and chambers are proposed. The analysis is carried out with the software PLAXIS 2D and 3D.

Finally, the most likely failure mechanism and representative network for the stability of the dike is assessed. Indications around the influence of animal burrowing for the safety of a levee are stated and recommendations on their analysis in future cases are presented.

13 July 2015

13 July 2015

Table of Contents

13 July 2015

List of Figures

13 July 2015

List of Tables

1 Introduction

1.1 Background

On the 19th January 2014, around 6am, river Secchia created a breach in a dike in San Matteo (Modena, Italy). The failure took place in a section with coordinates: 44° 41' 57.6"N, 10° 56' 41.5"E, located between a railway track and a small bridge.
The widening of the dimensions of the breach continued till reaching, 9 hours after the failure, the maximum width, equal to 80 meters, and maximum depth till the surface level (around 6 meters deep).
The water volume flowing out of the breach flooded the surrounding countryside and the villages of Bastiglia and Bomporto. Around a thousand of people evacuated and one man died during the relief operations. 600 volunteers helped during the emergency operations, while 400 million euro was the estimated damage of the event.

Figure 1.1 Flood in the Modena province (19 January 2014)

During the months after the failure, a scientific committee, composed by six members of five Italian universities, investigated the causes leading to the event. In July 2014, the Investigative Evaluation Report "*Relazione tecnico-scientifica sulle cause del collasso dell'argine del fiume Secchia avvenuto il giorno 19 gennaio 2014 presso la frazione San Matteo*" (Technical-scientific rapport about the causes leading to the collapse of the levee of Secchia river, which took place on 19th January 2014) was published (D'Alpaos et al., 2014).

Figure 1.2 The breach at San Matteo, Modena (19th January 2014)

Two witnesses reported that the breach started from an opening located in the upper part of the dike. Giovanni Russo, who lives nearby the location of the failure, saw, around 6.30am, water flowing out of the dike from an opening placed 2 meters beneath the crest: the width of the breach was around 2 meters at 7am and, at 8.30am, it increased to 6 meters.
Alfredo Baraldi instead saw a breach 3-4 meters wide around 5.30-6 am, while the water level was 1-1.5meters below the crest of the levee.

Both the witnesses and the study of the report exclude the possibility of overflow: when the failure took place, the simulated water level was between 35.78 and 36.04 m amsl (metres above mean sea level), while the crest of the levee is placed at 37.30 m amsl. Other failure mechanisms are also excluded such as erosion at the outer slope; the photos taken immediately after the breach show that the vegetation is still intact. Due to the characteristics of the foundation soil, deep filtration underneath the embankment can also be excluded, while liquefaction is not considered because the earthquake solicitations are not significant in this location. Finally, the levee was likely not fully saturated when the event took place. The dike still had residual strength, proved by the fact that trucks were passing on the crest of the dike to repair the breach after the event took place.

According to the Investigative Evaluation Committee, the creation of the breach was facilitated by the presence of large amount of animal burrows, in particular foxes and other wild animals. The cavities, the high precipitation and water level in the river during the days before the event would have thus increased the probability of failure.
Internal erosion and macro-instability may have been the causes of the breach and the two mechanisms may have acted independently or in combination. Internal erosion may have happened inside the animal burrows, facilitated by a reduction of strength of the soil due to precipitation. The network of animal burrows with the infiltration of rain and the high water level may have instead also reduced the shear strength of the soil, leading to macro-instability.

Presence of animals in the locations is proved by pictures of footprints and dens taken during the same day of the breach and days after of the event. In particular, the footprint belongs to a badger (Figure 1.3).

Figure 1.3 Footprint of a badger and animal burrow near the location of the breach

Moreover, on the 19th January another breach happened in the right riverside of Panaro river, in Tronco street, around 10 kilometres far from the breach location (Figure 1.4). The breach was due to internal erosion, as it is possible to see from the picture. The breach was immediately repaired by placing soil and a tarp above it. The same section was already under monitoring because of the large activity of animal burrowing, in particular of porcupines.

Figure 1.4 Internal erosion due to animal burrows in the right riverside of Panaro river (19th January 2014)

1.2 Relevance

During the workshop on *Plant & Animal Impacts on Earthen Dams (Federal Emergency Management Agency, 2000)* which was conducted at the University of Tennessee in 1999, the participants were asked to determine the most important questions to solve in the close future. The survey defined research and development as the most relevant aspects to consider.

The problem of animal burrows in dikes is present all around the world. Just to name few examples, recently a great plague of mice occured in the South West of Friesland (Netherlands), with densities up to 2,500 mice per hectare. Beavers are abundant in Germany, where many cavities were seen in the levees along the Oder river after the flood of summer 2010 (Clauß, 2013). Piping resulting by tunnels of gophers was observed in Arizona, along the San Pietro River (Carrol, 1949). The Truckee

Canal Embankment, in Colorado, instead failed in 2008 because of a diffused network of muskrat burrows (J.W.France and Moler, 2008).

The badgers, which are the main animals considered in the current study, are a significant dike safety issue in 17% of the American surveyed states (Federal Emergency Management Agency, 2000). Badgers, porcupines and foxes are, instead, very dangerous for the Italian dikes. During the last monitoring around 300 burrows were individuated only for Secchia and Panaro rivers. Finally, much literature about these animals is related to Ireland, due to their abundance in this country: a survey of 2007/08 estimates the presence of 33,500 badgers in the only Northern Ireland (Byrne et al., 2012).

Despite the need of research and intervention, little literature is available about the contribution of the presence of animal burrows in the failure of dikes.
For this reason, deep understanding of their influence is lacking and a further research is needed.

1.3 Problem Definition

The conclusion of the report presents hypotheses on failure mechanisms, indicating that internal erosion and macro-instability are possible causes of the breach. The presence of animal burrows could have contributed to the formation of these phenomena.

Animal burrows, such as root canals, cracks, fissures and sub-surfaces erosion, are defined as *macro-pores*, that are cavities with diameters>75µm. The macro-pores induce preferential flow, which depends on the size, shape, direction and distribution of the macro-pores. The preferential flow accelerates the movement of water in certain parts of the soil profile, resulting thus in its irregular wetting profile (Stadler et al., 2011).
If macro-pores are present, the infiltration, which depends on initial conditions and rainfall intensity, is significantly faster (Stadler et al., 2009). The infiltration takes place in the unsaturated zone above the water level (vadose zone), where the preferential paths created by the macro-pores allow the water to penetrate deeper.

When then the outside water level increases, the phreatic line changes with a shape and rate depending on the properties of the soil body. The heterogeneity introduced by the animal burrows influences its trend and the pore pressure distribution, such as Figure 1.5 illustrates. In such a way, if the pore water pressures would increase, the effective stresses and so the shear strength would be reduced and macro-instability could occur.

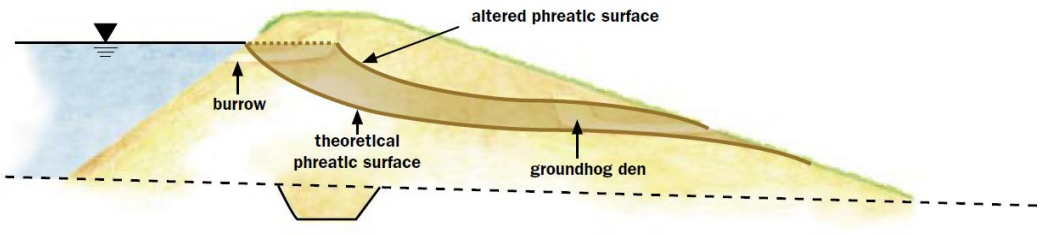

Figure 1.5 Shortening of seepage path due to animal burrow (2005)

Another possibility is that, if the burrows link the two sides of the levee, the water which freely flows inside them erodes their surface and enlarged them until failure eventually takes place. This phenomenon is known as internal erosion.

However the Investigative Evaluation Committee did not reach a final conclusion on how the breach failed. The analyses performed by the committee refer to macro-instability with the use of SEEP software. Internal erosion, assumed as a possible failure mechanism, is not investigated in the report.

Moreover, in the Investigative Evaluation Report, the presence of the burrows is simulated by reducing the soil stress, in particular tanφ, by 20%. This estimated reduction reflects the assumed 20% reduction of material due to the voids of the cavities, whose distribution is not a-priori known. As a matter of fact, the burrows are implicitly assumed to be homogeneously distributed in the levee and an investigation over the geometry and distribution of animal burrow systems is also missing in the report.

1.4 Research Objective

First of all, the research aims to understand the geometry, patterns and distribution of burrowing systems inside a dike. This can give an indication of the level of danger of these systems for levees.

Second, the study analyses the influence of animal burrowing on the pore water pressures and so the groundwater flow inside the dike body, for different proposed scenarios, positions of burrows and distribution.

Finally, the main goal of the current study is to gain an insight upon the failure mechanism of the levee of San Matteo along the Secchia River and the influence of animal burrowing to the breach. In such a way, the research aims to understand how animal burrowing affects the safety of a dike and to provide recommendations for the analysis of the influence of animal systems on levees for future cases.

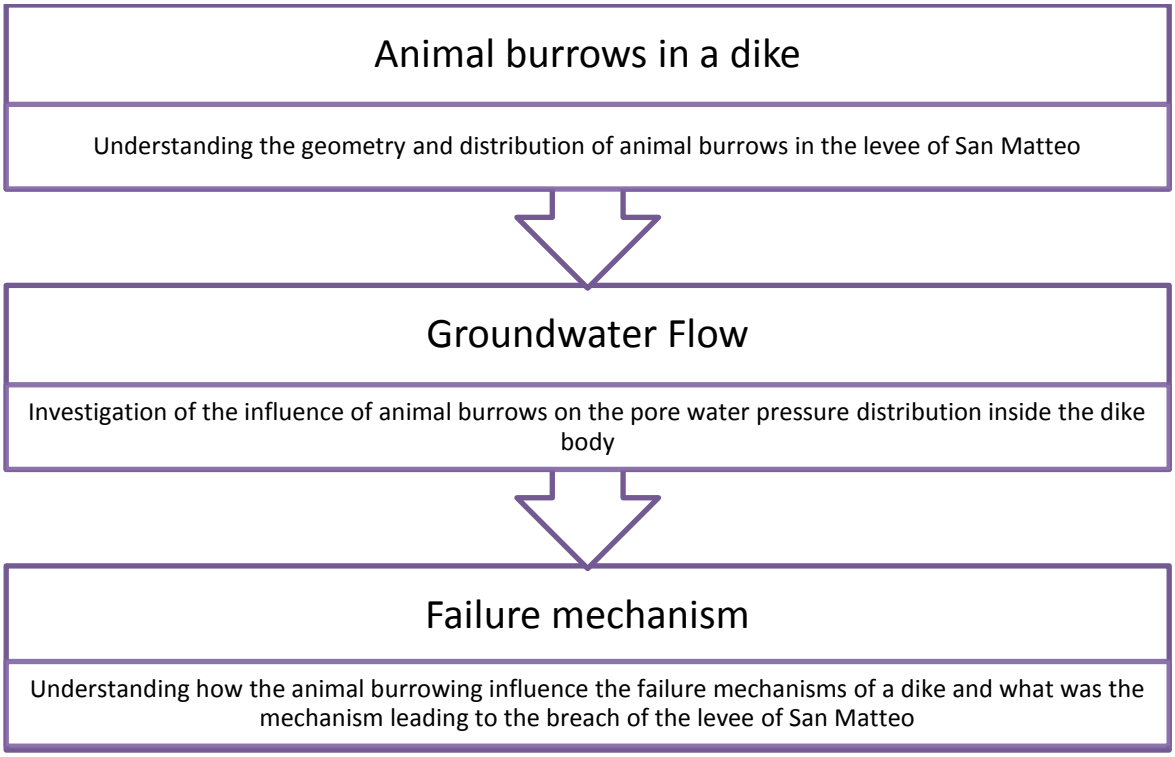

Table 1.1 Research objective.

1.5 Research Questions

The main questions leading the research are the following:

What was the failure mechanism leading to the breach of the levee of San Matteo?

How do preferential paths due to animal burrows influence the resulting water pressure distribution?

How can animal burrows influence dike safety?

Sub-questions will also be addressed:

What is the geometry of the burrows under analysis and how can their distribution be defined?

What was the critical geometrical distribution of animal burrows for the failure of the case under analysis?

1.6 Research Approach

The approach used in the research is presented below:

- Literature study
  - Analysis of report and assignments of inputs for the analysis
  - Research on animal burrows for definition of simplified geometry and 3d distribution
  - Historical cases of dike failures due to animal burrowing
  - Literature study on failure mechanism under analysis and influence of animal burrowing in these failure modes
- Analysis of influence of animal burrows on groundwater flow with FEM using Plaxis 2D
  - Analysis without cavities
    - steady-state solution
    - transient flow (considering both rainfall and changes of outside water level)
  - Analysis with cavities
    - steady-state solution
    - transient flow (considering both rainfall and changes of outside water level)
- Analysis of influence of animal burrows on groundwater flow with FEM using Plaxis 3D
  - Implementation of different scenarios of burrows distribution
  - Analysis of different results with Plaxis 2D and Plaxis 3D
- Definition of failure mechanisms:
  - Investigation of possible failure modes
  - Macro-stability analysis with PLAXIS 2D/3D with φ-c reduction method
  - Micro-stability investigation through interpretation of groundwater flow analyses with PLAXIS
  - Assessment of Internal Erosion with approach from Hole Erosion Test

In order to answer the research questions, a few steps need to be taken into account.

First of all, the literature review is carried out. The data available, regarding soil properties, dike profile, water levels and rainfall, are analysed in order to obtain the needed parameters as inputs for the

following analyses. Second, the types of animals causing the burrows, the geometry of tunnels and chambers and the complexity of their distribution inside the dike need to be investigated and assumed.

The current study then looks at the influence of animal burrows on the resulting water pressure distribution. The analyses are carried out for steady state and transient flow conditions, the latter with rainfall and water level changes in the river. The solutions of groundwater flow analyses with no animal burrows inside the dike body are compared to the results of the cases in which they are implemented. Different scenarios and distributions of animal burrowing inside the dike body are investigated. The study is carried out with the Finite Element Program PLAXIS, both for two and three dimensional analyses.

Finally, possible failure mechanisms of the levee of San Matteo and the influence of animal burrowing on them are investigated. The safety of the levee can be analysed and conclusions can be drawn about the failure mechanism leading to the event.

1.7 Thesis Outline

The general information of the study is given in chapter 1.

Chapter 2 presents a summary of the Investigative Evaluation Report. Chapter 3 describes the failure mechanisms which could have happened in the levee of San Matteo and investigates the particular influence of animal burrows for the stability of the dike. In chapter 4, the shapes, dimension, properties and distribution of the animal burrows are defined.

Chapter 5 defines the inputs data and boundary conditions of the problem to be used in the FEM analysis. The performed analysis with FEM implemented in Plaxis 2d and 3d are illustrated in chapters 6 and 7, where the simulations consider different direction and distributions of the animal burrows and analyse their influence for the pore-water pressure. In particular the results are compared for steady state vs transient flow and with vs without animal burrowing for the 2d and 3d solutions.

Chapter 8 investigates the possibility of instability of the inner slope to have caused the failure of the levee of San Matteo, by looking at the results of the macro-stability analyses performed with Plaxis. Chapter 9 investigates micro-instability and internal erosion as possible failure mechanism which happened in the right side of Secchia river on 19th January 2014.

Finally, conclusions and recommendations are treated in chapter 10.

Introduction	Chapter 1	Background and thesis outline
Background	Chapter 2	Summary of Investigative Evaluation Report
Literature review	Chapter 3	Failure mechanisms influenced by animal burrows
	Chapter 4	Animal burrows
Groundwater flow	Chapter 5	Input data and boudary conditions
	Chapter 6	2D Analysis:
	Chapter 7	3D Analysis
Failure mechanisms	Chapter 8	Instability of the inner slope
	Chapter 9	Micro-instability and internal erosion
Conclusions	Chapter 10	Conclusion and Recommendations

Table 1.2 Thesis outline.

.

2 Summary of the Investigative Evaluation Report

2.1 Introduction

On 7 february 2014, the president of the Emilia-Romagna region Francesco Verrani issued a decree (ordinance n. 17 of 7 february 2014, PPG/2014/23) according to which a committee composed by six members of five different universities would have investigated the reason of the failure of the levee of San Matteo.

The final report was published on 9 July 2014 in Bologna. In 89 pages, it describes the environment of Modena, the dynamics of the event, such as the hydraulic conditions, the development of the breach and the flooding. Site investigation and laboratory tests have been performed in order to gain a better insight on the soil properties and to run macro-stability analyses. Finally, the Investigative Evaluation Committee hypothesizes the causes and failure mechanisms of the breach.

2.2 Study area

The breach formed in a section of an earth dike in San Matteo (Modena, northern Italy) with coordinates: 44° 41' 57.6"N, 10° 56' 41.5"E, located between a railway track and a small bridge.

Figure 2.1 Geographic position (left) and localization of the breach (right)

The area is flat with altitude around 30-31 m amsl while the levees are 7-8 meters high. The river Secchia has a straight trend for 2.5km and the distance between its two sides is constant.

2.3 Reconstruction of the event

2.3.1 The breach

Two witnesses (G. Russo and A. Baraldi) interviewed by the Investigative Evaluation Committee report that the breach started from the upper part of the dike.

According to the reconstruction of the event, at 6am, a trapezium with base of 10meters and 2.5meters high, which is the top part of the levee, is removed and the crest drops till 35m amsl. The widening of the dimensions of the breach continues with time till reaching, 9 hours after (at 3pm on 19/01/2014), the maximum width of 80 meters, and maximum depth till the surface level (around 6 meters deep).

Figure 2.2 Reconstruction of the development of the breach at 10.11am and 12.22 (left) and picture of the breach at 10.11am (right). (D'Alpaos et al., 2014) (D'Alpaos et al., 2014)

2.3.2 The flooding

The water volume flowing out of the breach varied between 36.3 x $10^6$and 38.7 x 10^6 m^3, which flooded the surrounding countryside and the villages of Bastiglia and Bomporto. The dynamics of the flooding and the water depths are also simulated in the report, but not reported here since considered significant for the current study.

2.4 Hydraulic boundary conditions

2.4.1 Rainfall

The report by the Investigative Evaluation Committee presents a hyetograph of the intensity of rainfall (Figure 2.3) in the section of the breach between 18-01-2014 at 0:00 and 20-01-2014 at 0:00, obtained by the interpretation of radar maps. The rain was light during all the day before the failure until 8pm, when its intensity increased presenting a peak of heavy rain during the night. Around 2am of the 19th January the intensity decreased and moderate rain was present at 6am when the failure took place.

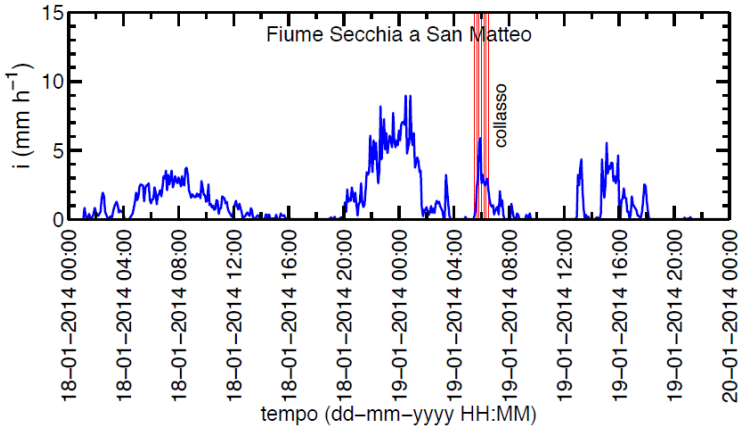

Figure 2.3 Hyetograph of the intensity of rainfall between 18-01-2014 at 0:00 and 20-01-2014 at 0:00 in the section of the breach. The intensity of the rain (y-axis) is plotted against the time (x-axis). The moment of the breach is indicated by the vertical red line at 6am on 19-01-2014. (D'Alpaos et al., 2014)

2.4.2 Water level in the river

The Investigative Evaluation Report presents several models for the simulation of the outside water level in the section of the breach between 15-01-2014 and 27-01-2014, obtained through the elaboration of observations in sections upstream and downstream of the location of failure.

All the models present minimum water level equal to 29 m amsl on the 17th January and they have similar trends: the water level increases during the afternoon of the 17th until reaching its peak after the breach, which is not taken into account in the simulation. The time in which failure happened is assumed at 6.00am, even if the breach was not instantaneous and some time was required to its development. At that time, the water level in the river is around 36 m amsl, so it was below the crest which was placed at 37.5 m amsl.

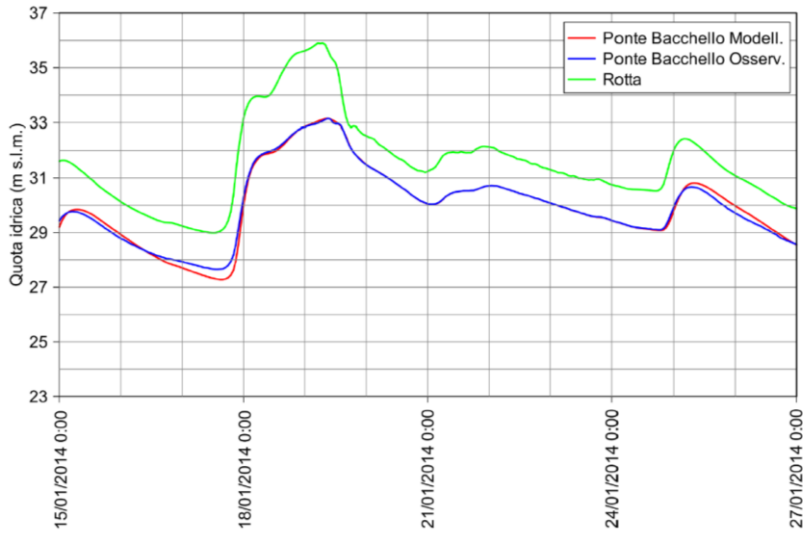

Figure 2.4 Water level in the river between 15-01-2014 at 0:00 and 27-01-2014 at 0:00. In green, the water level in the section of the breach, while in the other colours the comparison between the observed (blue) and simulated (red) level in another location, where data were registered. (D'Alpaos et al., 2014)

2.5 Geology of the area

The failure took place few kilometers in the north of Modena, which is a city of northen Italy and it belongs to the region Emilia-Romagna. The south of the region is characterized by Appennini mountains and hills, while flatland dominates its upper part.

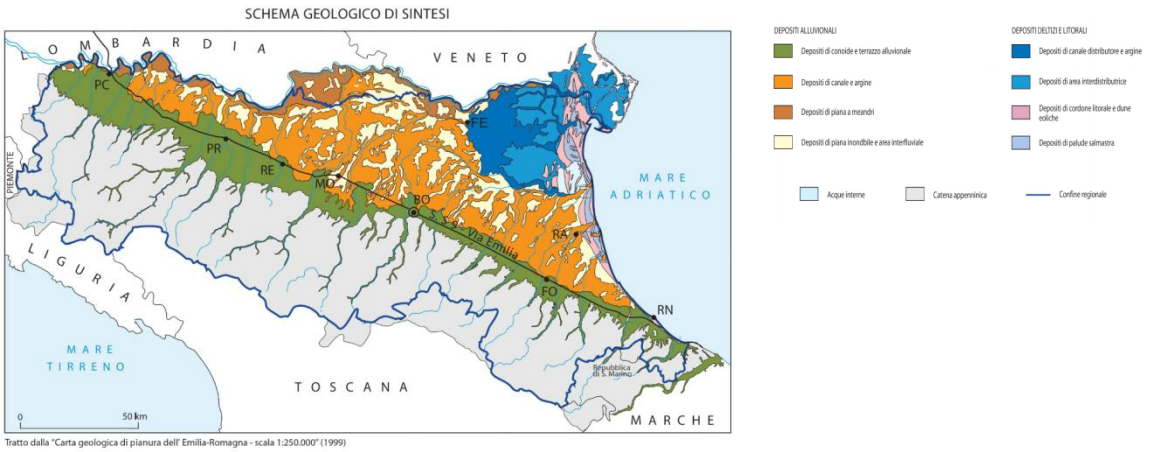

Tratto dalla "Carta geologica di pianura dell' Emilia-Romagna - scala 1:250.000" (1999)

Figure 2.5 Geological map of Emilia-Romagna, the region where the failure took place. In particular, the orange colour represents deposits of channels and embankments. (1999)

The sediments of

the flat area where Modena is located are deposits of channels and embankments. Their origin is due to the deposition and erosion of the rivers Secchia and Panaro, which are two tributaries of the Po river at its right riverside (Po).

The superficial stratigraphic unit until 300-450 m deep is constituted by the AES (Sintema Emiliano-Romagnolo superiore), which dates between 400.000 years old and the present. Underneath the AES, more sandy soil is present, belonging to Unit AES7 (sub-system of Villa Verucchio).

The first 20-30 meters from the surface level are characterized by fine sediments of its sub-system of Ravenna (AES8), which were deposited in the Holocene and whose sediments vary from medium sand to clay and are constituted by silty sand, sandy silts with clayey silty layers. In particular, the superficial part of the sub-system (until 5-8m deep) is the Unit of Modena (AES8a). Its origin is linked to the river environment and so the unit is formed by sandy silt or clayey silt with many iter-bedded sand layer, caused by the floods and the river dynamics.

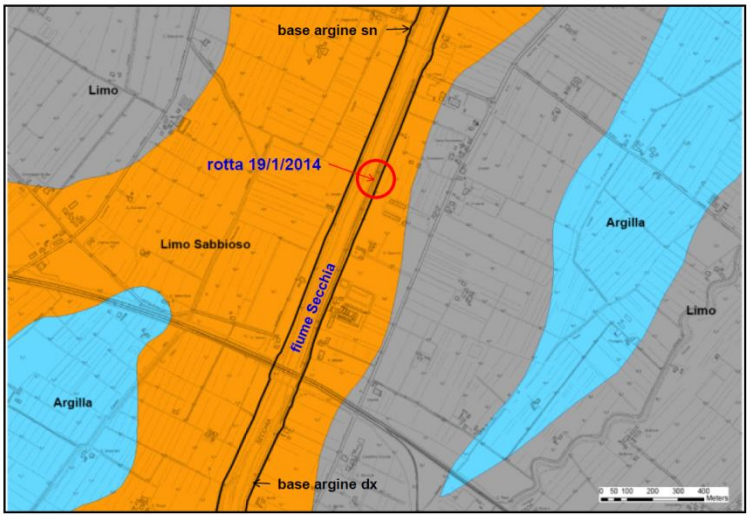

Figure 2.6 Geological map of the area. All the sediments belong to the Unit of Modena (AES8a); sandy loam is orange, clay is blue, loam is grey. The location of the breach is indicated with a red circle. (D'Alpaos et al., 2014)

2.6 Site investigation and laboratory tests

2.6.1 In-situ and laboratory tests

In order to define the stratigraphy and soil properties, field and laboratory tests were performed in three sections (Figure 2.7). The first section is on the right riverside, around 900 meters upstream of the breach. The second is in front of the breach, in its opposite side. The third section is on the right riverside, just downstream of the breach.

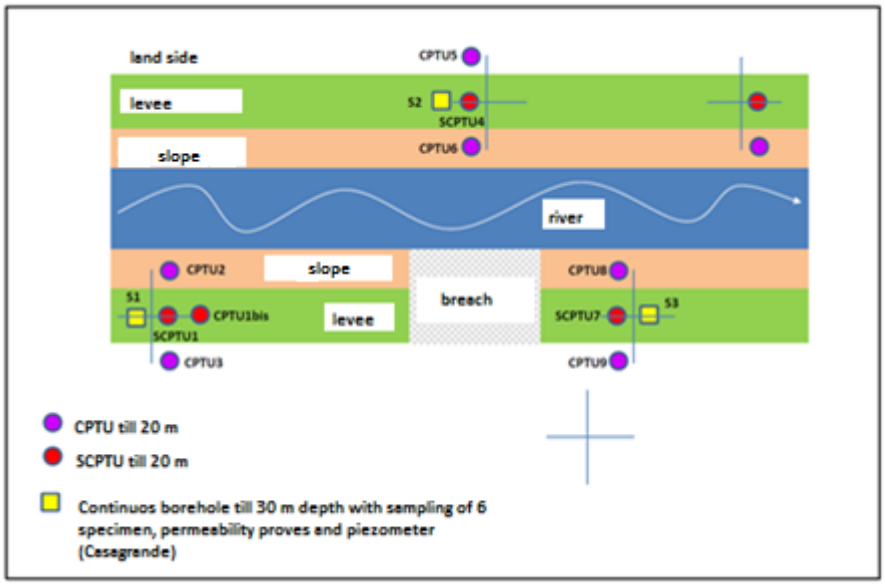

Figure 2.7 Position of geotechnical proves. (D'Alpaos et al., 2014)

The in-situ tests consist on CPTU, SCPTU, continuous boreholes, permeability and piezometric tests. Cone Penetration Test CPTU gives the values for the q_c (tip resistance), the f_s (lateral friction), the pore pressure u and the penetration tilt angle. Seismic cone penetration testing SCPTU gives, in addition, the value of the shear and compressional wave velocities.

Core samples have also been taken in these three locations and laboratory tests have been performed. The reader can find the results of the field and laboratory tests which are available in the report in Appendix A.

2.6.2 Stratigraphy

The dike is thus formed by three layers: Figure 2.8 represents the stratigraphy of first section under analysis, the profiles of the tip resistance q_c and the porewater pressure u, varying with depth.

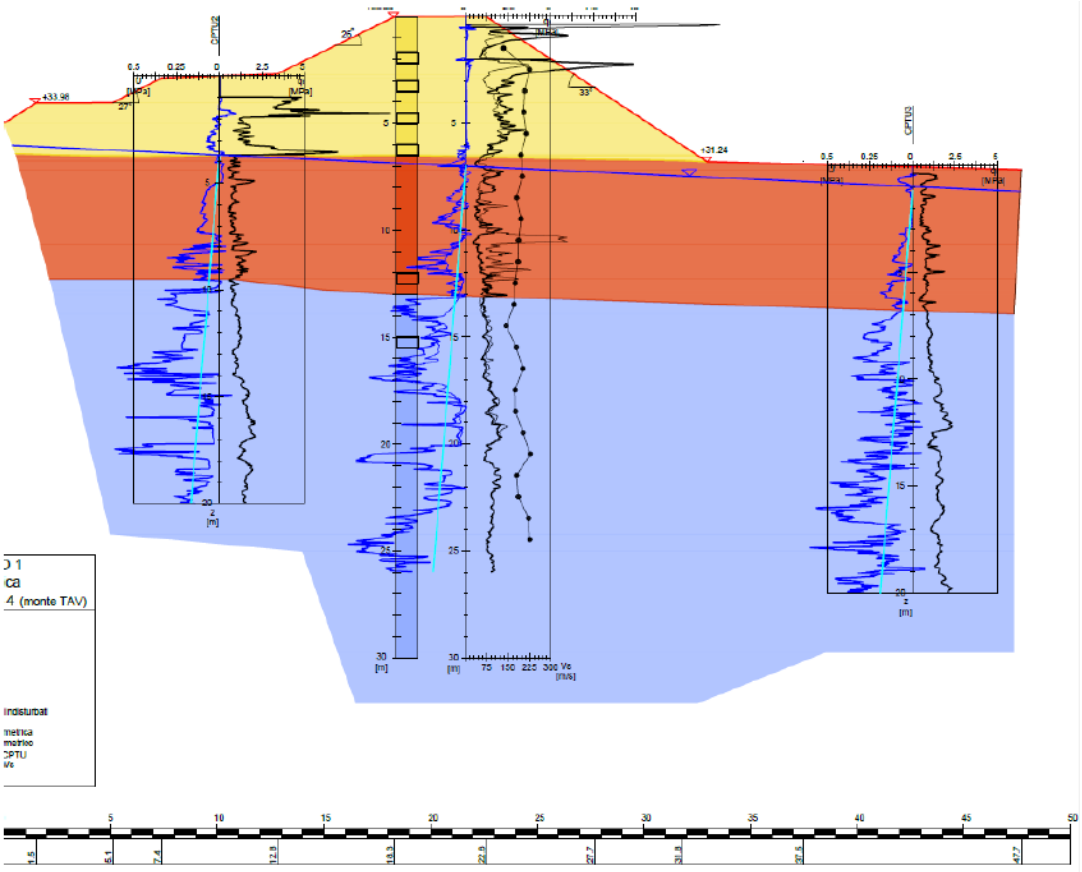

Figure 2.8 Stratigraphic profile in section 1: from the top, Unit AR (yellow), Unit B (orange) and Unit C (blue), with the profiles of the tip resistance q_c(black) and the porewater pressure u (blue) in three locations. (D'Alpaos et al., 2014)

In the Investigative Evaluation Report the three layers are called *Unit AR, Unit B and Unit C,* starting from the top. *Unit AR* forms the levee body and it is composed by silt with sand and sandy silt. Underneath, *Unit B* has sandy silt, locally with clay, and formed with sub-horizontal layers. The deeper unit is *Unit C,* which is mostly composed by clay and, locally, sand and silt are present.

Unit AR has a low permeability index (IP<10%) and $w_n < LP$ (Water Content smaller than Plastic Limit) so the consistency is semi-solid. Unit B presents similar lower plasticity than unit A but the consistency is fluid or plastic-fluid, since some results present $w_n > LL$ (Liquid Limit). Unit C is formed by very plastic clay.

The parameters for the strength and deformability have been calculated through interpretation of the laboratory tests or by correlation with the results of the field tests. Units AR and B are described with the peak friction angle Φ'_p and the friction angle in critic conditions Φ'_{cv}. For unit C, the undrained shear strength s_u and the peak friction angle Φ'_p have been calculated.

2.7 Presence of animals burrows in the levee

Presence of animals in the area has been confirmed during field visits with pictures of footprints and dens. The area was already under monitoring because of the large presence of animals. Photos in Figure 2.9 were taken during the same day of the breach and days after of the event. In particular, the footprint belongs to a badger.

Figure 2.9 Footprint of a badger and animal burrow near the location of the breach. (D'Alpaos et al., 2014).

Moreover, on the 19th January another breach happened on the right riverside of Panaro river, around 10 kilometres far from the breach location.

Figure 2.10 Internal erosion due to animal burrows in the right riverside of Panaro river (19th January 2014). (D'Alpaos et al., 2014)

The presence of burrows in the section of the breach was post-investigated by the Investigative Evaluation Commitee through two aerial photos with high resolutions by 2010 and 2012. Two entrances can be individuated in the picture of 2010, while they are four in 2012 (Figure 2.11). The pictures also correlate the positions of the entrances with the development of the breach.

Figure 2.11 State of the levee on 27-03-2010 (left) and 29-03-2012 (right). The position of the burrows entrances is indicated by the red circle, T1,T2.. indicate trees used as reference points, while the red arrows indicate the development of the breach. (D'Alpaos et al., 2014)

In the areal photo of 2012, four burrows are observed: three are placed along the inner slope, while only one in the outer slope. The distance between the three entrances along the inner slope is around 3meters between each other, while the longitudinal distance between them and the entrance in the other side is around 10 meters.
The entrance of the burrow along the outer slope is at 36.3 m amsl, that is around 30 cm above the maximum water level reached during the night of the 19th January 2014.

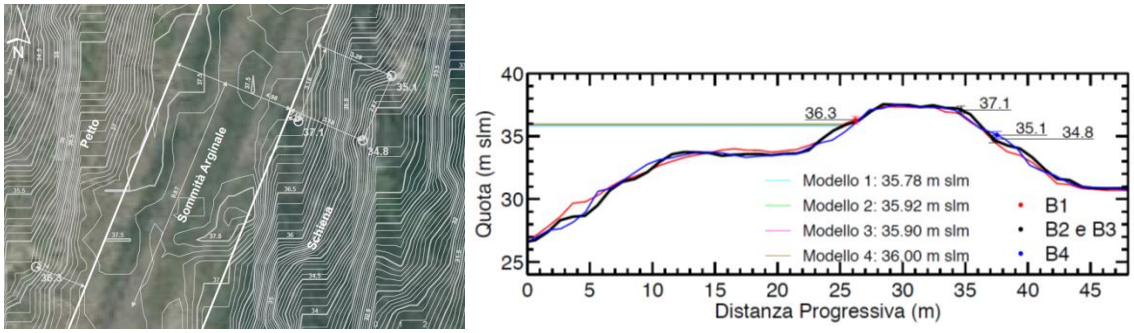

Figure 2.12 Reconstruction of planimetric position (left) and altimetry (right) of animal holes done in the report. On the right graph, the progressive distance(m) is on x-asis, while the altitude(m) on y-axis. (D'Alpaos et al., 2014)

2.8 Analysis

2.8.1 Introduction

The profile used for the stability analysis is obtained from the stratigraphic profile of section 3 and the initial phreatic level is equal to 29.50 m amsl.
The stability analyses are carried out with the software SEEP and they have been performed with the method of Morgenstern&Price and failure model of Mohr-Coulomb. Steady state and the transient flow analyses have been performed.

2.8.2 Steady state

The steady state calculations evaluate the failure of the levee without any change in time of the water level in the river. The analyses in the report evaluate the safety factor for different water levels and for two types of slip plane (shallow and deep). In order to take into account the uncertainty related to the soil properties, several Monte-Carlo simulations are performed for different values of friction angle.
The fragility curves in Figure 2.12, which give the probability that failure occurs (the y-value) for several water levels in the river (the x-value or independent variable), are the outputs of the analyses.

They are given for two types of slip planes (shallow and deep) and evaluate the probability of failure for different water levels in the river and, in particular, the maximum level reached before the breach happened.

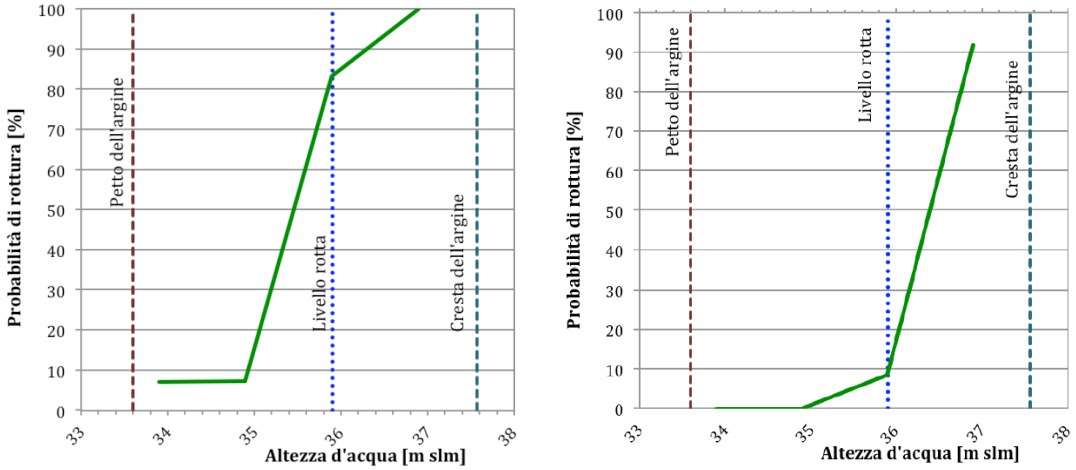

Figure 2.13 Fragility curves for the shallow slip plane (left) and deep slip plane (right) for different water levels in the river: probability of failure (y-axis) versus water level (x-axis). The dashed blue line indicates the water level at the moment of the breach at 36 m amsl and the green dashed line the top of the levee.

The input values and the analyses are further described in Appendix B.
However, according to the Investigative Evaluation Committee, steady state calculations are not representative for the breach and they just give an indication for the stability of the levee in case of high water level in the river which are constant for a long period of time.

2.8.3 Transient flow

2.8.3.1 Initial and boundary conditions

The transient flow analysis reproduces the behaviour of the levee just before the breach in order to have a better insight on the failure mechanism (back-analysis).
The initial conditions used in the analysis are characterized by negative pore water pressure inside the soil body, with a minimum suction pressure of -40 kPa (Figure 2.14). The pore water pressure distribution is extrapolated from literature review and considered realistic for the levee under analysis by taking into account its soil properties and the winter period.

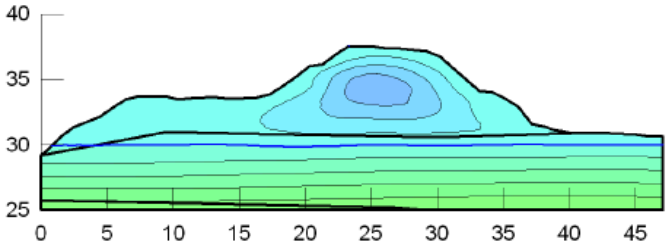

Figure 2.14 Pore water pressure distribution at the beginning of the analysis. The bold line represents the phreatic line and the difference between the iso-lines is 10 kPa. (D'Alpaos et al., 2014).

The Soil Water Retention Curve and the Hydraulic Conductivity Function (Figure 2.15) correlates the negative pore-water pressure respectively to the volumetric water content and the hydraulic

conductivity. The hydraulic properties of a single sample (sample #44) are used, since they are considered representative for the all levee.

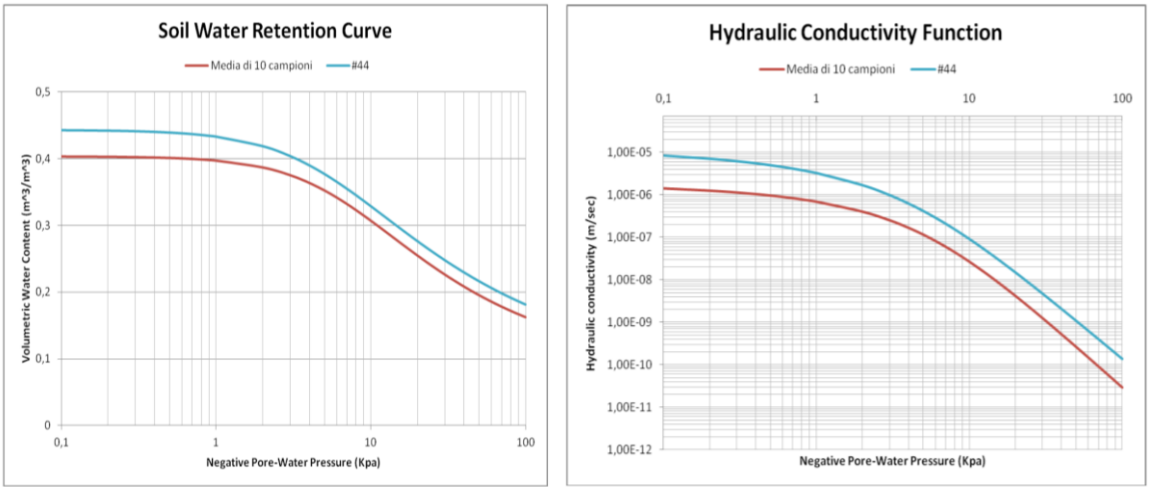

Figure 2.15 Soil Water Retention Curve and Hydraulic Conductivity Function. (D'Alpaos et al., 2014)

These curves are constructed with the model of Van Genuchten-Mualem and the used parameters used are summed up in Table 2.1.

Campione #44						
θ_r	$\theta_0 = \theta_{sat}$	α_{VG}	n_{VG}	$m_{VG}=1-1/n_{VG}$	K_0	τ_{VG}
($cm^3\ cm^{-3}$)	($cm^3\ cm^{-3}$)	(cm^{-1})	(-)	(-)	($cm\ h^{-1}$)	(-)
0.0719	0.443	0.01948	1.409	0.290	4.684	0.5

Table 2.1 Parameters used for the Van Genuchten-Mualem model from sample #44. (D'Alpaos et al., 2014)

2.8.3.2 *Analysis*

The back-analysis is performed for macro-instability of the inner slope for four types of failure surfaces, namely from I to IV: the firsts are shallower and surfaces III and IV are the ones that according to the committee happened to fail. The simulation period used in the transient flow analysis is from 17/01/2014 to 19/01/2914, during which rainfall and water level data are then applied to the section.

First, the analysis doesn't consider the presence of animal cavities. The dike is assumed homogeneous with no macro-voids or discontinuities and the soil parameters obtained by the field and laboratory tests are used as inputs.
The results of these first analyses (Figure 2.16) present the FS above 1 for surfaces III and IV. The equipotential surfaces and the water content are also calculated. The results can be found in Appendix B.

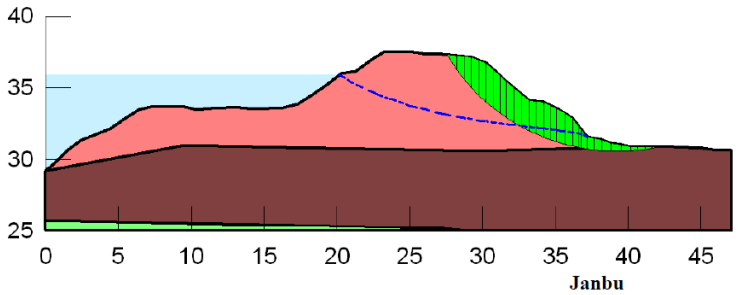

Morgenstern & Price
Media FS = 1.16
P (F) = 0.95 %

Media FS = 1.12
P (F) = 3.30 %

Figura 116 - Superficie I, assenza di cavità.

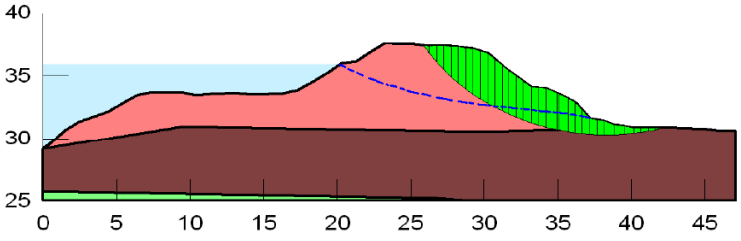

Morgenstern & Price
Media FS = 1.22
P (F) = 0.25 %

Janbu
Media FS = 1.17
P (F) = 0.95 %

Figura 117- Superficie II, assenza di cavità.

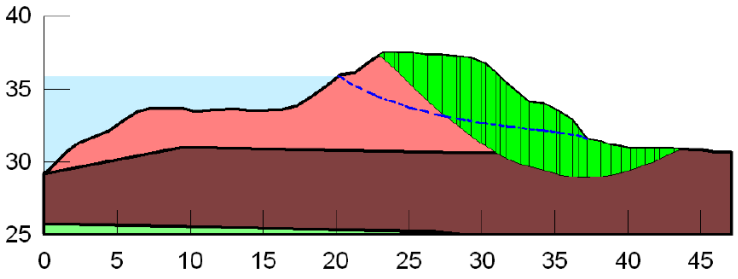

Morgenstern & Price
Media FS = 1.23
P (F) = 0.40 %

Janbu
Media FS = 1.15
P (F) = 2.00 %

Figura 118 - Superficie III, assenza di cavità.

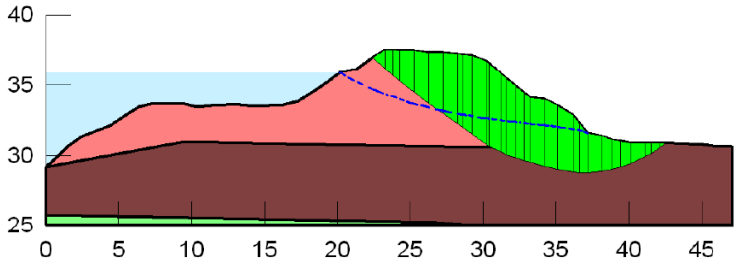

Morgenstern & Price
Media FS = 1.26
P (F) = 0.15 %

Janbu
Media FS = 1.18
P (F) = 1.10 %

Figura 119 - Superficie IV, assenza di cavità.

Figure 2.16 Transient flow analyses for the levee without taking into account animal burrowing, with failure surfaces I to IV, starting from the top. (D'Alpaos et al., 2014)

Then, the analysis is repeated by taking into account the presence of animal burrows and their influence to the breach. The cavities are implemented with the reduction of the tangent of the friction angle tanφ by 20%, in order to simulate the reduction of resistance that they introduce. The burrows are thus assumed homogeneously distributed along the dike body.
The FS now decreases and the values are still above 1 for surfaces III and IV.

Surface	Morgenstern & Price	Janbu
I	0.95	0.91
II	1.03	0.97
III	1.09	1.02
IV	1.14	1.06

Table 2.2 Values of FS for the analyses performed in the Investigative Evaluation Report with animal burrows homogenously distributed inside the levee

2.9 Conclusion of the report

According to the Investigative Evaluation Committee, the failure was facilitated by the presence of large amount of animal dens, in particular foxes and other wild animals.
The committee indicates two failure mechanisms that may have acted singularly or combined. The first is internal erosion, which is facilitated by the presence of animal burrowing and precipitation, such as it happened along the Panaro river. Once the internal erosion enlarges the cavities, the dike body above it collapse determining the start of the breach.
The second mechanism is macro- instability, which has been facilitated by the saturation and presence of cavities, and so the consequent loss of effective stress.
Finally, according to the committee, independently on the failure mode, the presence of burrows was necessary to cause the breach.

2.10 Further Considerations

Few aspects are not fully clear in the Investigative Evaluation Report and need a further investigation:

- The animal burrows have been implemented in the analysis by reducing the tangent of the friction angle φ of all the dike body by 20%. However, this method corresponds to a manual implementation of the φ-c reduction method (paragraph 8.3) by reducing the tanφ until failure occurs. Moreover, no correlation is given between the missing volume excavated by the animals and the correspondent assumed reduction of strength.
- By reducing the overall properties of the dike body, the burrows are implicitly assumed to be homogeneously distributed in the levee. The possible network and the geometry of the burrows are not presented in the report. However only through their investigation it is possible to assess their influence to the failure or, at least, to establish a correlation between the excavated network and the overall reduction of tanφ.

3 Overview of failure mechanisms influenced by animal burrows

3.1 Introduction

The failure of a flood defence can be initiated by different mechanisms, whose most important are illustrated in Figure 3.1.

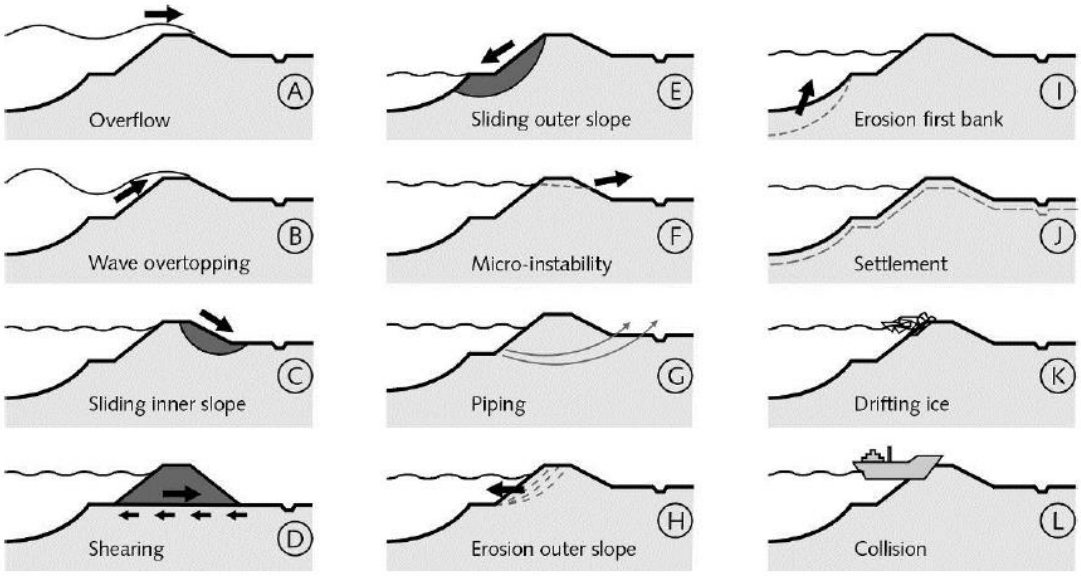

Figure 3.1 Possible failure mechanism of flood defences. (Jonkman and Schweckendiek, 2015)

Their meaning and their relation with the breach of San Matteo are discussed below:

A. Overflow: it happens when the water level in the river is higher than the levee crest, so that water flows above it. This failure mechanism is excluded as the cause of the event of San Matteo: when the breach took place, the simulated water level was between 35.78 and 36.04 m amsl while the levee crest is placed at 37.30 m amsl.

B. Wave overtopping: even if the still water level in the river is below the top of the levee, the waves cause the overtopping of the crest. The waves in the Secchia river on 19/01/2014 were negligible, as it will be described in paragraph 5.2.2.1, so also this failure mechanism can be excluded.

C. Sliding Inner Slope: a sliding plane is created in the inner slope due to higher saturation and pore pressure, with consequent reduction of effective stresses. This failure mechanism is further described in Paragraph 3.2, since it may have been the cause of the breach.

D. Shearing: sliding along the base of the dike body, due to horizontal forces exercised by the water in the river. Two testimonies report that the breach started from an opening located in the upper part of the dyke, excluding so this failure mechanism.

E. Sliding Outer Slope. When the water level in the river suddenly drops, the high water pressure in the soil body, which is not supported anymore by the water load in the river, causes the sliding of the outer slope. This failure mechanism didn't take place for the breach of San

Matteo, since the water level recorded was increasing and no *sudden draw-down* was registered.

F. Micro-instability: the water level inside the dike body increases until its exit point is above the toe at the inner slope of the levee and water starts seeping out of the inner slope. This phenomenon is investigated for the levee of San Matteo.

G. Piping. The high water pressure inside the dike body cause the erosion of particles: starting from the inner slope, cavities called *pipes* develop towards the outer slope, leading to the sliding of the all levee body. Since this mechanism is significant for the levee of San Matteo, it will be further discussed in Paragraph 3.4.

H. Erosion of Outer Slope. The current and waves in the river can cause the erosion of the outer slope. In the case under analysis, this mechanism can be excluded: the photos taken immediately after the breach don't show any erosion at the outer or inner side, where the trees are still intact.

I. Erosion Foreshore. Due to *liquefaction* or *unstable breaching*, the effective stresses of the soil reduce to zero. The slope failure consequently happens, leading to the so-called *flow slide*. Liquefaction is not considered in the case under analysis because the earthquake solicitations are not significant in this location. Moreover this failure mechanism is excluded when considering the testimonies and the photos after the event.

J. Settlement: The crest of the levee decreases compared to its design value due to consolidation and creep. As a consequence, overflow and overtopping can occur. However, this phenomenon is not relevant for the case under analysis.

K. Drifting Ice. The ice present in the river pushes the water to overflow the crest or causes erosion of the outer slope by colliding against it. Also this mechanism didn't happen in the case under investigation: no ice was present on 19January 2014 in the Italian locality of San Matteo.

L. Collision by vessel: it is also not relevant in the not navigable Secchia river.

As a conclusion, Sliding of the Inner Slope, Micro-instability or Internal Erosion are the mechanisms which may have led to the breach. Before analysing these phenomena, few considerations need to be done.
During a field trip to the location of the breach in March 2015, pipelines were not individuated inside the dike body.
Moreover, according to Stefano Orlandini, member of the Investigative Evaluation Committee and interviewed on 24th March 2015, the levee was not saturated when the event took place. The dike still had residual strength, proved by the fact that camions were passing on the crest of the dike to repair the breach after the event took place.

3.2 Instability of the inner slope

3.2.1 Introduction

Instability occurs when actual shear stress exceeds the shearing resistance along a plane, where sliding will happen.

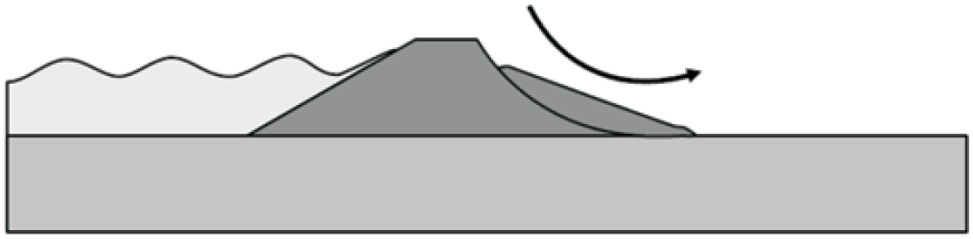

Figure 3.2 Instability of the inner slope

According to Terzaghi's principle, the effective stresses depend on total stresses and pore pressures:

$$\underline{\sigma}' = \underline{\sigma} - \underline{m} \cdot p_w \qquad (3.1)$$

Whe:

$$\underline{\sigma} = \left(\sigma_{xx}\sigma_{yy}\sigma_{zz}\sigma_{xy}\sigma_{yz}\sigma_{zx}\right)^T \text{ and } \underline{m} = \left(1 \quad 1 \quad 1 \quad 0 \quad 0 \quad 0\right)^T \qquad (3.2)$$

$\underline{\sigma}$ is the vector with total stresses, $\underline{\sigma}'$ is the vector with effective stresses, p_w is the pore pressure and $\underline{m}$ is a vector with terms equal to 1 for normal stress components and equal to 0 for shear stress components. The infiltration of water into the soil body, due to rainfall or increase of water load acting on the levee, changes the pore water pressures inside the dike body. As the pore water pressures inside the levee increase, according to formula (3.1), the effective stresses σ' decrease.

The decrease of effective stresses causes the decrease of shear strength (Reddi, 2003). As a matter of fact, according to Mohr-Coulomb criterion, the shear strength τ, which consists on cohesive and frictional resistance, depends on the normal stress on the plane of shear failure:

$$\tau^{\lim} = c + \sigma_n' \cdot \tan\phi \qquad (3.3)$$

where τ^{lim} is the limit shear strength along the sliding plane, σ'_n the normal effective stress on the failure plane and ϕ the angle of internal friction of the soil.

Moreover, the saturation of the soil due to the infiltration of water increases the soil weight, which also contributes to the driving moment and thus increase the probability of instability.

3.2.2 Influence of animals on the instability of the inner slope

The fragility curve in Figure 3.3 gives the probability that failure occurs (the y-value or dependent variable of the fragility curve) as a function of the external load, which is the water level in the river (the x-value or independent variable). The figure illustrates that the probability of failure severely increases when animal burrows are present. In particular, the most dangerous burrows belong to badgers.

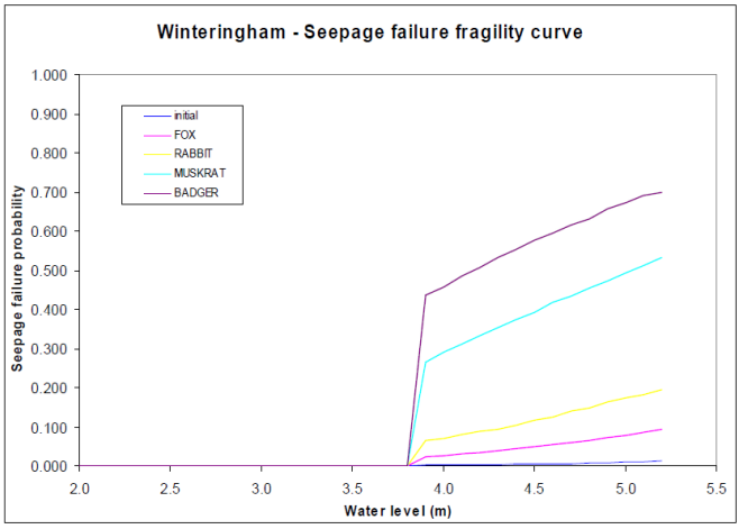

Figure 3.3 Fragility curves: the probability of failure depends on the type of animals creating the burrows and it increases compared to the case of no burrow (2012)

When the water level in the river increases, the phreatic line changes with a shape and rate depending on the properties of the soil body. Thus the heterogeneity introduced by animal burrows influences its trend such as Figure 3.4 illustrates.

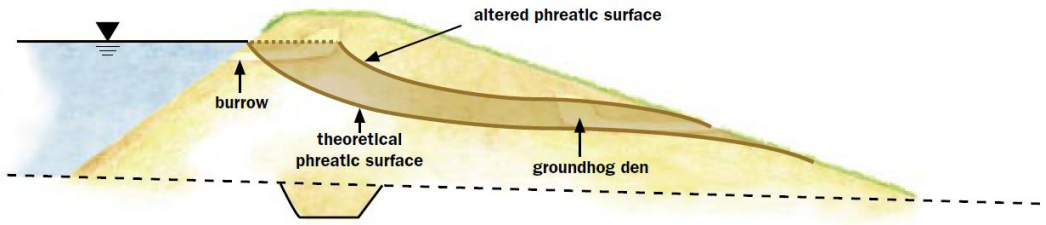

Figure 3.4 Shortening of seepage path due to animal burrow (2012)

The animal burrows can reduce the seepage length and the phreatic line can rise, posing a risk to the stability of the dike. For this reason, the probability of failure increase in case of animal burrows.
The reduction of seepage length depends on the geometry of the cavity and so on the species creating the burrow. Badgers create complex burrows with many tunnels and entrances. According to a study performed by Deltares (2012), their presence can reduce the seepage length up to 6 meters and their typical diameter is assumed equal to 0.4. Foxes, instead, reduce it up to 2meters, while rabbit up to 3m and muskrat up to 5m.

3.3 Micro-Instability

3.3.1 Introduction

If the phreatic line exits at a point above the toe of the inner slope and seepage flow develops, micro-instability can occur (Vorogushyn et al., 2009). Failure starts at the exit of the phreatic line at the inner slope when the weight above and the forces created by the flow exceed the resisting shear resistance. Particles at the exit point are detached and carried away by the seepage flow and the process gradually retrocedes towards the upstream side of the levee.

Figure 3.5 illustrates the failure due to micro-instability. In particular, the slide height is indicated by h_a.

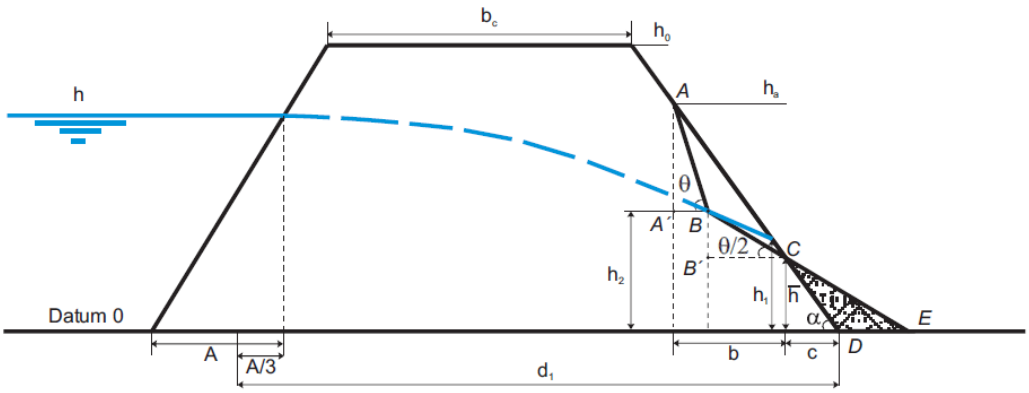

Figure 3.5 Slope failure due to micro-instability (Vorogushyn et al., 2009).

Non cohesive soil, erodible material and unprotected exit are favourable conditions for the development of micro-instability.

3.3.2 Influence of animals on micro-instability

The presence of animal burrows can raise the phreatic line (Figure 3.4). If it exits above the inner toe of the dike and the seepage forces are high enough, the probability of seepage and micro-instability increases.

3.4 Internal erosion

3.4.1 Introduction

The generic term “piping” is used for several mechanisms which can be identified as followed (Richards and Reddy, 2007):

a) Backwards Erosion. The inter-granular seeping water create tractive forces, which are higher at the exit point where the flow concentrates: they act as erosive forces and flush the particles away from the soil matrix. Micro-instability is also known as backward erosion.
b) Internal Erosion. The soil particles are removed by tractive forces along pre-existing openings such as cavities or voids.
c) Tunneling or Jugging. The rainwater causes the chemical dispersion of clay soils in the vadose zone.
d) Suffusion and Suffosion. The first refers to the gradual migration of fine particles in the coarse matrix, while the second indicates the collapse and loss of all the soil structure.
e) Heave. If a semi-permeable layer is situated above a more permeable zone, when the water pressures in the pervious zone increase and exceed the vertical effective stress of the layer above, uplift at the base of the semi-permeable barrier takes place.

The most favourable soil to internal erosion is highly erodible, permeable and uncompacted. Silts and silty sands with low clay content, generally with low dry density, high void ratio and collapsing properties are the most susceptible soils to piping (Masannat, 1980).

3.4.2 Influence of animals on internal erosion

The presence of animal burrows facilitates the “internal erosion as evolution of defects”, such as piping is defined when cracks and microfissures are present in the soil matrix (Bonelli, 2006). As water flows

into the cavities, the seepage forces act along the surface, eroding them and removing the subsurface soil.

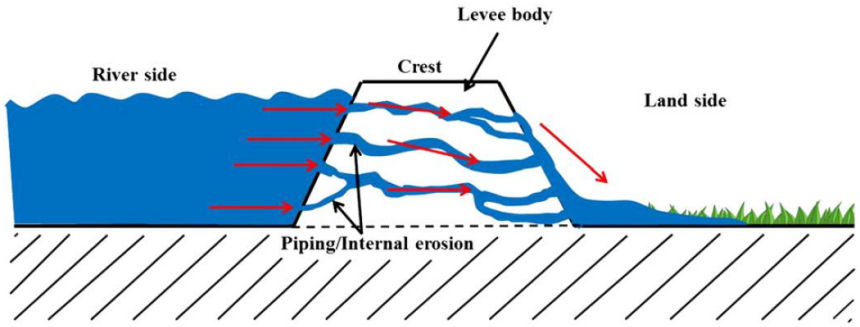

Figure 3.6 Internal erosion in presence of animal burrows (Chlaib et al., 2014)

3.5 Historical cases

Piping resulting by animal holes was observed in Arizona, along the San Pietro River (Carrol, 1949). The pipes were created by gophers and eroded becoming huge tunnels which connected to the main one (Figure 3.7).

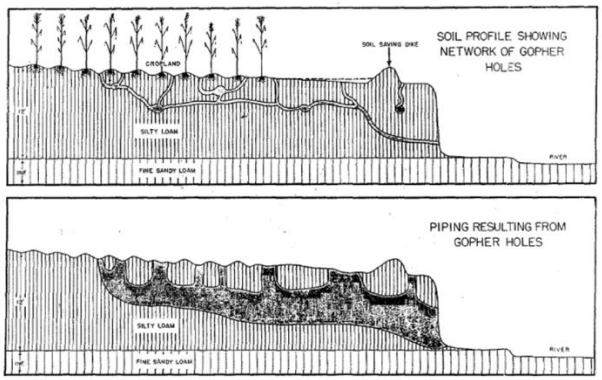

Figure 3.7 Internal erosion facilitated by gophers burrows along San Pietro River, Arizona (Carrol, 1949)

On 5 January 2008, a failure occurred in the Truckee Canal (Fernley, Nevada). The post-investigation revealed that the flow rates were not exceptional and that the extensive network constructed by animals caused piping to occur (Paul and Slaven, 2009). Water, entering and flowing through the cavities, acted at high pressures against the tunnels, creating hydraulic fractures throw the levee and opening other seepage paths. Thus the resulting piping and erosion led to failure. Finally, the fact that higher water levels occurred in the past without leading to previous failures supports the hypothesis of evolution of the underground animal system in time.

Figure 3.8 Canal breach and network of muskrat burrows Truckee Canal (Fernley, Nevada)

Other historical failure caused by internal erosion due to animal burrowing are the followings (Richards and Reddy, 2007): Big Sand Creek Str Y032032, MS (1996), Lower Stichcomb, GA (1978), Mallard Lake, TN (1996) and Prospect Reservoir Dam, CO (2002).

3.6 Correlation between animal burrows and failure for the levee of San Matteo

According to the Investigative Evaluation Report, at 6am on 19th January 2014, the top part of the embankment was removed. It had a trapezoidal shape with base 10m wide at 35m amsl.
The reduced width of 10meters indicates that a particular weakness was present in that location in order to create the breach. As a matter of fact, no other breaches happened along the levee, even if the level of water in the river further increases after the failure, as it will be described in paragraph 5.3.2.2.

The breach width corresponds to the maximum distance between the burrows entrances: the breach occurred where probably the main sett was located, such as indicated in Figure 2.11 for the times 10:11am and 11:22am.

Moreover, the depth of the breach corresponds to the estimated position of the bottom of the tunnels: according to two testimonies interviewed by the Investigative Evaluation Committee, it started from 1.50-2 meters below the crest. Assuming that the entrance tunnels go down for 1meter, the system is located at that exact depth.

Finally, the burrows could have constituted preferential tunnels for water, which infiltrated due to water level in the river and high precipitation during the days when the event took place. Even if the water level in the river was 30cm below the entrance of the burrow at the outer slope, the water table inside the levee could have been situated above the tunnels, since they usually penetrate in depth compared to their entrance.

3.7 Conclusion

The current chapter have investigated the possible mechanisms which caused the failure of the levee of San Matteo and the influence of animal burrowing in causing them. While evaluating the breach, the possible failure mechanism that happened are reduced to Instability of the Inner Slope, Micro-Instability and Internal Erosion.

Sliding of the inner place takes place when the higher saturation and pore pressures decrease the effective stresses and so the shear resistance of the sliding plane. Animal burrowing increase the probability of instability of the inner slope by raising the water table and so the pore pressures inside the dike body. First the pore pressure distribution inside the dike body and the effects of animal burrows on it are investigated (chapter 6 and 7). Then stability analyses are carried out in Chapter 8.

Micro-instability occurs when the water level inside the dike body increases until its exit point is above the toe at the inner slope of the levee and water starts seeping out of the inner slope. The presence of animal burrows can raise the phreatic line and, if the seepage flow exits in a point above the inner toe of the dike, the probability of micro-instability to occur increases. The position of the water level in investigated through the groundwater flow analyses (chapter 6 and 7) in order to conclude about the possibility of micro-instability to have caused the breach of San Matteo (chapter 9).

Internal Erosion can take place in pre-existing voids such as animal burrows when the water, flowing into the burrows, exercises seepage forces and remove the surrounding soil. This mechanism is investigated, through the analysis of the development of radius in time, with an approach obtained by the Hole Erosion Test in Chapter 9.

Finally, some observations suggest the influence of animal burrowing in the creation of the breach. As a matter of fact, it was approximately 10 meters long and localized at the same location of the burrows entrances and so also of the underground system digged by the animals. Moreover, the depth of the breach according to testimonies corresponds to the depth of the assumed realistic burrow network.

4 Animal Burrows

4.1 Introduction

The current chapter focuses on the burrowing activity of European badger, Red foxes and Crested porcupines, that are the animals considered responsible for the creation of the burrows entrances registered in the Investigative Evaluation Report.

First of all, the types of animals and the environment in which their dens are digged is presented. Second, the investigation concentrates on defining the geometry of tunnels, the underground systems and the amount of excavated volume. Finally, the analysis concentrates on the levee of San Matteo. Starting from the recorded position of entrances, scenarios of underground systems are assumed, by also taking into account the growth of the system with time.

In conclusion, through literature review, the current chapter provides a description of the geometry and spatial distribution of underground burrowing systems. In such a way, realistic scenarios are proposed that will be implemented in the following analyses (chapter 6 and 7).

4.2 Types of animals

Accoding to D'Alpaos, chairman of the Investigative Evaluation Committee, the European badger (*Meles meles*), Red foxes (*Vulpes vulpes*), and Crested porcupines (*Hystrix cristata*) are the animals responsible for the creation of the burrows along the levee of San Matteo. The phenomenon of animal holes in the dikes of the area is recent since these animals have been present in Northern Italy for few years.

4.2.1 European badger, Foxes and Crested porcupine

European Badgers are medium-sized omnivorous with nocturnal life habits. They live in Europe and eastern Asia, in clans, that are family groups up to 12 members. Their presence near the levee was confirmed by footprints taken near the location of the breach during the same day of the event.

Figure 4.1 European Badger (Meles meles): from left to right, the animal, the distribution and their footprints in the location of the breach

Crested porcupines are present in Italy, North Africa and sub-Saharan Africa and they live in different environments such as forests, dry rocky areas, farmlands and deserts. They are nocturnal animals, known to be solitary foragers that live in small family groups formed by the adult pair and several young members. The porcupines are monitored in the area of the breach and they were responsible for the breach that took place on the 19th January in the right riverside of Panaro river.

Figure 4.2 Crested porcupine (Hystrix cristata): from left to right, the animal, the distribution and the failure in the right riverside of Panaro river.

Red Foxes are present in Europe, Canada, USA, Asia, Australia and North Africa. They live in family groups even if their life habit is solitary and they are mainly active during the night. Dens created by foxes were observed few the months after the breach of San Matteo in Carpi, that is a town 15 km far away from the location of the breach.

Figure 4.3 Foxes (vulpes vulpes): from left to right, the animal, the distribution and their burrows in the close town of Carpi.

4.2.2 The Myocastor coypus

The coypu (Myocastor coypus), which is a semiaquatic rodent with South-American origins, is very present in the area and was firstly assumed to be the animal responsible of the burrows. However, later its responsibility has been excluded. L. Fortunato, former director of AIPO (Inter-regional Agency of Po river) explains that coypu is a semi-aquatic animal whose burrows are at water level in normal regime, thus lower than the ones present in the location. These animals are not taken into account in the Investigative Evaluation Report.

However, their responsibility in the event cannot be completely excluded. These animals are a real danger for the dikes along Secchia river: the recent numerous campaigns for their capture demonstrate the awareness of the danger that they cause to dikes (Tongiorgi et al., 1998).
Theirs burrows start from the toe of the levee at the outer slope, below the water level. The diameter of the tunnels is among 20-40 cm and they rise for approximately 6 meters till the chamber, located in a dry place.

Despite these considerations, the current study takes the same assumptions of the Investigative Evaluation Committee and so excludes the burrows of coypus from the analysis. As a matter of fact, the locations and amount of coypus burrows are not recorded in the location of the breach, making difficult their consideration for the following analysis.

4.3 Sett

4.3.1 3d complexity and distribution

The burrows geometry depends on the animals which make them. European badgers and crested porcupines create similar systems, which they often share with foxes.
European badgers create complex burrow systems called setts, which are mostly located in low altitude and in steep slopes, preferably with cover. The dens of the foxes are in forests, scrubland, prairies but also in urban environments, in particular in locations where the soil is well drained. The systems created by foxes have simple structure, usually consisting of a burrow leading to a den, from which many lateral passages branch. Crested porcupines can live in existing holes, such as caves, rock crevices and holes created by other animals, or they dig their own burrows within an extensive and elaborate system.

Since the structures created by European Badgers and Crested Porcupines are very similar, it is assumed that their setts are present in the area of the levee of San Matteo and shared with foxes.
Most of the setts are constructed in loam, sandy and clay soils. The preference for sandy and dry soils is justified by the fact that they are more friable and thus it is easier to dig on them (Kruuk, 1978, Reddi et al., 2008).
The presence of setts is facilitated by vegetation cover, slope and diggable soil type. The vegetation protects them, the roots provide structural support to the tunnel system and facilitate the drainage. Also slopes can improve drainage, keeping the setts dry (Byrne et al. 2012). Moreover, slopes provide a favourable environment where to dig on.

The setts can be used by more clans and they consist on complex underground systems, which are composed by several passages and chambers. The central part is constituted by a main sett, occupied by most of the colony's members. It has several entrances, it is permanently occupied and its function is breeding.
Close to it, 50m up to 150m far away, there are non-main setts, which can further divided into annexe, subsidiary and outlier setts, depending on the frequency of use and the connectivity with the main set. Outlier setts are not often occupied and they have only one entrance; annex setts, which are close to the main sett, have few entrances and are usually occupied; subsidiary setts, which are far from the main sett, have many entrances and are sometimes occupied. In Ireland, the results conducted by five studies show that 77% of the surveyed setts don't invest a principal role (Byrne et al., 2012). Outlier setts, when unused or abandoned, can also be taken over by foxes (Vulpes vulpes) and European rabbits (Oryctolagus cuniculus).

One sett can have between 1-2 and 44-50 entrances, among which some can be very used and other abandoned. The factors that affect the size and complexity of the sett are its function, the soil type and its age. In particular, main setts are larger than annexes, subsidiary and outliers setts; more the soil is diggable and more the system is developed; finally oldest systems are the biggest and most complex.

The number of entrances, chambers, tunnels length and internal volume of the three setts reported in Table 4.1 give an idea of the size of the excavations performed by the badgers.

Sett	Entrances	chambers	Tunnel network (m)	Total volume (m^3)
1	16	57	310	15
2	38	78	360	25
3	178	50	879	39

Table 4.1 Size and dimension of three badgers setts explored in Ireland in 1976 (Roper, 2010)

The complexity of the systems is also illustrated in Figure 4.4.

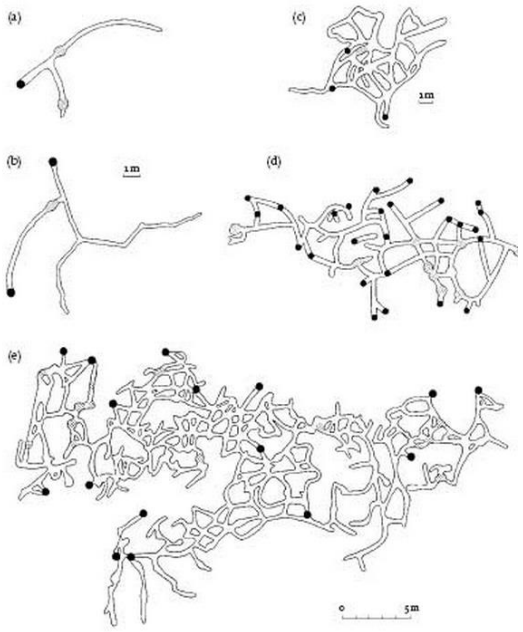

Figure 4.4 Schematization of badgers setts of different size and complexity: outlier setts (a and b), subsidiary sett (d) and main setts (c and e). The entrances are indicated by the filled circles. (Roper, 2010)

After the failure of the Truckee Canal Embankment (Colorado) in 2008, the embankment has been excavated and the grouting, previously inserted, reveals the system underneath (Figure 4.5).
The network of burrows belongs to muskrats, whose system is different from the one excavated by badgers, porcupines and foxes. However the example gives an idea on the complex systems which animals can build in a dike body.

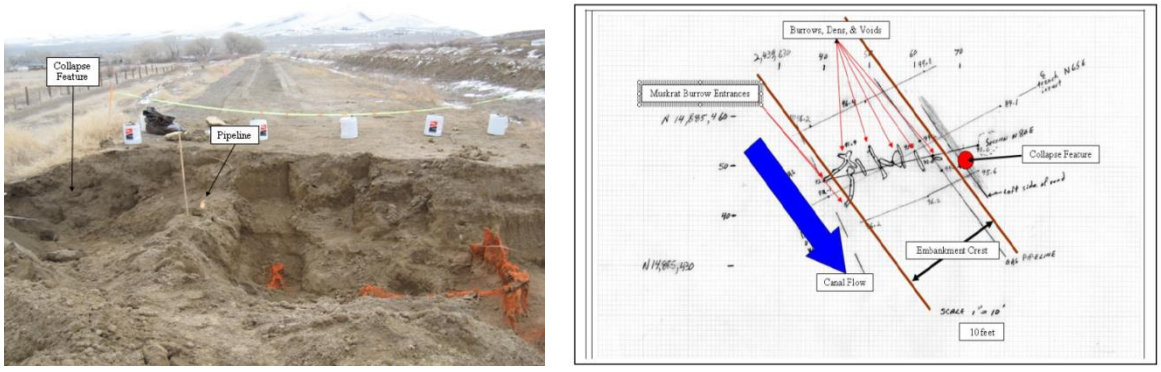

Figure 4.5 View of excavation of Truckee Canal Embankments, where the orange painted grouting reveals the networks of voids and tunnels of muskrats (left) ; their representation in a map (right) (Paul and Slaven, 2009).

4.3.2 The excavated volume

By using data from badger setts in Wytham Woods, Oxfordshire, UK, M.A. Coombes and H. A. Viles developed a model to correlate the population dynamics and the zoogeomorphic activity (Coombes and Viles, 2015). The surface area A (m^2), defined as the “extend of existing mounds and spoil”, can be calculated as:

$$A = 8.7a + 1.0X_{yr} + 15.5c - 7.2u - 20.7 \quad (4.1)$$

where *a* is the minimum number of years for which the sett exists, X_{yr} is the number of excavation years (years of residency of the badgers in the sett), *c* is sett fecundity (number of cubs) and *u* is the number of adults resident in the sett.
The volume *V* (m^3) that has been excavated in the subsurface is correlated to the surface area by Coombes & Viles (2015) and defined as:

$$V = 0.03A - 0.14 \quad (4.2)$$

4.3.3 Geometry

Despite of the complexity of these underground systems, some geometrical patterns do repeat in every sett.

The burrows of badgers are tunnels with semi-circular (arched) or squashed elliptical form, wider than higher(Heptner and Sludskii, 1988). The tunnels have typical height of 0.20 m and are 0.30-0.35 m wide (Nichol et al., 2003).
The nesting chambers have squashed spherical shape with arched roof and their horizontal section is roughly circular (Roper, 2010). The dimensions of the chamber can be wider if more badgers occupy it.

The geometry assumed for the system is summarized in the Table 4.2.

Tunnel	Shape	Semi-circular / squashed ellipse
	Width	0.3 m (0.25-0.35 m)
	Height	0.2 m (0.17-0.25 m)
	Inclination	40-45° downwards
	Depth	0.5-2.5 m (above groundwater level)
	Length	5-10 m
Chamber	Shape	Squashed sphere
	Width	0.57 m (till 1 m)
	Length	0.42 m (till 1 m)
	Height	0.3-0.4 m

Table 4.2 Geometry assumed for the network of animal burrows

As illustrated in the reproduction of a sett in Figure 4.6, at least one entrance of the burrows is higher than the others in order to promote ventilation to the chambers and the entrance tunnels are inclined to ensure drainage.

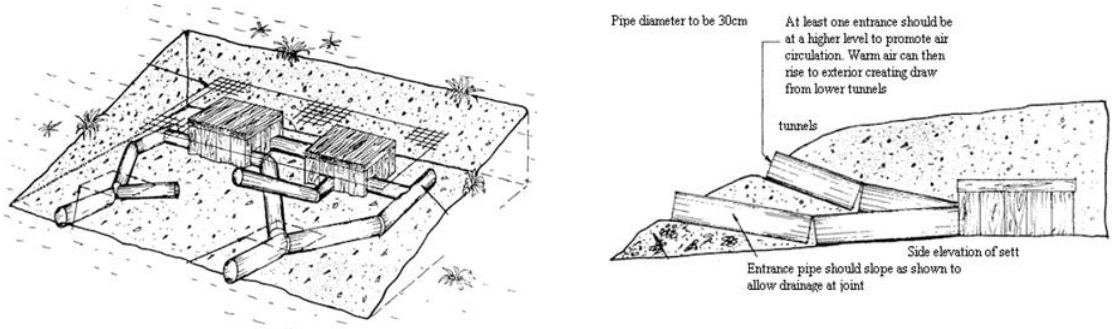

Figure 4.6 Reproduction of badger's sett.

The tunnels usually don't go deeper than 1 meter underneath the entrance and they are located in a dry place above the groundwater level. The tunnels initially go down (with an inclination of 40-45°) but they can also run horizontally. If then the same soil is present, the depth of tunnel systems is approximately constant.

Two tunnels intersect at 90°, while three tunnels at 120°. They can split in separate chambers, which are usually situated at the end of the burrows (5-10 meters from the opening entrance) or the chambers are a widening of the tunnels themselves. The chambers are used for sleeping or rearing the young family members. A family unit has three sleeping chambers, which are isolated from one another or open at both ends. If two chambers are present, the main chamber is occupied by the primary pair and the other by a secondary pair.

The chambers can be situated in levels of different depths creating a complex 3d structure. However, in case of slopes, the entrances are usually located along a horizontal line and the tunnel network can be approximated as 2dimensional.

4.4 Burrows in the section of the breach

4.4.1 The environment of the levee of San Matteo

The levee of San Matteo offers an ideal environment for the diffusion of badgers, porcupines and foxes. Even if little grass was present along the slopes, the vegetation at the inner side of the dike and the isolation of the levee from human presence attract the animals. Few houses are present next to the embankment and the road is around 100meters far from it.

The height of the levee is around 7-8meters, ensuring dry places where to build setts, which are usually not reached by the water level in the river. The soil consisting on silty sand is also an ideal soil where to dig on.

Due to the favourable conditions that this environment offers, more and more animals are building setts along the Secchia river. Their diffusion is a recent phenomenon that the local authorities are dealing with, first with inspections and then with remediation.

Figure 4.7 Vegetation cover of the embankments of the Secchia river

4.4.2 Position of entrances

The Investigative Evaluation Report presents two aerial photos from 2010 and 2012 where entrances of burrows are individuated (Figure 2.11 and Figure 2.12).
By looking at the pictures it is possible to recalculate their location and elevation (Figure 4.8).
The entrances are located almost at the top of the levee, since badgers, porcupines and foxes dig in dry places. Only in rare occasion the water level in the river would cover the entrance placed in the slope at the water side. As a matter of fact, during the night of the 19th January 2014, the water level was around 30cm below it.

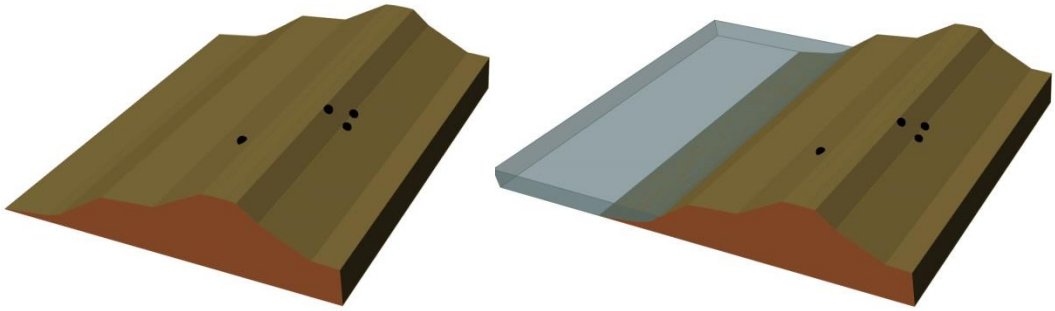

Figure 4.8 Position of animal dens in the dyke body (left) and the water height at 29 m amsl, which is the average water level in the river over the year (right)

4.4.3 Subsurface network

The mean number of entrances is between 7 and 12 for every sett (Byrne et al., 2012). Small setts have 1-6 entrances and the biggest setts recorded in Ireland have between 28 and 60 entrances. The width of the sett is usually very large, with connection of main and annex setts from 50 to 150m.

The system of the levee of San Matteo under analysis has 4 entrances and the maximum distance between them is around 10 meters. Thus, it is reasonable to assume that the entrances belong to the same main sett: the three entrances along the inner slope are linked to the one in the outer slope.

The geometry of the subsurface network is not a-priori known and it can be reasonable assumed. The tunnels, modelled as cylinders with diameter equal to 0.2m, start from the known entrances and go down for 1meter with slope of 45°; then they go horizontally until reaching the centre of the levee. There the tunnels are linked together forming a whole system (Figure 4.9).

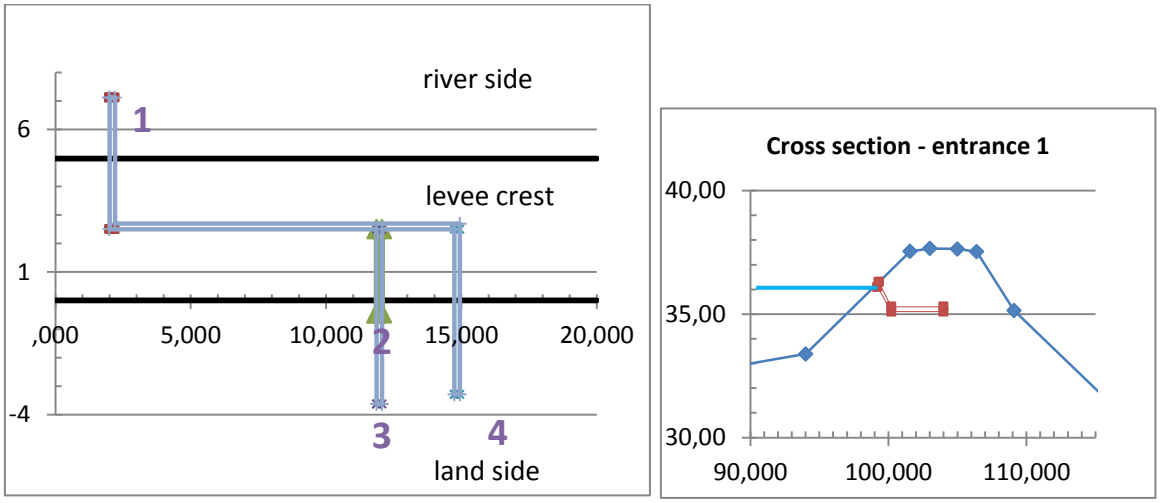

Figure 4.9 On the left: Top view of the assumed network. The black lines indicate the crest of the levee, the numbers indicate the position of the entrances and the blue lines are the tunnels connecting them
On the right: Cross section showing the tunnel at entrance 1.

In the proposed network, the total length of the tunnels is 32 m and the total excavated volume is equal to 1 m^3. For simplicity, the presence of chambers in not considered in the assumed network.

4.4.4 Development of the system between 2012 and 2014

In Figure 2.11 from the Investigative Evaluation Report, only two burrow entrances are recognized in the photo in 2010 while four entrances are individuated in 2012. Thus, the sett develops and enlarges with time with two new entrances in 2012 compared to 2010.
It is then luckily that the system developed also between March 2012, when the four entrances were recorded, and January 2014, when the breach occurred.
Thus, the current paragraph investigates the growth of the system and proposes a scenario for the system in 2014.

The enlargement of the sett is typically a function of several factors, such as the sett age, the size of the social group using the sett, the change in the size of the social group and the soil characteristics (Roper, 2010). By knowing the volume of the network and by defining the number of new entrances and their position, it is possible to reconstruct the internal structure.

First of all, in order to estimate the development of the sub-system, the approach proposed in paragraph 4.22 is used. In Formula (4.1), the excavated volume V in 2012 is known and equal to 1 $m^{3.}$ The sett age *a* and excavation year X_{yr} are assumed being equal to 3 years in 2012. As a matter of fact, entrances were already recorder in 2010, so that the presence of badgers can be assumed starting from 2009, when the excavation took place. Combining formulas (4.1) and (4.2):

$$V_{2012} = 0.03(8.7a + 1.0X_{yr} + 15.5c - 7.2u - 20.7) - 0.14 \qquad (4.3)$$

Knowing V_{2012}, *a* and X_{yr}, it is possible to calculate the unknown: $(15.5c - 7.2u)$.

In 2014, the sett age *a* and the excavation years X_{yr} are equal to 5years. Assuming the sett fecundity *c* and numbers of adults *u* constant and so equal to the situation in 2012, it is possible to calculate, with formula (4.3), the excavated volume in 2014. Finally V_{2014}=1.582 m^3, corresponding to total tunnel length of 50.4 m.

Second, according to Roper (2010), the average growing rate of badger setts is one entrance every two year. For this reason, a new entrance is assumed in the analysis.

Third, the more influent and dangerous position of the entrance, when evaluating its effect in the creation of the breach, is along the outer slope. Since the entrance is assumed to be excavated in 2012, after the photo was taken, the new system should have been not dangerous for the dike stability until 2014 when the dike failed.
A peak of water level in Secchia river was recorder on 05/04/2014 and it was equal to 35.7 m amsl. This level was 30 cm below the one recorded on 19/01/2014 at 6am when the breach took place (paragraph 5.3.3). It is then assumed that the burrow excavated during the last 2years had its entrance between 35.7 and 36 m amsl: the cavity would have not been filled of water in April 2013 but in January 2014.

Finally, the assumed sett present in 2014 consists on a system with one new entrance, placed along the outer slope at 35.7 m amsl. It is connected to the other burrows and the excavated volume is V_{2014}=1.582 m^3 with total tunnel length of 50.4 m. Thus the additional length of the tunnels, compared to the system in 2012, is equal to 18.4 m. In order to satisfy these assumptions, the following network is assumed: the entrance is placed 1.5 meter next to the pre-existing one along the outer slope; the burrow is connected to the other three entrances in the inner slope with a central tunnel of 14 meters, parallel to the one already present in 2012. The network is shown in Figure 4.10.

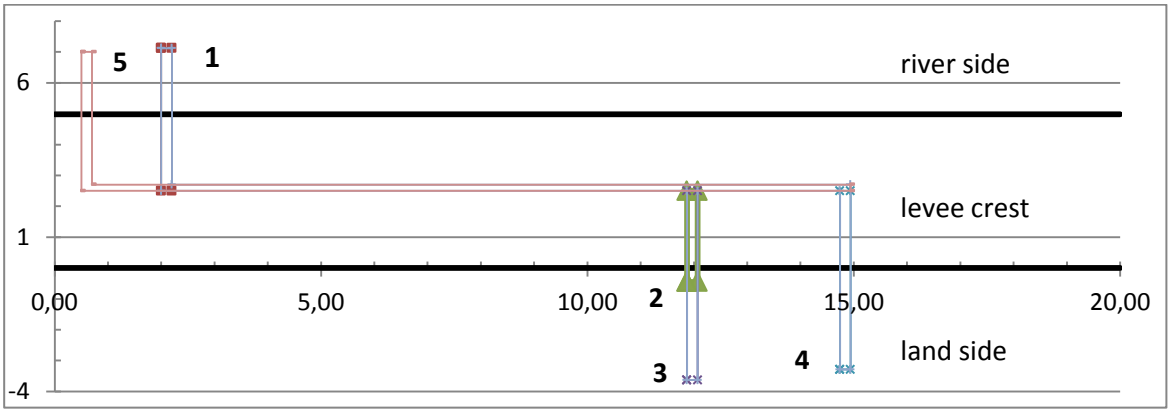

Figure 4.10 Top view of the scenario in 2014.

5 Groundwater flow: initial and boundary conditions

5.1 Introduction to groundwater flow analysis

Groundwater flow analysis is essential when evaluating the stability of a slope. The total stresses are divided into effective stresses and active pore pressures:

$$\underline{\sigma} = \underline{\sigma}' + \underline{m} \cdot p_{active} \qquad (5.1)$$

where $\underline{\sigma}$, $\underline{\sigma}'$ and $\underline{m}$ have been introduced in paragraph 3.2.1, while p_{active} is equal to the water pressure in the saturated case as described in paragraph 5.3.1.
As the pore pressures inside the levee changes due to the applied hydraulic boundary conditions, the effective stresses σ' change as well. The stability of a dike depends on the shear strength τ, which varies with the effective stresses according to Mohr-Coulomb criterion (equation (3.3)).
Thus, when the hydraulic boundary conditions lead to groundwater flow inside the dike body, it is necessary to assess the pore pressures inside the levee body in order to evaluate the stability of the dike.

Numerical methods, such as the Finite Element Method implemented in the software PLAXIS, as further explained in chapter 8, allow a *fully coupled flow-deformation analysis*. The deformations and pore pressures change in time according to time dependent hydraulic boundary conditions (2013b).
A fully coupled flow-deformation analysis considers time dependent boundary conditions, so that changing prescribed water levels and precipitation, the undrained behaviour above the water table and soil permeability are the inputs for the analysis.
The initial and boundary conditions for the analysis are illustrated in the current chapter.

5.2 Initial conditions

5.2.1 Dike profile and soil properties

The profile used for the analysis is illustrated in Figure 5.1. The top of the dike is placed at 37.66 m; underneath the levee body, the unit AES8a extends from 31.55 m amsl till 25.16 m amsl, where the sub-system of Ravenna (AES8) has its upper boundary. The phreatic level is placed at 29 m amsl.

The dike profile is a simplification of the section made by AIPO (Inter-regional agency for Po river) in 2002 in a section located few meters upstream of the breach. The boundaries of the layers and their denomination is the same assumed in the Investigative Evaluation Report: unit A (dike body, in yellow in the figure), unit B (unit AES8a , in orange) and unit C (sub-system AES8, in blue).

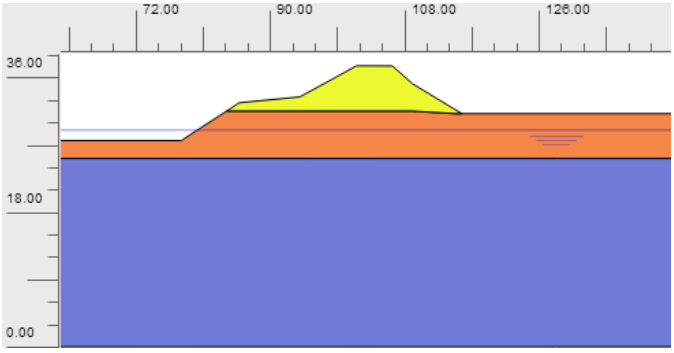

Figure 5.1 Profile used for the PLAXIS calculation.

The soil properties used for the analysis are derived from the data available in the Investigative Evaluation Report, as described in Appendix C, and they are summed up in Table 5.1. Unit B is a silty sand with vertical and horizontal permeability of 0.16 m/day. Unit A, which constitutes the dike body, is a silty sand with flow parameters defined by the van Genuchten-Mualem model for the unsaturated soil, as described in the following paragraph.

Unit	γ_{sat} (kN/m^3)	γ_{unsat} (kN/m^3)	E' (kPa)	μ	c (kPa)	φ' (°)	s_u (kN/m^2)	Sand (%)	Silt (%)	Clay (%)	kx (m/day)	ky (m/day)	e (-)
A	21.7	19.5	78.5E3	0.2-0.3	7	32		-	-	-	1	1	0.8
B	18.8	16.0	48.7 E3	0.2-0.3	7	28.8		26	68	6	0.162	0.162	0.8
C	18.9	16.0	54.2 E3	0.4-0.5			55	1	39	60	10^{-3}	10^{-4}	1

Table 5.1 Input data for Plaxis 2D calculation, using Mohr Coulomb Model.

Finally, both unit A and unit B have drained behaviour, while unit C, which is a clayey layer, has undrained behaviour.

5.2.2 Unsaturated zone: the dike body

The unsaturated zone is defined as the soil zone between the water table and the land surface, where values of water pressure are negative relatively to atmospheric pressure. The height above water table is defined as suction head.

In the so-called *capillary fringe*, situated above the water level until the *air-entry head*, the soil is essentially saturated. Then, above it, the air gradually displaces water from the soil pores so that the water content decreases with the suction head (Lu and Likos, 2004).
This trend is described by the soil-water retention curve, in terms of volumetric volume content versus suction head: the void space occupied by liquid can vary from fully saturated at the top of the capillary fringe to zero.

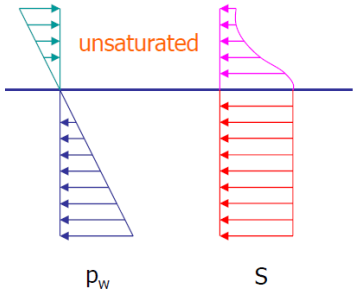

Figure 5.2 Pore suction and saturation in the unsaturated zone.

The permeability coefficient represents “the ease with which a fluid can flow through the pore space” (Pinder and Celia, 2006). Since the saturation corresponds to the ratio of the space available for the fluid over the entire pore volume, the permeability values decrease as a function of saturation. The permeability has its maximum value for saturation of 100% and it decreases not linearly above the water table in the unsaturated zone. The *relative permeability* is the ratio of the actual permeability value over the permeability in the saturated zone. Thus it is equal to 1 in the saturated soil and it decreases in the unsaturated zone.

It is necessary to define the relations between pressure head and saturation and between saturation and permeability in the unsaturated zone.
First of all, the van Genuchten equation defines the relation between pressure head and saturation:

$$S\left(\phi_p\right) = S_r + \frac{\left(S_s - S_r\right)}{\left[1+\left(\alpha\left|\phi_p\right|\right)^n\right]^m} \qquad (5.2)$$

Where S_s (-) is the maximum saturation at the water table, S_r (-)is the residual saturation at the top of the unsaturated zone, ϕ_p (m) is the pressure head, while α (m^{-1}), n (-) and m (-) are parameters that are fit to measured data.

The relation is used to define the Soil Water Retention Curve (Figure 5.3) in terms of relative saturation versus pressure head for the unsaturated soil in the levee of San Matteo, starting from the available data in the report (Appendix C for a further explanation).

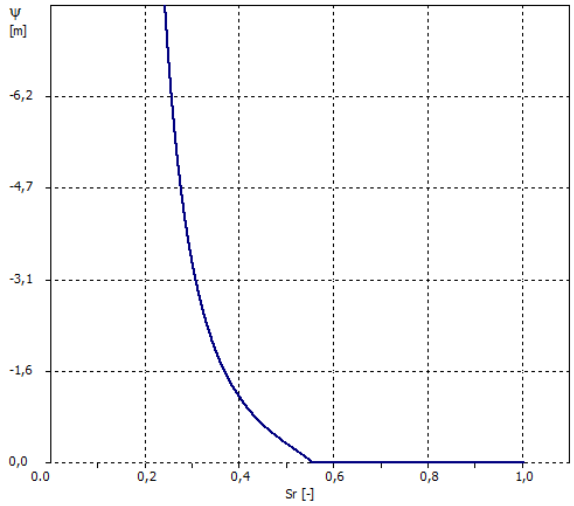

Figure 5.3 Relative saturation [-] versus pressure head [m] for the unsaturated soil of the dike body, defined with the van Genuchten model.

The effective saturation is defined as a normalized measure between the upper and lower limits of saturation S_s and S_r:

$$S_{eff} = \frac{S - S_r}{S_s - S_r} \qquad (5.3)$$

It is now possible to introduce the van Genuchten-Mualem equation which defines the relation between the relative permeability k_r (-) and the saturation:

$$k_r = \left(S_{eff}\right)^{1/2}\left\{1-\left[1-\left(S_{eff}\right)^{1/m}\right]^m\right\}^2 \qquad (5.4)$$

The relative permeability is one for S_{eff}=1 and so it is equal to the value of permeability defined below the water table, while the soil in the unsaturated zone becomes more impermeable as the suction increases.

The relationship between relative permeability k_r (-) and suction head ψ (m) used for the levee of San Matteo is calculated from the data available in the Investigative Evaluation Report (Appendix C) and it is the illustrated in the Figure 5.4.

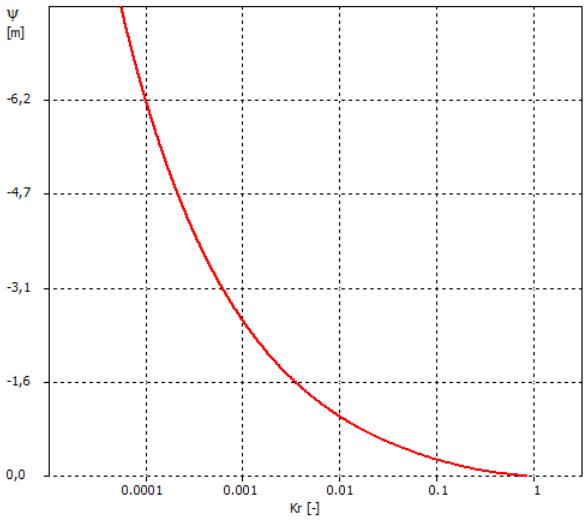

Figure 5.4 Relative permeability [-] versus pressure head [m] for the unsaturated soil of the dike body, defined with the van Genuchten-Mualem model.

By assuming an initial hydrostatic distribution of pore pressures in the unsaturated zone, the high values of suction at the top of the levee would lead to unrealistic low value of permeability. For this reason and by looking at literature review based on similar levees during winter conditions, the Investigative Evaluation Committee assumes in the report an initial pore pressure distribution with minimum value of 40 kPa in the centre of the dike body and water pressure equal to 10 kPa at the top of the levee (paragraph 2.8.3.1). This initial pore pressure distribution is adopted in the current study (Figure 5.5).

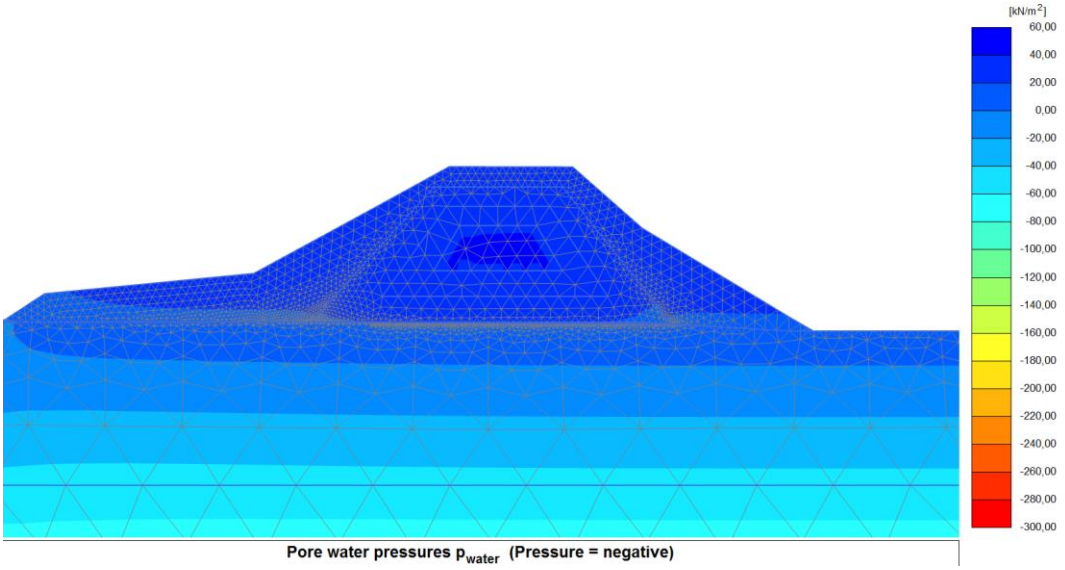

Figure 5.5 Initial pore water pressure distribution assumed for the analysis with PLAXIS 2D.

5.2.3 Animal burrows: properties

The burrows are implemented in the analysis as soil tunnels with unique values of permeability and porosity in all their domain, according to the dual porosity and dual permeability model (Stadler et al., 2011). In order to simulate the void of the burrow and the ease of the water to flow into the cavity, high values of porosity and permeability are implemented. In particular, the porosity is equal to n=0.999 and so the void ratio is $e = \frac{n}{1-n} = 999$. The permeability is 100 times higher than the one of the surrounding soil (k=100m/day) and it is uniform all over the cavity (initial saturated condition).

The stregth parameters are posed equal to the surrounding soil, in order to avoid the local collapse of the soil above the cavity.

5.3 Hydraulic boundary conditions

5.3.1 Groundwater flow analysis

The groundwater flow analysis calculates active pressures which are necessary to obtain the effective stresses and so assess the stability of the dike, as previously described (paragraph 5.1).

The active pressures are defined as effective saturation S_{eff} times the pore water pressure p_{water}:

$$p_{active} = S_{eff} \cdot p_{water} \qquad (5.5)$$

Therefore p_{active} and p_{water} differ when the soil is partially saturated ($S_{eff} < 1$).

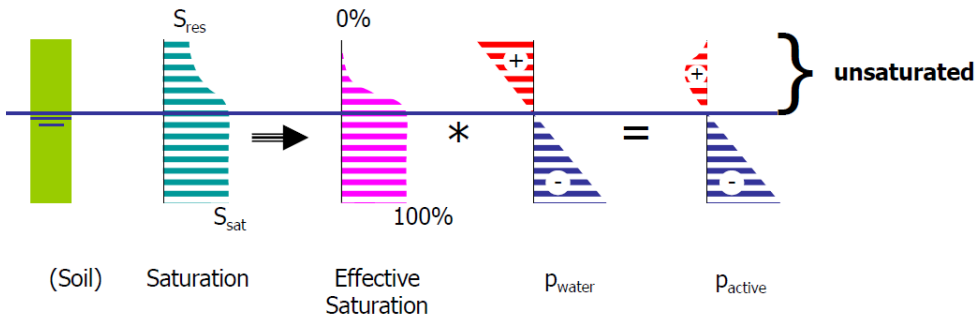

Figure 5.6 Calculation of active pore pressure from effective saturation and water pressures

As a consequence, in the unsaturated zone, the effective stresses are calculated as :

$$\underline{\sigma} = \underline{\sigma}' + \underline{m} \cdot (S_{eff} \cdot p_{water}) \qquad (5.6)$$

The groundwater flow analysis can be steady state or transient flow. The differences in the calculations are here explained.

5.3.1.1 Steady state analysis

The steady state groundwater flow calculation is based on hydrostatic distribution from defined water levels and the pore water pressures are calculated for a steady state condition (for $t \rightarrow \infty$). The steady state solution represents the condition for which the time is not considered.

The analysis is based on defined phreatic level: the pore pressures distribution is hydrostatic and their value is based on water weight and the distance below the water level (Figure 5.7). Therefore no flow and deformation are taken into account in their calculation.

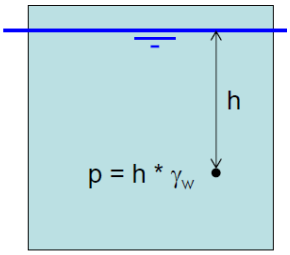

Figure 5.7 Pore pressure calculation in steady state groundwater flow calculation

In the case under analysis, steady state analysis is carried out for water level in the river equal to the maximum reached during the night of the 19th January 2014 at 6am and so equal to 36 m amsl.

5.3.1.2 Transient flow analysis

This type of analysis considers time dependent boundary conditions and the generation of excess pore pressures for undrained behaviour.
The pore water pressures are defined as the sum of steady-state and excess pore pressures:

$$p_{water} = p_{steady-state} + p_{excess} \quad (5.7)$$

The steady-state pressures are determined before the deformation analysis for steady-state condition: the results of the steady state calculation are inputs for the transient flow analysis. Instead, the excess pore pressures are result of deformation calculation and occur as a consequence of stress changes in undrained materials.
The time dependent boundary conditions that are used for the case under analysis, such as rainfall data and water level changing, are presented in the following paragraph.

5.3.2 Time dependent boundary conditions

5.3.2.1 Rainfall

The Investigative Evaluation Report presents a hyetograph of the intensity of rainfall in the section of the breach between 18-01-2014 at 0:00 and 19-01-2014 at 8:00, illustrated in Figure 2.3 and simplified in Figure 5.8. The rain was light during all the day before the failure until 8pm on 18/01/2014, when its intensity increased presenting a peak of heavy rain during the night of the 19th January. Around 2am the intensity decreased and moderate rain was present at 6am when the failure took place.

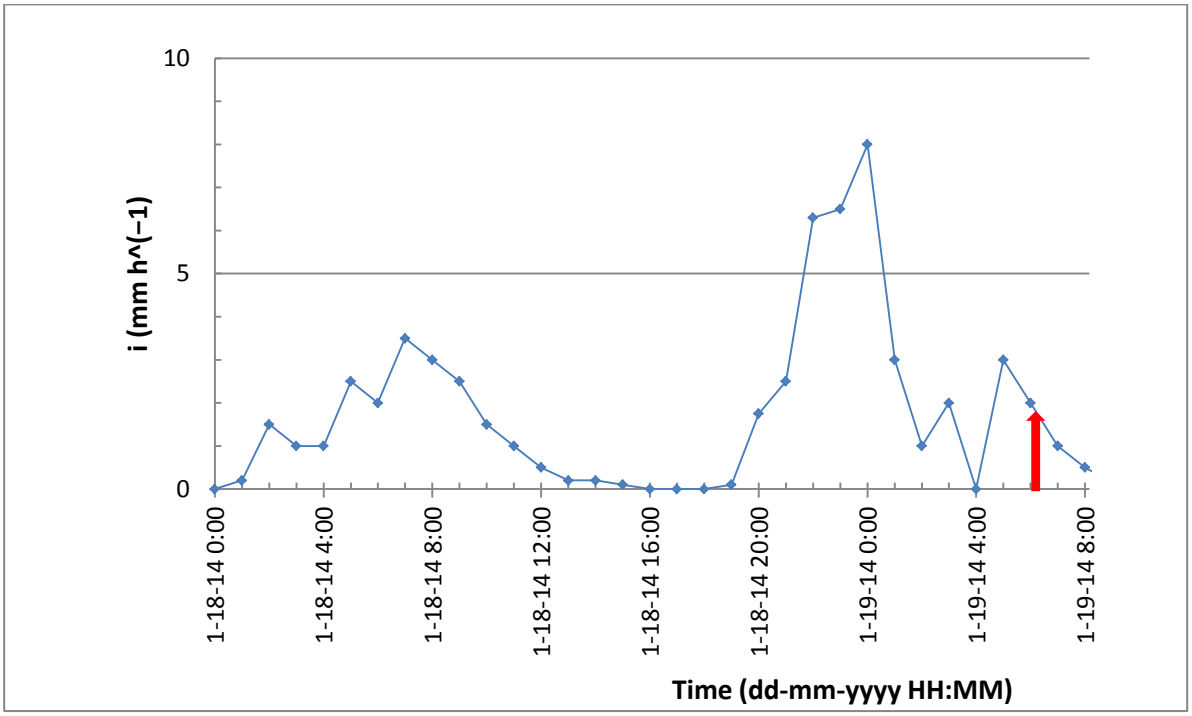

Figure 5.8 Hyetograph of the intensity of rainfall between 18-01-2014 at 0:00 and 20-01-2014 at 0:00 in the section of the breach used in the current study, that is a simplification of the hyetograph given by the report.

Continuous rainfall data are also made available by ARPA-SIM (Servizio IdroMeteorologico dell'ARPA dell'Emilia-Romagna) for a section located 1.2 km from the section of the breach (Lon. 10.956703 Lat. 44.702144, with World Geodetic System - WGS 84). When compared with those elaborated in the report, a shift in time and a lower trend of the former can be recognized: the difference in the measurements can be justified by the fact that the measurements refer to tow different sections.

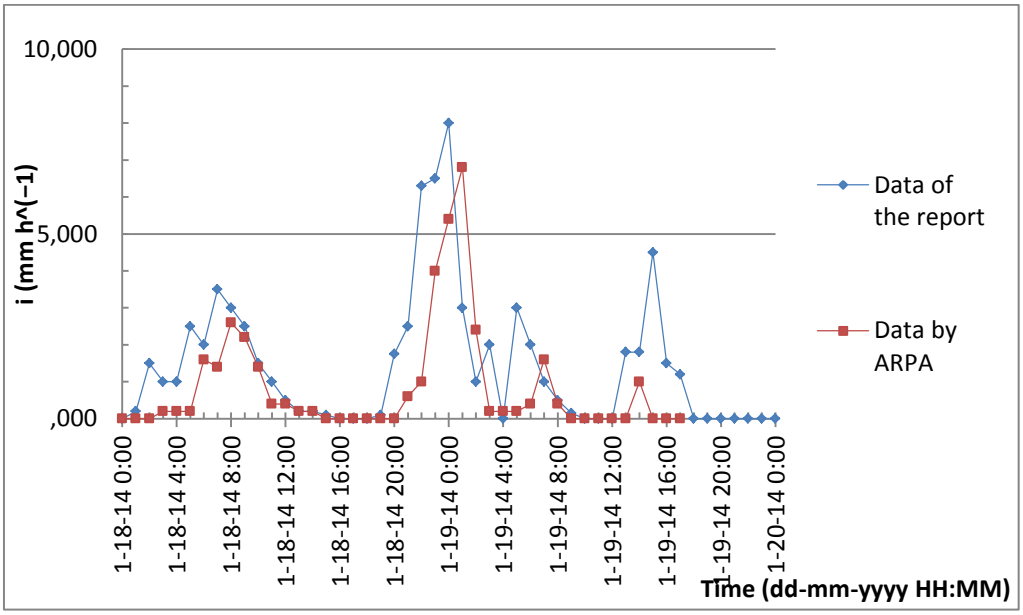

Figure 5.9 Comparison of data in the report and given by the ARPA service between 18-01-2014 at 0:00 and 20-01-2014 at 0:00.

In order to reproduce the scenario which caused the failure, the data of the Investigative Evaluation Report are used as input for the analyses of the current study.

5.3.2.2 Water level changing

The models in the Investigative Evaluation Report with simulation time between 15-01-2014 and 27-01-2014 present a minimum water level of 29 m amsl on 17th January 2014. Then, the water level rose during the afternoon of the 17th January 2014 until reaching its peak after the moment of the breach. At 6.00am on 19/01/2014, when failure took place, the water level in the river was equal to 36 m amsl, that is 1.50meter below the levee crest (Figure 5.10).

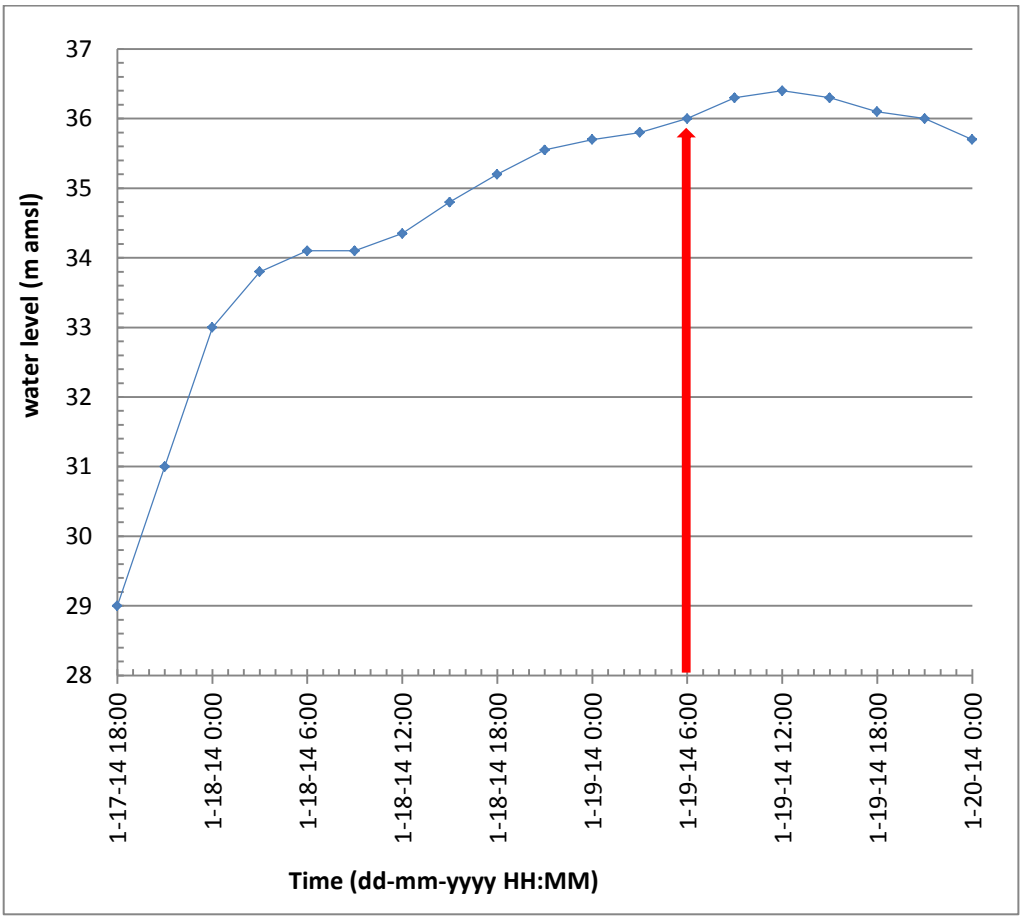

Figure 5.10 Water level in the river between 17-01-2014 at 18:00 and 20-01-2014 at 0:00 in the section of the breach for the current study and obtained by the elaborations of the several models present in the report. The water level after 19-01-2014 at 6:00 considers no failure occurrence.

Figure 5.11 illustrates the water level in Secchia river during January 2014 for a section located 7km upstream of the breach (Coordinates with the World Geodetic System - WGS 84 in Decimal Degrees (DD): Lon. 10.899344 Lat. 44.669669), with data provided by ARPA.

The minimum value was equal to 26.4 m amsl, while peaks are recorded after the rain on 05/01/14 and on the 18th of January. The rise of water level before the failure was imminent, so that steady state condition doesn't realistically represent the hydraulic boundary conditions.

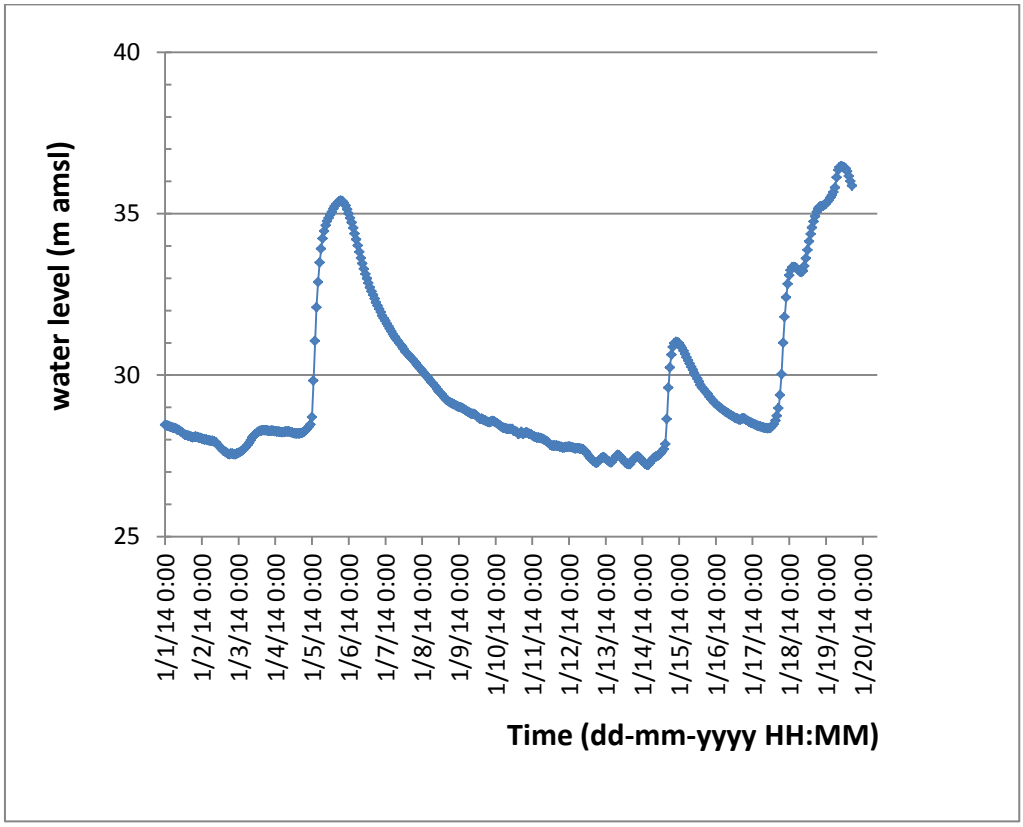

Figure 5.11 Water levels in Secchia river by ARPA service between 1-01-2014 at 0:00 and 20-01-2014 at 14:00 in the location with Lon. 10.899344 Lat. 44.669669 (with World Geodetic System - WGS 84).

In order to validate the data by ARPA, they are compared to the ones from the Investigative Evaluation Report. Since the first are measured from a section localized 7km upstream of the breach, they are shifted in time with approximately one hour of delay in order to fit the data in the report. It is then possible to calculate the average velocity in the river equal to v = 7 km/h =1.94 m/s.

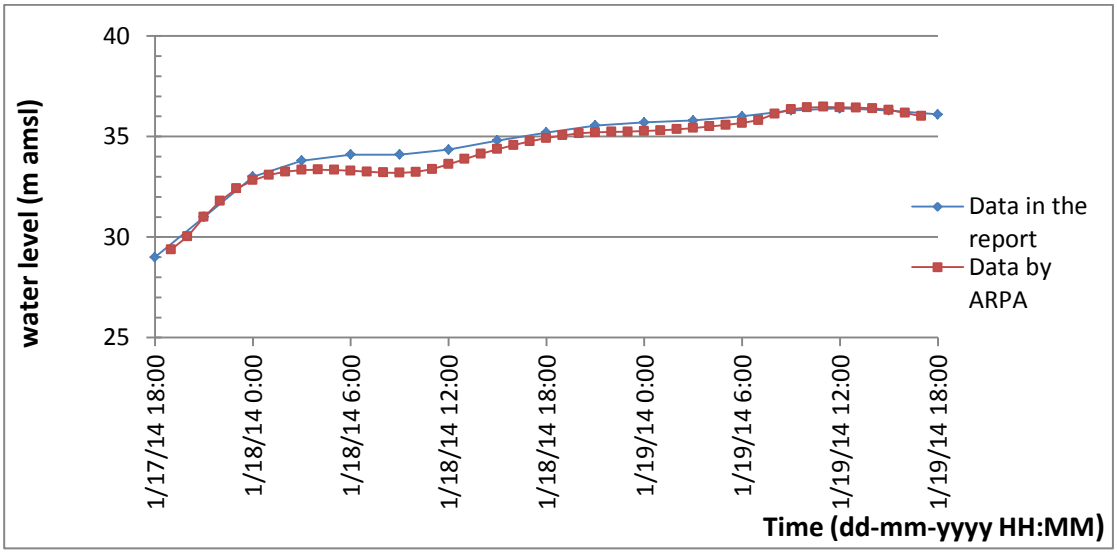

Figure 5.12 Comparison of data in the report and given by the ARPA service between 17-01-2014 at 18:00 and 19-01-2014 at 18:00.

5.3.2.3 Wave height

The maximum water level in the river at 36 m amsl is below the entrance of the burrow recorded by the photo in 2012 at the outer slope (at 36.30m amsl, Figure 2.12). However the waves could have made it possible for the water to directly flow into the cavity. In the same way, waves, if very high, could have caused the overtopping of the levee.

In order to study their influence, the method of Sverdrup-Munk-Brettschneider is used (Sorensen, 1993). By knowing the water depth *h* (m), the length *F* (m) over which the wind is effective and the wind velocity u_w (m/s), it is possible to calculate the wave height H_s (m):

$$H_s = \frac{u_w^2}{g} 0.283 \tanh\left[0.578\left(\frac{gh}{u_w^2}\right)^{0.75}\right] \tanh\left[\frac{0.0125\left(\frac{gF}{u_w^2}\right)^{0.42}}{\tanh\left[0.578\left(\frac{gh}{u_w^2}\right)^{0.75}\right]}\right] \qquad (5.8)$$

The water depth used as input data is *h = 10 m*, that corresponds to the maximum level reached before the breach, calculated from the river bed. The wind velocity is $u_w = 2\, m/s$, which was registered by the ARPA data and corresponds to light air. The analyzed length is *F = 75 m*, which corresponds to the minimum distance between the crests of dikes at the rigth and left hand side of the river.

The resulting weight height is H_s =0.01 m: the river presents ripples without crests, which don't raise the water level significantly and can be neglected in the analysis.

5.3.3 Considerations upon water level in the river and rainfall

In order to gain a better insight on the particularity of water level and rainfall leading to the breach, it is necessary to compare the data during the days before the event with values recorded in a large period of time.

Figure 5.13 presents a hyetograph with rainfall data from 1st January 2013 to 19th January 2014 (source: ARPA). The values during the event were not the highest recorded during the year more frequent precipitation was registered in March 2013.

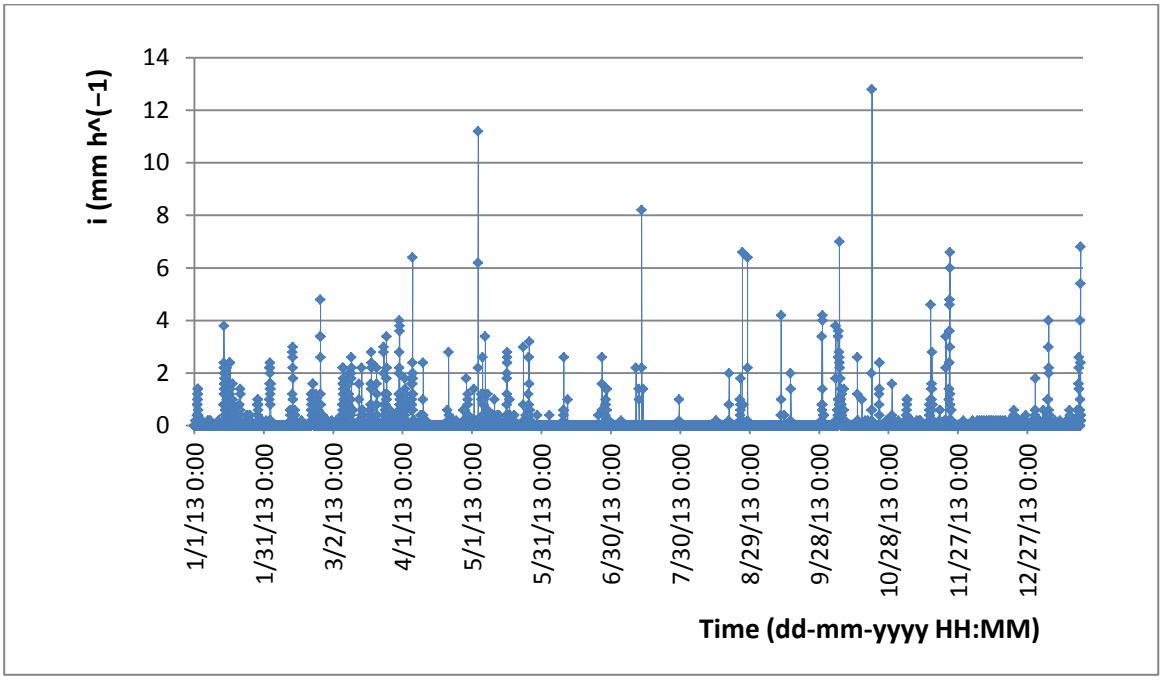

Figure 5.13 Hyetograph of the intensity of rainfall between 1-01-2013 at 0:00 and 20-01-2014 at 0:00 by ARPA-SIM for the location Lon. 10.956703 Lat. 44.702144 (World Geodetic System - WGS 84), that is 1.2 km from the section of the breach.

Also the water levels in Secchia river registered from 1st January 2013 to 19th January 2014 (Figure 5.14) reveal that the values recorded before the failure were not anomalous. As a matter of fact, just few months before the breach, on 05/04/14, the water level had a peak equal to 35.7 m amsl, that is 30cm below the maximum water level at 6:00 at the moment of the breach.

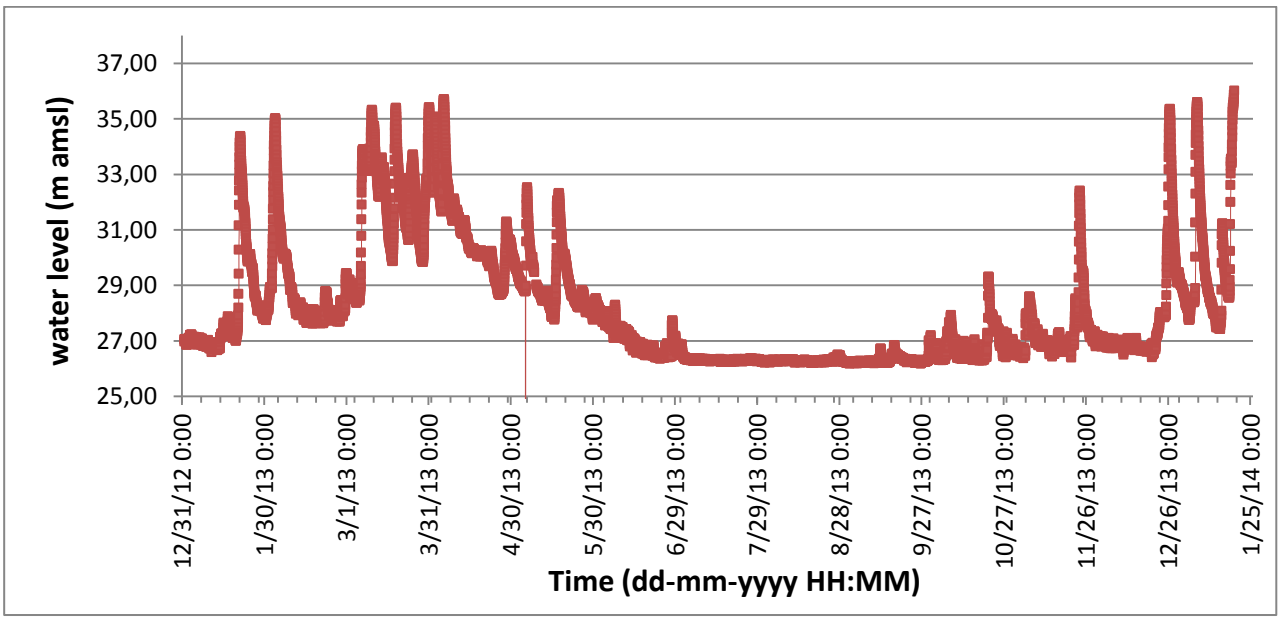

Figure 5.14 Water levels in Secchia river by ARPA service between 1-01-2013 at 0:00 and 20-01-2014 at 14:00 in the location with Lon. 10.899344 Lat. 44.669669 (World Geodetic System - WGS 84), that is 7 km upstream of the section of the breach.

As a conclusion, the values of river water level and rainfall leading to the failure were not exceptional, compared to other events during the previous year.
However, the peaks of rainfall and high water level in the river occurred at the same time during the night of 19th January 2014 and this is a particularity of these data compared to the other events during 2013. As a matter of fact, during the other peak events over the year, the interval between the heavy rain and the peak of water flow in the river varied between 6 and 10 hours. The rain usually occurs upstream in higher altitudes and then, after few hours, the peak of water arrives downstream. Instead, during the night when the breach occurred, the rain hit directly the levee when also the river had a high water level.

Moreover, the breach occurred when the water in the river was not at its maximum level yet and the peak that came after didn't cause other breaches along the levee. This observation confirms the hypothesis of a localized weak area along the dike where failure eventually occurred.

Finally, the water level at 6am on 19th January 2014 was at 36 m amsl, that is 30 cm below the entrance of the burrow at the outer slope reported in the Italian study. This aspect will be further analysed in the following chapters.

6 Two dimensional analysis

6.1 Introduction

The current chapter describes the groundwater flow analyses performed with PLAXIS 2D. Once the initial conditions are implemented, the steady state calculation is performed. After it, transient groundwater flow analyses are carried out, first without and then with animal burrows. As a matter of fact, through groundwater flow analyses, it is possible to investigate the influence of animal burrows to the pore water pressures distribution inside the levee and therefore get an insight about the possible failure mechanism that led to the breach of San Matteo, such as previously described in chapter 3.

PLAXIS is a finite element computer program used to perform deformation and stability analyses for several geotechnical applications.
The program is chosen to investigate the case study in order to analyse the groundwater flow while implementing transient boundary conditions. Moreover PLAXIS allows performing three dimensional analyses (chapter 7) and the Finite Element Method is preferred to the Limit Equilibrium Method for the assessment of the stability of the dike (chapter 8).

6.2 Profile: dimension and mesh

The model used for the analysis is 143 meters wide and 38 meters high: high dimensions ensure no influence of the boundaries in the results. The soil profile is constituted by three layers: unit A (dike body), unit B and unit C (paragraph 5.2.1).

Coordinates boundary	Values (meters)
Min_x	57,0
Min_y	0,00
Max_x	200,0
Max_y	38,00

Table 6.1 Model dimensions for 3d analysis.

The used mesh in the Finite Element Method is fine. In particular, it is coarser in the lower layer while it refines closer to the levee. The top part of the dike is very fine, since only a fine mesh allows the infiltration of rainfall. The mesh has 4975 elements and 10212 nodes, with average element size of 1meter. When burrows are introduced in the levee body, the mesh is further refined in the dike core.

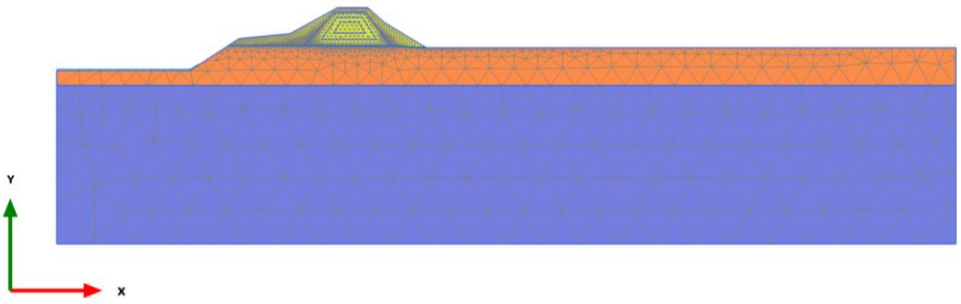

Figure 6.1 Model dimension and mesh used for PLAXIS 2D.

The vertical boundaries are “open” for the groundwater flow while the bottom horizontal boundary is “closed” to simulate an impermeable layer underneath. Referring to the deformations, full fixity is

imposed at the base of the geometry, while vertical but not horizontal displacement is allowed along the vertical boundaries.

6.3 Initial Condition

In the initial conditions the phreatic line is placed at 29 m amsl. The initial pore water pressures are manually implemented by the user as suggested in the Investigative Evaluation Report(paragraphs 2.8.3.1 and 5.2.2): they are null along the phreatic line, while their distribution is hydrostatic below it. In the unsaturated zone, their value increases until the maximum of 40 kPa (positive value indicating suction) in the centre of the dike body while the water pressures at the surface are equal to 10 kPa. The initial stresses are automatically determined by Plaxis.

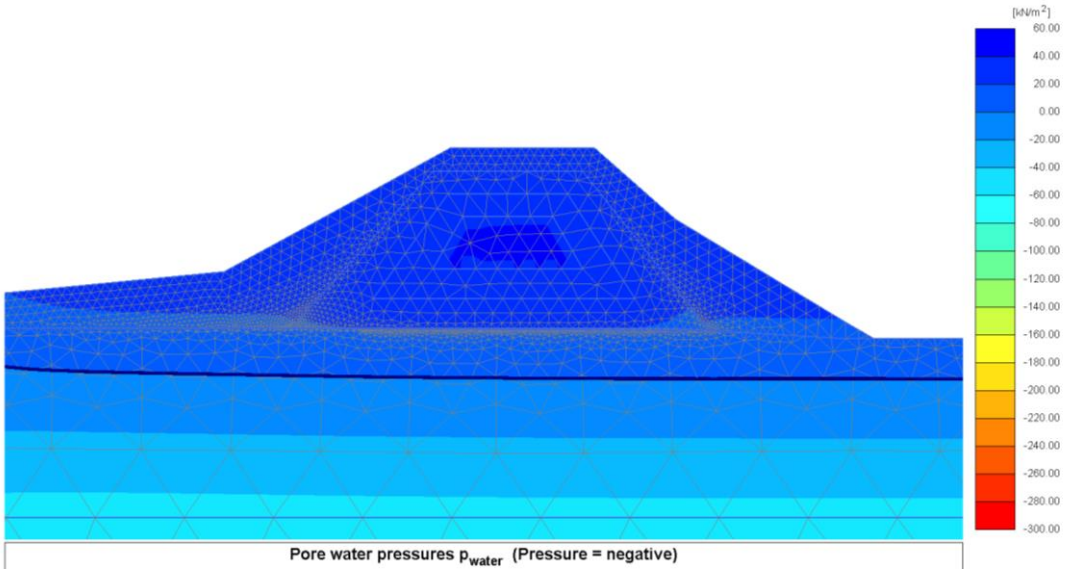

Figure 6.2 Initial water pressure distribution assumed for the simulation on 01-01-2014

6.4 Steady state

6.4.1 Introduction

The steady state solution represents the condition for which time is not considered (Paragraph 5.3.1). The water level in the river is equal to the maximum reached during the night of the 19th January 2014 at 6am and so equal to 36 m amsl. On the inner side the phreatic line is placed at 29 m amsl. Non-flow conditions are assumed along the lower horizontal boundary, while free flow is applied at the vertical boundaries.

6.4.2 Results

Figure 6.3 illustrates the pore water pressure distribution given by the steady state analysis.

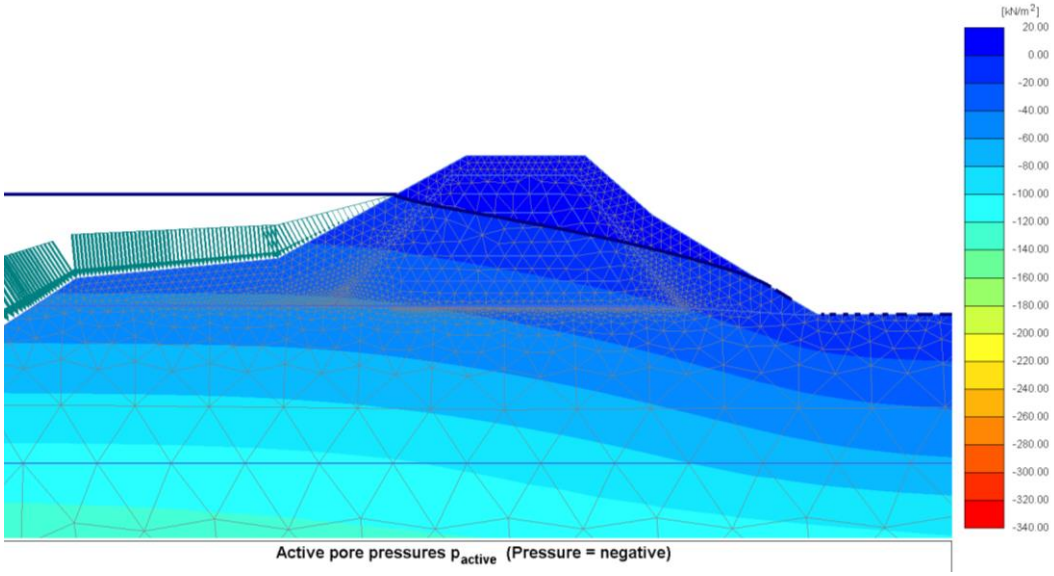

Figure 6.3 Pore water pressure distribution for steady state solution with water level at 36 m amsl

The water table crosses the levee body and it exits in a point placed 1.5 meter above the inner toe of the dike. The iso-pressure lines are almost parallel to the water level in the levee: the infinite time given to their development allows their homogeneous distribution.
The validity of the steady state analysis is confirmed in the results by the fact that the pore pressures coincide with the steady state water pressure, while the excessive pore pressures, which would result from the short-term undrained behaviour, are null.

Figure 6.4 shows the profile of groundwater head ϕ (m):

$$\phi = \psi + z \qquad (6.1)$$

where ψ (m) is the pressure head $\psi = \frac{p}{\rho g}$ (p is the pressure, ρ the water density and g the gravitational acceleration) and z (m) is the elevation. The equipotential lines connect points with same piezometric head: the flow direction is normal to these lines. Therefore water flows from the outer to the inner side while no concentration of flow is visible next to the inner toe.

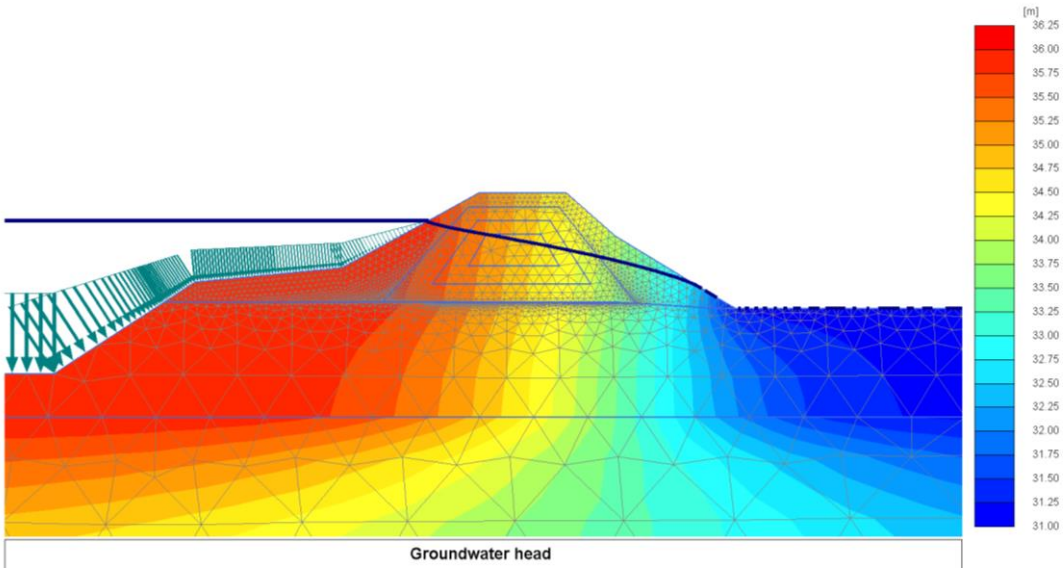

Figure 6.4 Groundwater head for steady state solution with water level at 36 m amsl

Figure 6.5 shows the profile of the effective saturation (formula (5.3)). Its value is one below the water table, where it is equal to the saturation value S_s, which is an input parameter of the van Genuchten model used in the dike core. The permeability depends on the effective saturation (formula (5.4)) and it has its maximum value in the saturated case where $S_{eff} = 1$.

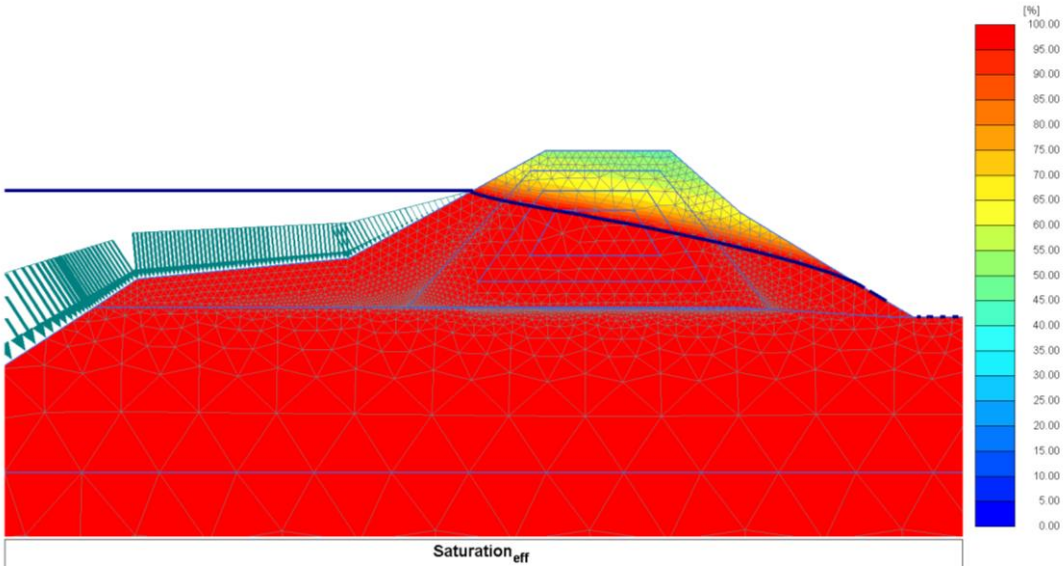

Figure 6.5 Saturation profile for the steady state analysis

6.5 Transient flow

6.5.1 Introduction

The transient flow analysis is more complex and requires more computational time than the steady state calculation. However it is suitable for the current case study, which depends on the infiltration of water due to rain and changing water level in the river (paragraph 5.3).

The river water level and precipitation are the applied boundary conditions to the analysis as a function of time. The changing water level is implemented for a simulation time of 3.25 days, from 16/01/2014 at 0:00 till 19/01/2014 at 6:00, with data recorded every 3hours. By comparing the results with inputs for a longer period (19 days, starting from 01/01/14), the similarity of the outputs justify the use of shorter simulation time for which shorter computation time is also required.
Hourly rainfall data are instead implemented for 1.25 days, from 18/01/2014 at 0:00 to 19/01/2014 at 6:00, that is the time when the rain contribution is significant.
The data used have been previously introduced in paragraph 5.3.2.

6.5.2 Results

Figure 6.6 shows the pore pressure distribution at the last stage of the transient groundwater flow analysis. The resulting water table is lower than the phreatic line of the steady state solution (in blue in the figure). As a matter of fact, more time is required for the pore water pressures inside the levee body to rise and to finally reach the steady state solution.

At the inner side, the phreatic line exits at the toe of the dike due to the presence of water at the surface because of the intense rain.

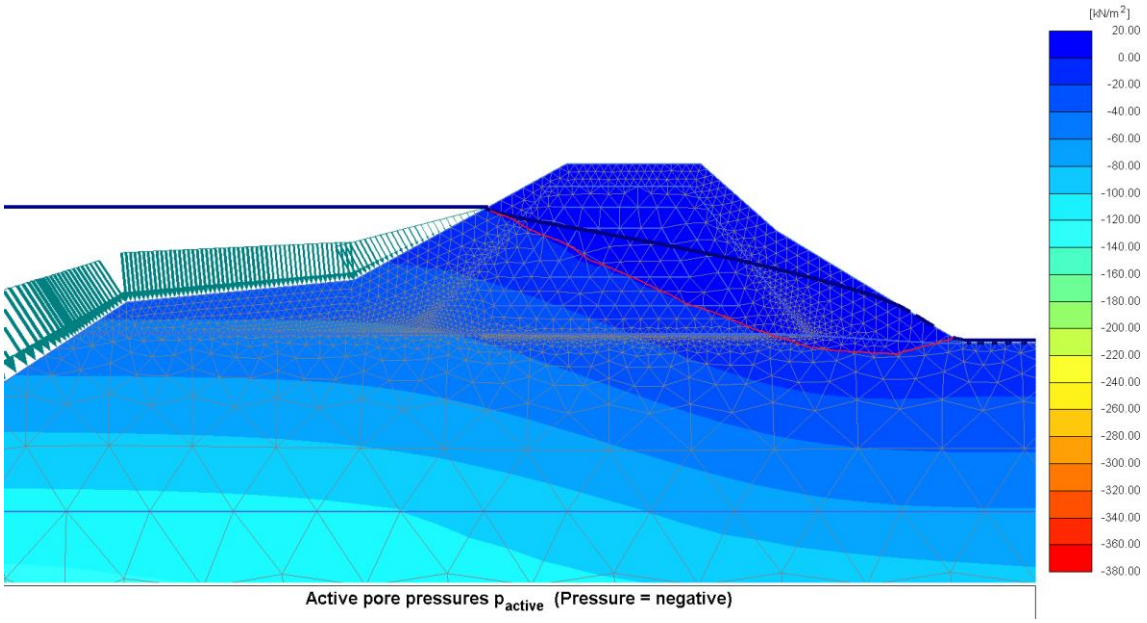

Figure 6.6 Pore water pressure distribution for transient flow analysis. The phreatic of the steady state solution is indicated by the thick blue line with the water table at the end the transient flow analysis is indicated by the red line.

The development of pore water pressure is analysed for point B, posed at 36m amsl along the slope (Figure 6.7). The point is chosen as indicative because its altitude is the same of the water level when failure occurs.

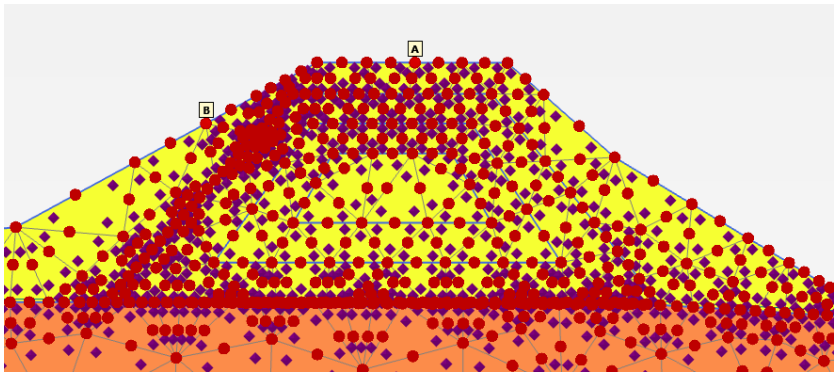

Figure 6.7 Chosen nodes for the analysis of results

Figure 6.8 shows a rapid increase of pore water pressure in point B on 18/01/2014 at 0:00. Due to the fast rise of water level in the river, the pore water pressures jump from negative values (positive values indicate suction) to value close to zero. The rapid change in water pressure causes the equal sudden decrease of effective stresses, according to Terzaghi's law (equation (3.1)).

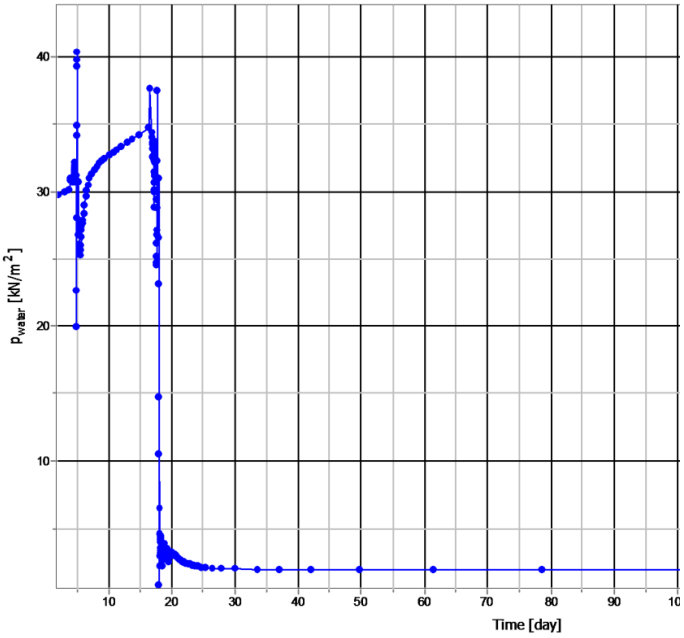

Figure 6.8 Pore water pressure p_{water}(kN/m^2) of node B versus Time (day). The values of pore pressures are reported in their absolute values.

Figure 6.9 shows the saturation profile. The soil underneath the water table is saturated, such as the top part of the levee, due to the infiltration of rain. There the relative permeability is one, according to the van-Genuchten model.

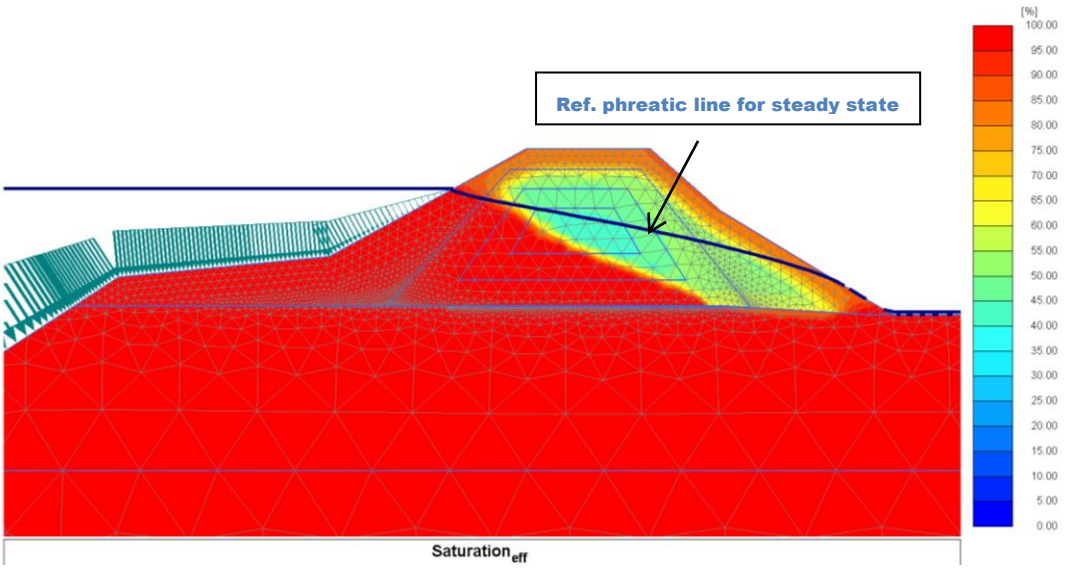

Figure 6.9 Saturation profile for the transient flow analysis. The line indicates the reference phreatic line obtained with the steady state analysis.

6.6 Animal burrows

6.6.1 Introduction

The current paragraph investigates the influence of the burrows to the groundwater flow in order to later assess their contribution to the failure of the levee of San Matteo.

The burrows can be simplified as cylinders with diameter of 0.2m and higher permeability and porosity (paragraph 5.2.3). In the following calculations, the 3d nature of the animal burrows is taken into account in the 2d analysis by means of a reduction factor for the unit weight of soil (Armitage, 1999). The reduction factor is equal to the percentage area occupied by the burrow.
Considering a slice of soil 1m wide and 2r high (Figure 6.10), the burrow with radius r occupies an area equal to πr^2. The percentage area is then ($\pi r/2 \cdot 100$) and, for the assumed diameter of 20 cm, the reduction factor is 15.7 %.

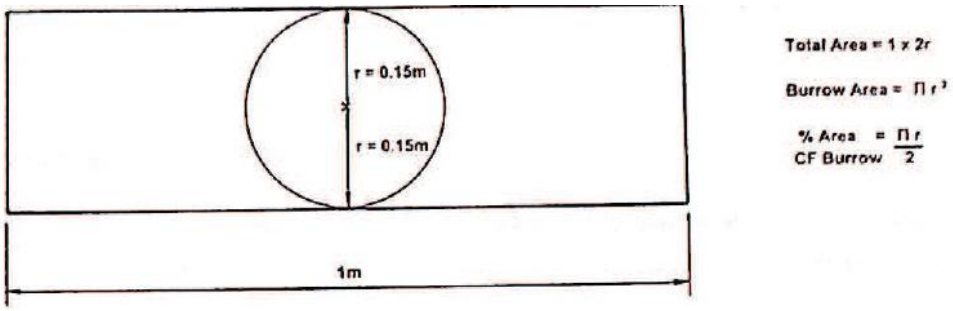

Figure 6.10 Slice of soil considered for calculating the reduction factor(Armitage, 1999)

Also the network of tunnels and chambers is a three dimensional system, while the only section which can be realistically implemented in a two dimensional analysis, without the need of simplifications, is represented in Figure 6.11. It is a cross section of the tunnel which longitudinally crosses the embankment for around 10 meters and links the entrances at the inner and outer slopes forming a whole connected network.

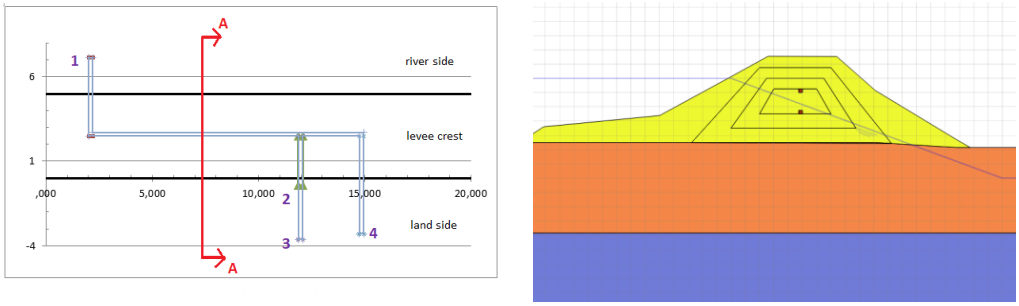

Figure 6.11 Section A-A of the levee (left) and its implementation in PLAXIS (right)

However, the two dimensional calculation reveals that the tunnels have hardly any influence in the groundwater flow. As a matter of fact, their possible contribution to the breach is caused by the fact that they link the entrances from the outer to the inner slope, thus acting as free channels transporting water. For this reason, their contribution to the breach has to be further analysed in a three dimensional analysis.

Several sections and scenarios, explained at the beginning of every analysis, are implemented in the following calculations. For a broader description of the burrowing network, please look at paragraph 4.3.
Moreover, attention is given to the results of transient flow analyses rather than the steady state solution, which will be just briefly introduced.

6.6.2 Burrow at the outer slope

The first analysis considers the burrow at the outer slope which was documented in the photography of 2012 of the Investigative Evaluation Report. Figure 6.12 illustrates the analysed cross section. The entrance of the tunnel is located at 36.3 m amsl, i.e. 30cm above the maximum water level in the river. The tunnel initially goes down for 1meter with slope of 45° and then horizontally until reaching the centre of the levee (Figure 6.12).

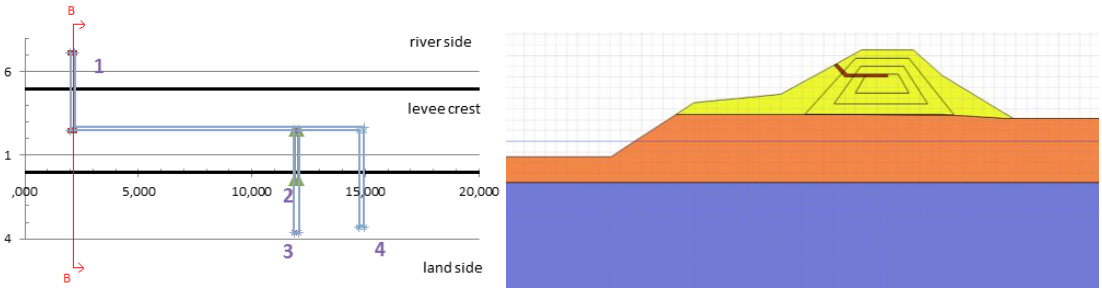

Figure 6.12 On the left: Top view of the assumed network. The black lines indicate the crest of the levee, the numbers indicate the position of the entrances and the blue lines are the tunnels connecting them. On the right: cross section B-B of burrow at the outer slope in PLAXIS.

The resulting water pressure distribution shows the influence of burrow at the outer slope for the steady state solution: the water table is horizontal and deviated by the burrow (blue line in Figure 6.13), so that the cavity acts as a preferential path which intercepts the phreatic line.
Instead, at the end of the transient flow analysis, the water table remains below the animal burrow and it is slightly influenced by it. The burrow doesn't have a significant influence on the values and distribution of active pore pressure: the relative low permeability of the soil of the dike doesn't allow the rise of pore pressure till the burrow in the considered simulation time. The pore pressure distribution is

similar to the case without any burrow (Figure 6.6) and the water level rises and exits at the inner toe due to rain.

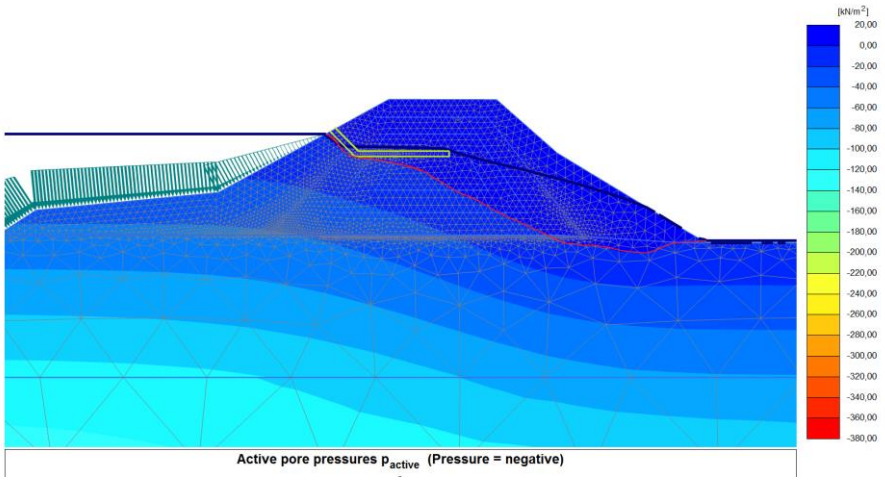

Figure 6.13 Active pore pressure distribution at the end of the transient flow analysis with animal burrow at the outer slope. The water table at the end of the analysis is the red line, while the phreatic line of the steady state solution is the blue line. The contours of the animal burrow are in green.

The saturation profile (Figure 6.14) is influenced by the animal burrow and so, as a consequence, also the values of permeability. The cavity is fully saturated as input for the analysis.

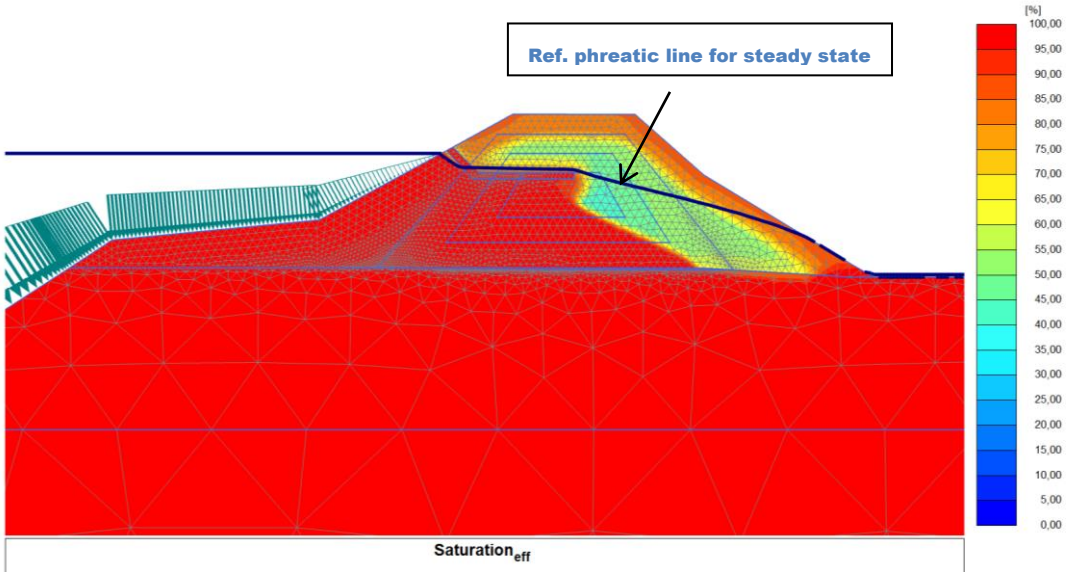

Figure 6.14 Effective saturation at the end of the transient flow analysis with animal burrow at the outer slope.

6.6.3 Burrow at the inner slope

Among the four entrances of animal burrows recorded in 2012, three are placed along the inner slope (entrances 2, 3 and 4 in Figure 6.15). The influence of the burrows in the land side is now investigated with a simplified straight geometry starting from the assumed central tunnel is used for the analysis (Figure 6.15).

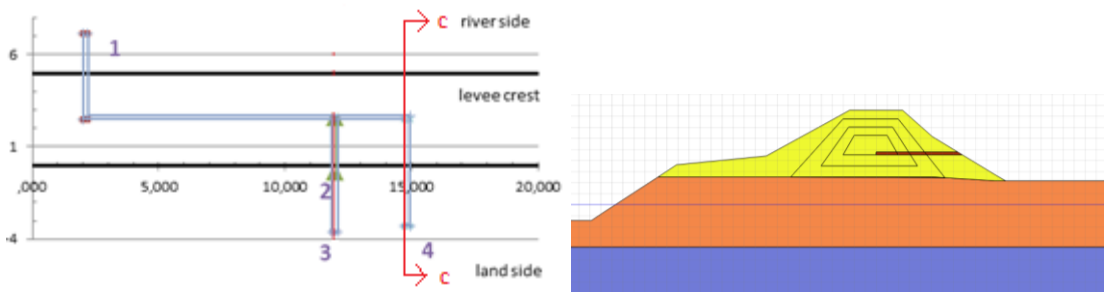

Figure 6.15 On the left: Top view of the assumed network. The black lines indicate the crest of the levee, the numbers indicate the position of the entrances and the blue lines are the tunnels connecting them. On the right: cross section C-C of burrow at the inner slope in PLAXIS.

The phreatic line at steady state is intercepted by the burrow at the inner slope (blue line in Figure 6.16). The cavity creates a preferential path for the phreatic line and shortens the seepage length.

The presence of the burrow at the inner slope is less relevant for the groundwater flow in the transient analysis. The pore pressure distribution when considering its presence (Figure 6.16) is very similar to the one without any burrow.

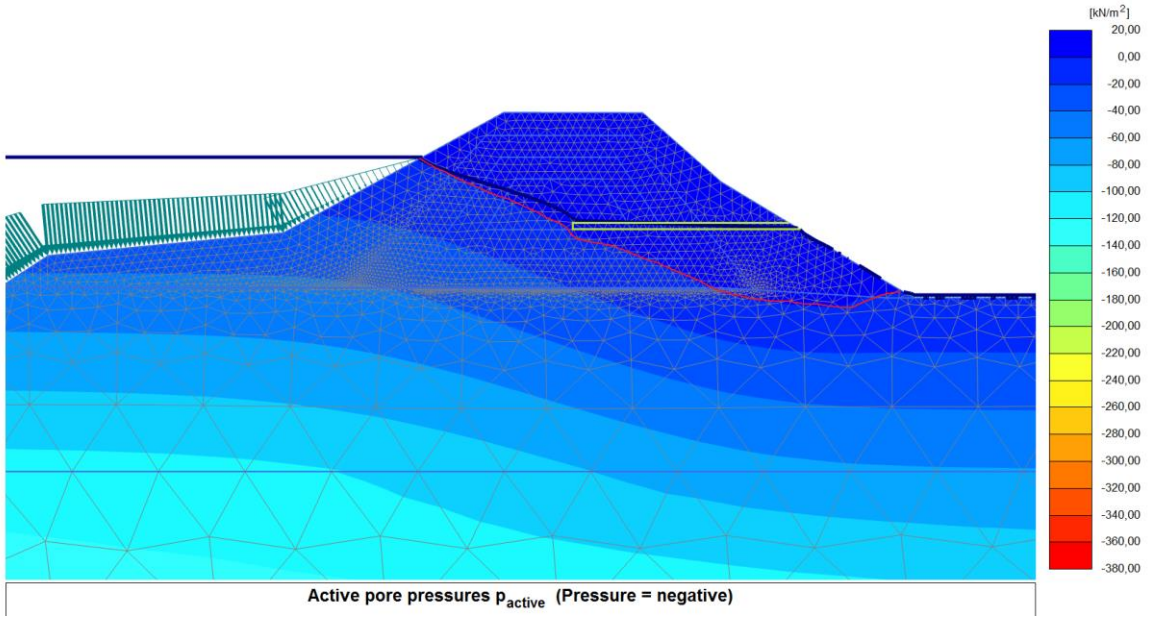

Figure 6.16 Pore pressure distribution at the end of the transient flow analysis with animal burrow at the inner slope. The water table is in red, while the phreatic line of the steady state solution is the blue line. The contours of the animal burrow are in green.

The saturation profile is also not affected by the burrow (Figure 6.17); the tunnel is fully saturated, as defined by initial condition.

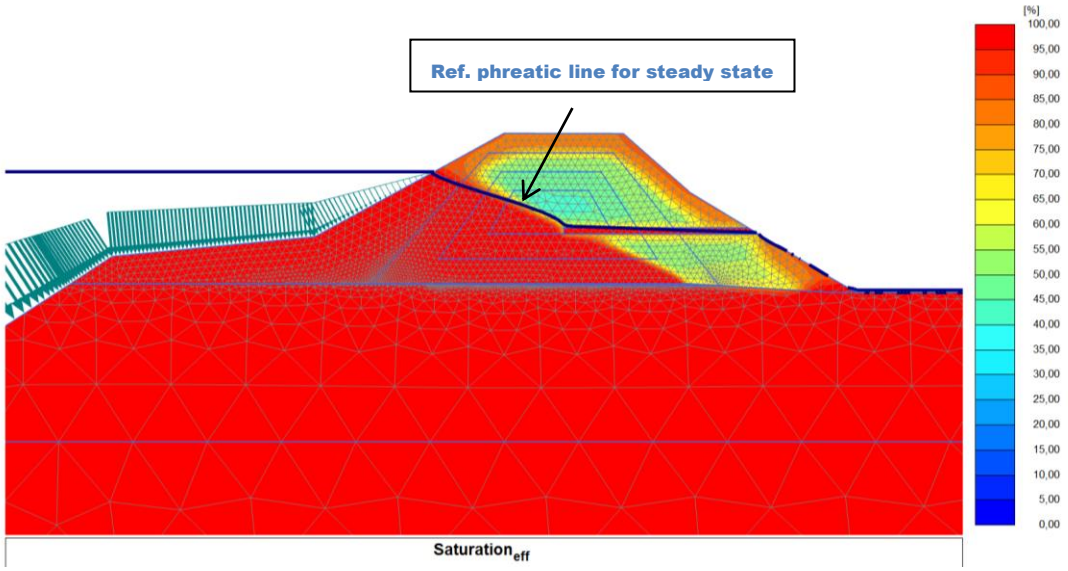

Figure 6.17 Effective saturation at the end of the transient flow analysis with animal burrow at the inner slope.

6.6.4 Burrowing system in 2014

The Investigative Evaluation Report presents burrow entrances recorded in 2012. However it is likely that the system developed in time between 2012 and 2014, when the breach occurred (paragraph 4.4.4).

The assumed network in 2014 was introduced in paragraph 4.3.4: it has two entrances at the outer slope, three entrances at the inner slope and two tunnels connecting the whole system (Figure 6.18).

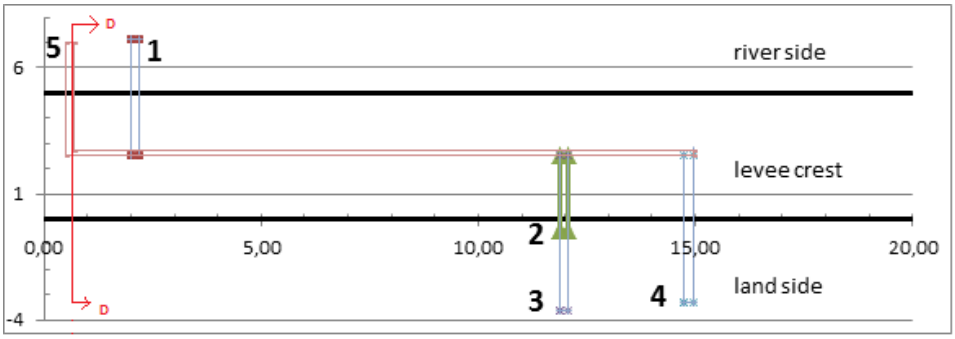

Figure 6.18 Assumed system in 2014. The cross section D-D in analysed with PLAXIS 2d.

One more entrance is present compared to the system in 2012 (entrance 5 in Figure 6.18): it is placed at 35.7 m amsl, that is 30cm below the maximum water level, and it is 1.50meter distant from the other entrance along the outer slope (entrance 1). It is implemented in PLAXIS as a tunnel with diameter 0.2 m; it initially goes down for 1-1.5m with slope 45degrees and then it runs horizontally until the centre of the levee where it turns perpendicularly to the tunnel connecting with the burrows at the outer slope.

The influence of this burrow is analysed with PLAXIS 2D (cross section D-D: Figure 6.18 and Figure 6.19).

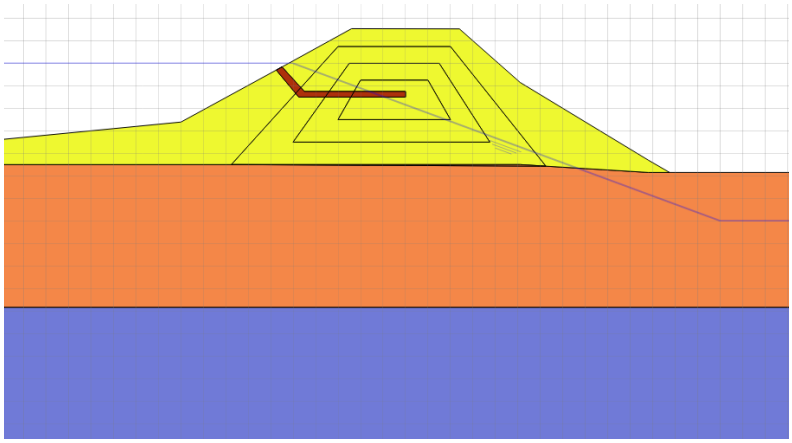

Figure 6.19 Configuration for PLAXIS analysis with documented burrow at the inner slope and entrance between 36.7 and 37 m amsl.

In the steady-state solution, the phreatic line is influenced by the burrow (Figure 6.20). As a matter of fact, it is initially horizontal and parallel to the tunnel. At the centre of the levee, where the burrow ends, it decreases until crossing the inner slope with an exit point higher than the case without burrow.

Also the results of the transient flow analysis show the influence of the burrow to the pore pressure. The water table approaches the steady state condition increasing so the pore water pressures. Its trend at the inner side is instead the same than without any burrow.

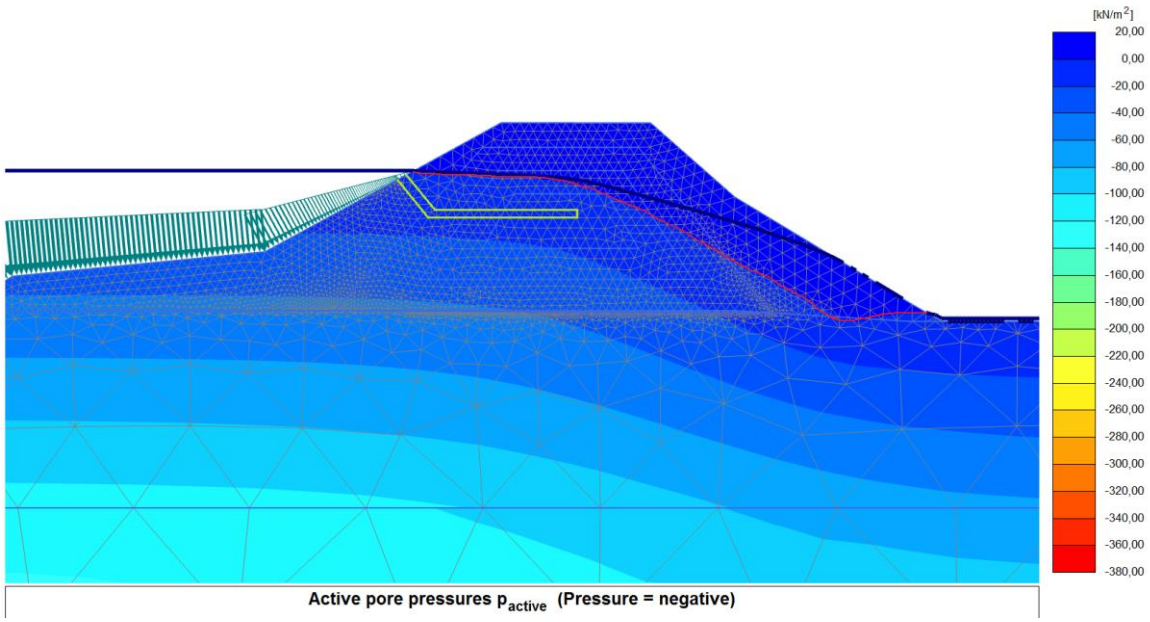

Figure 6.20 Pore pressure distribution at the end of the transient flow analysis with animal burrow with entrance at 35.75 m amsl at the outer slope. The phreatic line is in red, while the phreatic line of the steady state solution is the blue line. The contours of the animal burrow are in green.

The saturation profile (Figure 6.21) shows that, when the water level reaches 36 m amsl and rain is taken into account, most of the dike is fully saturated: the significant influence of the burrow placed

below the river water level is here evident.

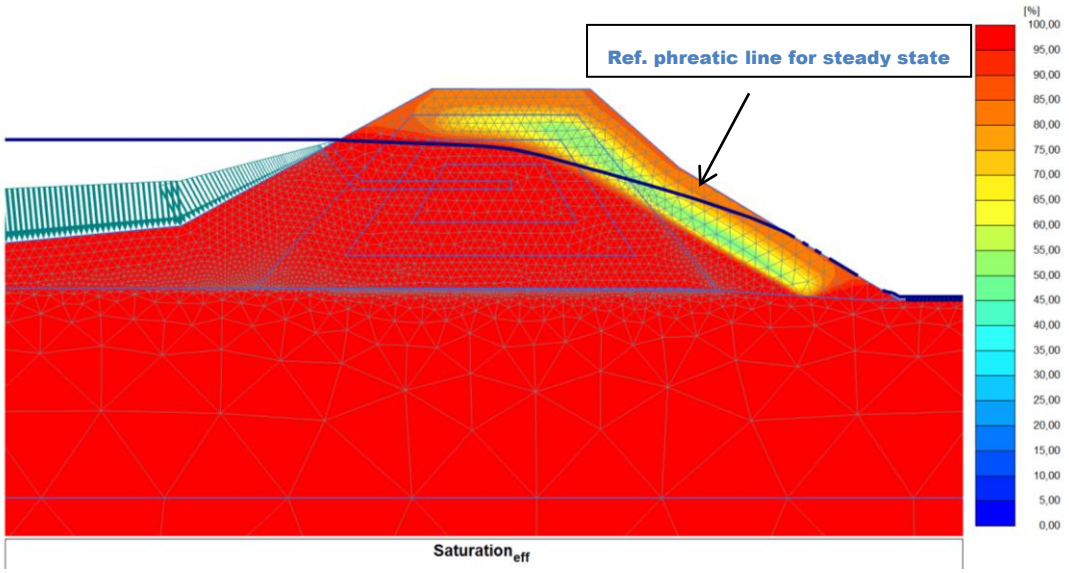

Figure 6.21 Saturation profile for the transient flow analysis with animal burrow with entrance at 35.75 m amsl at the outer slope

As a conclusion, the cavity present in 2014, under maximum water level in the river, represents a preferential path for water, increasing the pore water pressures and the saturation inside the levee. The transient flow results approach the steady state solution. The only differences are given by the phreatic line at the inner slope, which doesn't present an exit point for the transient flow analysis, and by the saturation profile, which is affected by the rain in this type of analysis.

6.7 Summary

The computer program PLAXIS performs groundwater flow analyses for steady state and transient calculations. The steady state solution represents the situation for which time is not considered and the water level in the river is posed equal to its maximum value, while transient flow analysis is carried out with time dependent boundary conditions: the water level changes in river Secchia for 3.25day and it rains for 1.25day. The initial pore pressure distribution has suction inside the dike core with maximum value of water pressures equal to 40 kPa: their values determine the permeability according to the van Genuchten-Mualem model. The burrows are implemented in the analysis as soil tunnels with diameter 0.2m, high permeability and porosity to simulate their voids while their 3d nature has been taken into account by introducing a reduction factor for the unit weight.

When not considering animal burrowing, the phreatic line of the steady state solution crosses the levee body and it exits in a point placed 1.5 meter above the toe of the dike. The transient flow analysis presents lower pore water pressures that the steady state solution, while, at the inner side, the water level exits at the dike toe due to the influence of rain. The infiltration of rain is also visible when looking at the saturation profile: the top part of the levee is fully saturated.

The first burrow under analysis is placed along the outer slope, 30cm above the maximum water level. Its influence in the pore pressure distribution at the end of the transient flow analysis is not significant, while it is evident for the steady state solution: the phreatic line runs across the burrow, which acts as a preferential flow path.
Secondly, the analysis is performed for a section with burrow at the inner slope. In the steady state solution, the phreatic line is intersected by the cavity. No significant influence is instead visible for the transient flow solution. Finally, if the burrow at the outer slope is situated below the water level, the

influence of pore pressures is significant for both steady state and transient flow analyses. The water table is situated above the burrow and parallel to it, while the values of pore water pressures in the dike body are higher than the previously analysed cases.

6.8 Conclusion

6.8.1 Position of animal burrows

The burrows are preferential flow paths which intercept the phreatic line and the resulting pore pressure distribution. The position of the entrances along the slopes determines how they influence it.
Burrows located along the outer slope raise the pore pressures as they are deeper. Figure 6.22 illustrates the water level in steady state condition in case of burrows. The sketch gives a qualitative representation of the influence of presence of burrows and their depth to the groundwater flow.
If the burrow is placed in the top part of the outer slope (case 1), it has no influence on the pore water pressures and the resulting water level is the same than the case for which no burrow in excavated in the dike. In case of lower burrow entrance, the cavity can act as a channel where water freely flows (case 2). Also in this case the water level and pore water pressures inside the dike body are higher than the case without burrow.
Burrows placed below the maximum water level can significantly modify the water pressures and the trend of the water table (case 3). In this case, the raise of water pressure can be significant not only for steady state but also for transient flow analysis.

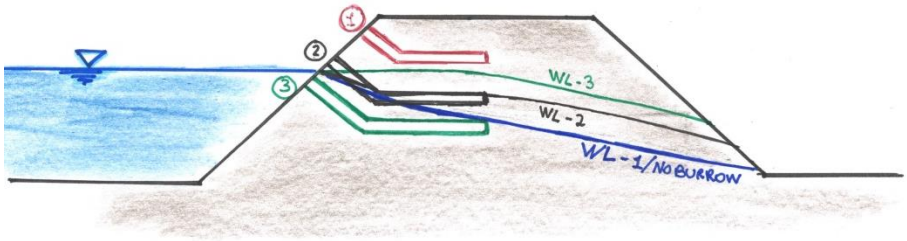

Figure 6.22 Influence of burrow entrances along the outer slope to the groundwater flow.

Also burrows with entrances at the inner slope can influence the water pressure distribution, by intercepting the phreatic line, which flows along them. The different scenarios are illustrated in Figure 6.23 for steady state solution.
If the entrance is placed at the highest part of the slope (case 1), it doesn't intercept the phreatic line and so its influence is null. In case of lower entrance (case 2), the burrow can intercept the water level: water flows along the tunnel exiting along the inner slope in a higher point compared to the other scenarios. In such a way, the raise of water level increases the water pressures in the soil body underneath.
Finally, burrows with entrance starting at the lower part of the inner slope act as drains, lowering the water pressures inside all the dike body (case 3).

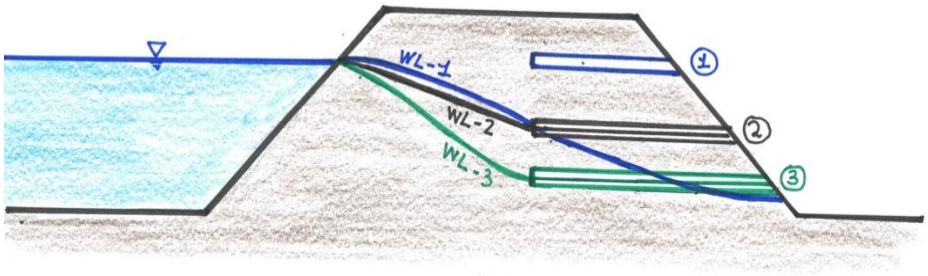

Figure 6.23 Influence of burrow entrances along the inner slope to the groundwater flow.

6.8.2 Steady state versus transient flow analysis

The pore water pressures are lower for transient flow that steady state analysis, since they would require more time to rise inside the levee body and finally reach the steady state solution. In all the analysed cases, the steady state solution presents the phreatic line with an exit point along the inner slope, while the water levels of the transient flow analyses are lower and exit at the inner toe of the dike due to the infiltration of rain.

The most pessimistic scenario (corresponding to higher pore water pressures) is given by the case of transient flow results approaching the steady state solution. In case of a burrow with entrance along the outer slope, the results of the transient flow analysis are similar to those of the steady state. The results differ only at the inner part, where the pore pressures are lower and do not have an exit point along the inner slope. In particular transient flow analysis approaches the steady state results in case of burrow with low entrance along the outer slope since the cavity is placed below water level for longer time.

In all the other analysed cases for transient flow analyses, the burrows give almost no influence on the results, since the water level is not intercepted by their presence.

In conclusion, the steady state solution represents the situation for which the animal burrows mostly influence the results by raising the values of pore water pressures inside the dike body. For this reason, it is suggested to perform steady state rather than transient flow analysis to investigate the highest influence of animal burrowing to the groundwater flow inside the dike body.

7 Three dimensional analysis

7.1 Introduction

The current chapter describes groundwater flow analyses performed with PLAXIS 3D for the levee of San Matteo. As previously done in two dimensions, both steady state and transient groundwater flow analyses are carried out, first without and then with animal burrows.

Three dimensional analyses are performed in addition to 2D calculations for a few reasons. First, the breach of San Matteo was around 10meters wide. The reduced width indicates the presence of a weakness in that location causing a three dimensional failure mechanism instead of a two dimensional infinitive long breach. Moreover, the nature of burrows and their network is 3dimensional. When burrows are implemented in two dimensional analyses, they are implicitly assumed as parallelepipeds infinitively long in longitudinal direction. This configuration also reproduces the case of many entrances located next to each other at the same altitude along the slope and similar underground pattern for the starting tunnel. However this configuration is not the one recorded in the levee of San Matteo, so that a 2d analysis is not considered sufficient and so 3d calculations are performed.

First of all, the 3d analysis is carried out for the levee without animal burrows. Transient groundwater flow calculations are performed, with water level changing in the river with a simulation time of 3.25days and rainfall for 1.25days, such as previously done in 2d. The steady state calculation is not directly performed: however, its resulting phreatic line is also illustrated in the outputs of the transient calculation, thus allowing the comparison with the 2dimensional calculation. Later the underground network digged by the animals is implemented for two different scenarios, previously introduced in paragraphs 4.4.3 and 4.4.4. Also in this case, transient flow analysis is performed and the results are analysed for sections crossing the burrow entrances.

7.2 The profile

The profile used for the 3d calculations is obtained by extruding the 2dimensional profile for 50 meters in the longitudinal direction. The model is 17.5m high and 80 m long (Table 7.1)

Coordinates boundary	Values (meters)
Min_x	60.00
Min_y	-20.00
Min_z	20.00
Max_x	140.0
Max_y	30.00
Max_z	37.55

Table 7.1 Model dimensions for 3d analysis.

The dimensions are shorter than the 2d profile in order to reduce the mesh size and so the computation time, which is particularly long for three dimensional calculations.
Moreover, since the element size depends on the model dimension (Plaxis, 2014), it is necessary to reduce the dimension of the model in order to have a better refinement of the mesh, in particular for small parts of the geometry such as animal burrows. Finally, the model dimension is chosen so that the results are not influenced by the boundary conditions.

The mesh has 14621 soil elements and 22838 nodes, with average element size of 2.2meters. When burrows are introduced in the levee body, the mesh is further refined in the dike core.

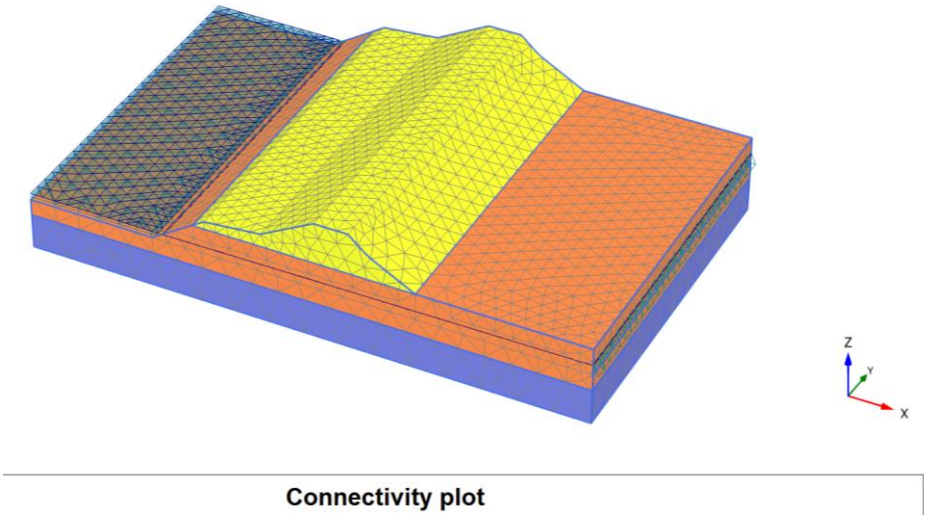

Figure 7.1 Model profile and mesh.

The groundwater flow boundaries are “closed” along the minimum and maximum x-z planes and in the bottom horizontal boundary in order to simulate an impermeable layer underneath. The other boundaries are instead “open” for the groundwater flow.
Referring to the deformations, the top surface is free to move while the bottom is fully fixed. The model boundary in the yz-plane with minimum x-value presents free displacement along the lateral and vertical direction; vertical displacements are instead not allowed for the yz-plane with maximum x-value. Finally, the model boundaries in xz-plane present fixity only in the y-direction, while movement is allowed along the other two axes.

7.3 Initial condition

The initial pore water pressure distribution in the Investigative Evaluation Report is assumed for the 3d analysis such as for the 2d-analyses previously performed (paragraph 6.3). However the interface of PLAXIS 3D doesn’t allow the user to easily implement them. Therefore the initial conditions have been simplified by imposing a hydrostatic distribution with value of suction equal to 40 kPa at the center of the levee and maximum value of 80kPa at the top.

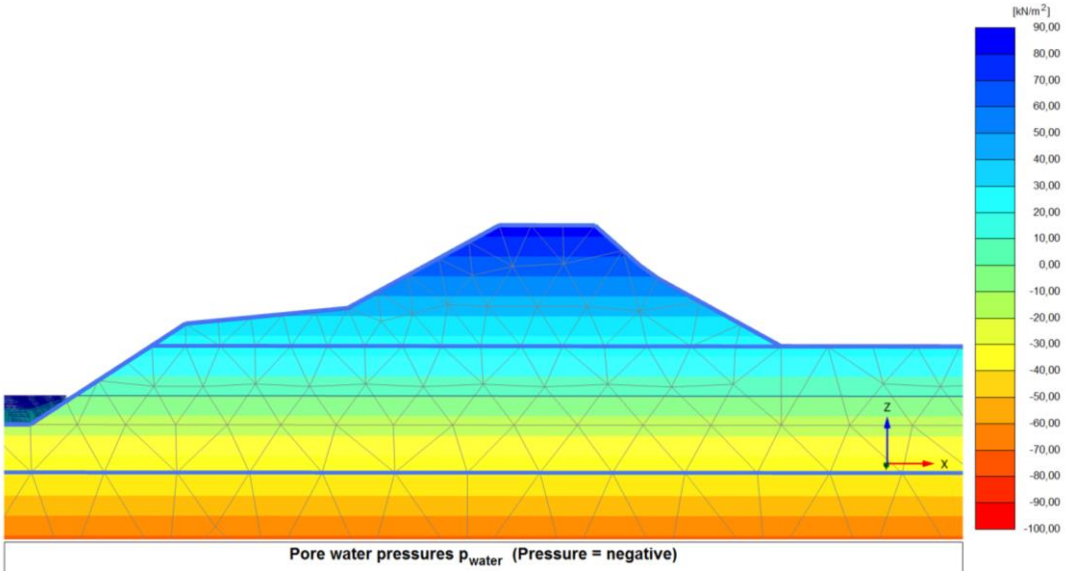

Figure 7.2 Initial pore water pressure distribution inside the levee for a section on the plane x-z

7.4 Steady state

The validation of the 3dimensional calculations is given by the comparison of the results with those of the 2d analysis.
When performing the transient analysis, the phreatic line of the steady state is calculated and used as input for the analysis. In this way, even when not performing a steady state calculation, its phreatic line can be visualized as the input for the transient flow analysis.

The phreatic line is represented by the blue line in Figure 7.3: it enters the levee at 36 m amsl and it exits at 32.5m amsl above the toe at the inner slope. Its trend is the same of the two dimensional analysis (Figure 6.3).

7.5 Transient flow

7.5.1 Introduction

The transient flow analysis with PLAXIS 3D takes into account the changing water level in the river and the rain. Such as for the two-dimensional analysis, the changing water level in Secchia river is simulated for 3.25days with data every 3hours, starting on 16/01/2014 at 0:00 until 19/01/2014 at 6:00, while rainfall hourly data of the last 1.25 day are used.

7.5.2 Results

The results are visualized for a section in the x-y plane. Figure 7.3 shows the final distribution of active pore pressures at the end of the transient flow analysis.

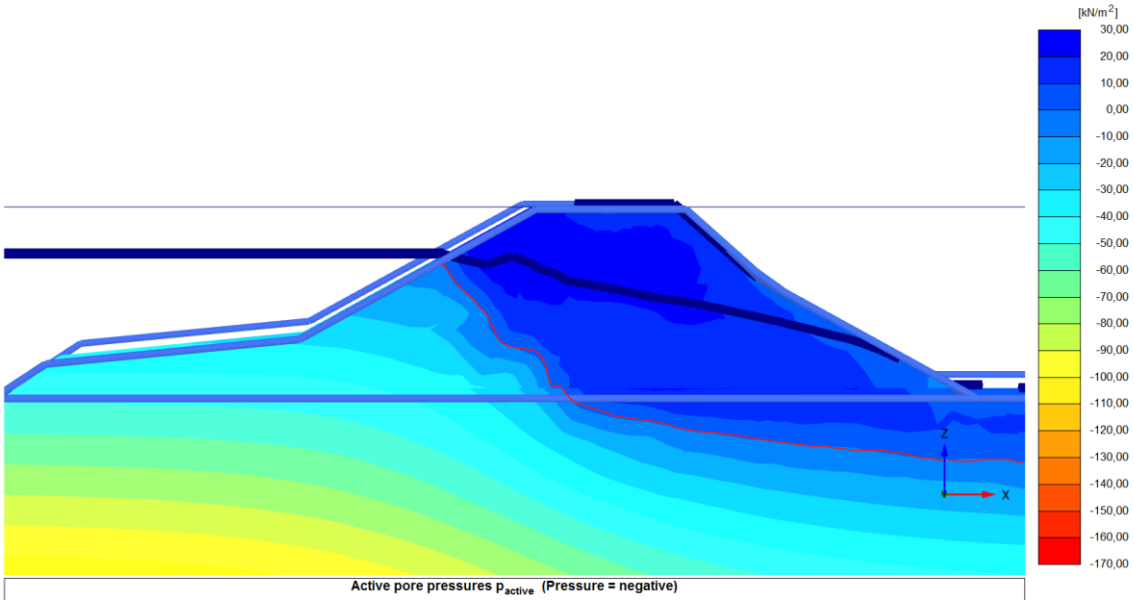

Figure 7.3 Active pore pressure distribution at the end of the transient flow analysis, having considered the changing of water level in the river and the rain until 6am on 19/01/2014. The phreatic line of steady state is the blue bold line, while the water table of the transient flow is in red.

The results are slightly different from those obtained with same boundary conditions in PLAXIS 2D (Figure 6.6): the pore pressures at the end of the 3D analysis are lower resulting in lower water table and absence of exit point of seepage flow at the inner slope.

The difference in results is due to a few reasons. First of all, as described in paragraph 7.3, the initial pore pressure distribution is simplified compared to that used at the beginning of the 2d analysis. In particular the initial pore pressures vary linearly, reaching high value of suction on the crest of the dike. In such a way, the pore pressures in the core are lower and their raise during the analysis is reduced compared to the 2D calculation.
Moreover, because of model size and computation time, the elements of the 3d analysis have double size (2.2 m) compared those used in 2d (1 m). However, only fine elements allow the infiltration of water, which is now minimized in the 3d analysis because of the large width of the elements. In such a way, the reduced rainfall decreases the values for the final distribution of pore water pressures.
Finally, the large mesh size also results in less precise 3d calculations compared to those obtained in 2d. For this reason, the resulting phreatic line has a less precise shape.

Figure 7.4 shows the saturation profile at the end of the analysis. Only part of the dike core is fully saturated, that is the zone below the water level at the end of the transient flow analysis. The top of the levee is only partially saturated while water penetrates in the lower part of the inner slope.

The results are similars to those obtained with the two dimensional calculation (Figure 6.9) but few differences are individuated. As a matter of fact, the dike in Figure 7.4 is less saturated in its core and the top of the levee is dry: the saturation due to rain is here missing. The infiltration of water is also not present in the upper part of the inner slope.

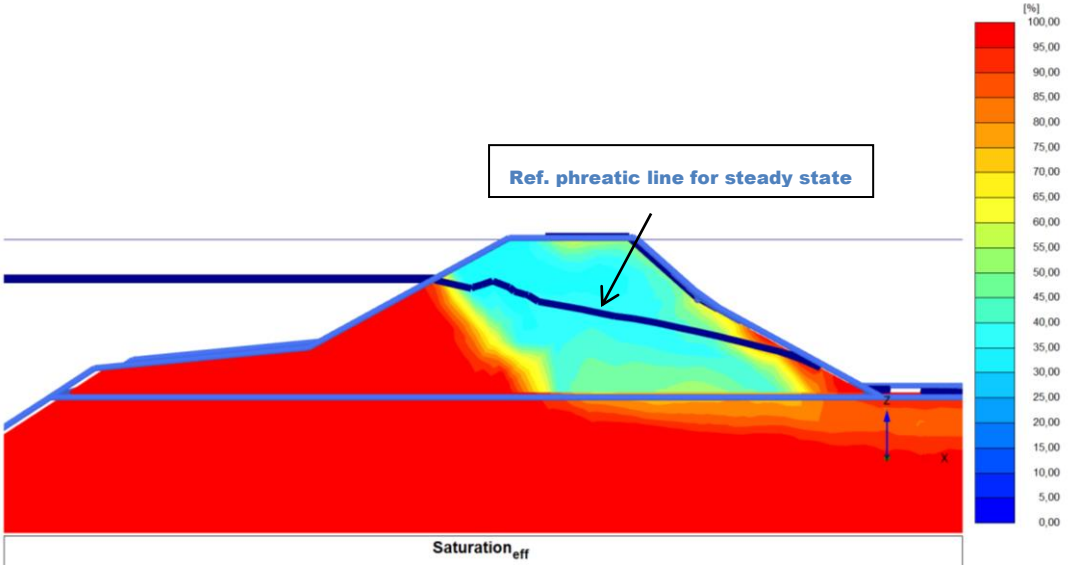

Figure 7.4 Saturation profile at the end of the transient flow analysis, having considered the changing of water level in the river and rainfall.

In order to gain a better insight on the rainfall effect in the 3d calculation, the saturation profile of Figure 7.4 is compared to the profile at the end of the analysis without considering the rain (Figure 7.5). After comparing, it is possible to conclude that rain is effective only in the lower part of the inner slope: in this location the levee of the complete analysis (Figure 7.4) is more saturated than that the dike of Figure 7.5.

The dike core of Figure 7.4 is also more saturated. As a matter of fact, during the 1.25days for which rainfall is implemented, the level in the river is kept stationary at its maximum level. This additional day allows the rise of water pressure and increase in saturation in the dike core in Figure 7.4, compared to the analysis without rain.

As previoulsy described, the infiltration of water due to rain is reduced because of the large element size used in the 3d analysis.

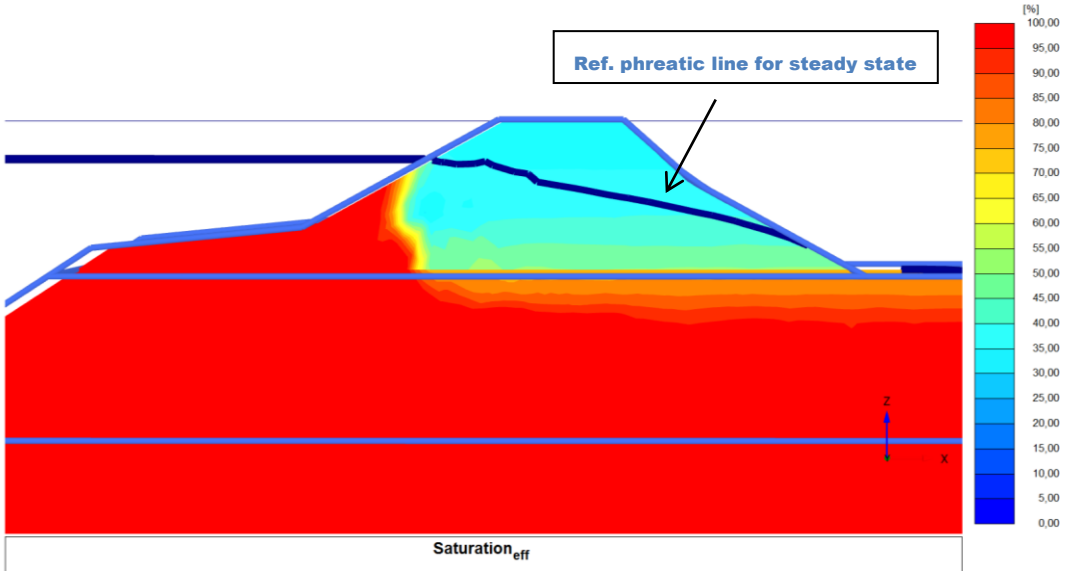

Figure 7.5 Saturation profile at the end of the transient flow analysis, having considered only the changing of water level in the river and not rainfall.

7.6 Animal burrows

7.6.1 Introduction

While the 2dimensional analysis investigates singular sections of the underground system, 3d calculations analyse the influence of the whole network to the groundwater flow.

The burrows are implemented as soil tunnels with high permeability and porosity, such as previously done for the 2dimensional analysis. The unit weight of soil is minimized to simulate empty cavities while all the other properties are equal to the surrounding soil.

Two scenarios, previously introduced in paragraphs 4.4.3 and 4.4.4, are carried out in the analysis: the first is the assumed 3d network of the sett with the entrances described in the Investigative Evaluation Report, while the second takes into account the development of the system in time.

7.6.2 First scenario

The system, which has been previously described in paragraph 4.4.3, is constituted by four burrow entrances, located at altitudes 36.3, 37.1, 15.1 and 34.8 m amsl, respectively from entrance 1 to 4 in Figure 7.6. The tunnels initially go down with a slope of 45° for 1-1.5meters and then they run horizontally until the centre of the levee. A central tunnel longitudinally crosses the dike for around 10meters linking the entrances at the inner and outer slope.

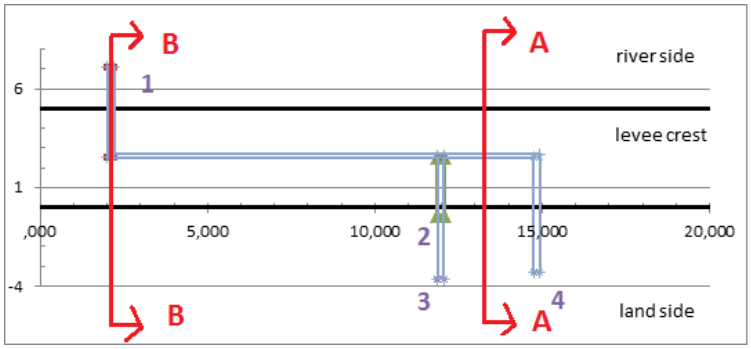

Figure 7.6 First scenario implemented in the 3d calculation.

The system implemented in PLAXIS 3D is shown in Figure 7.7. The burrows are soil cylinders with diameter of 20cm.

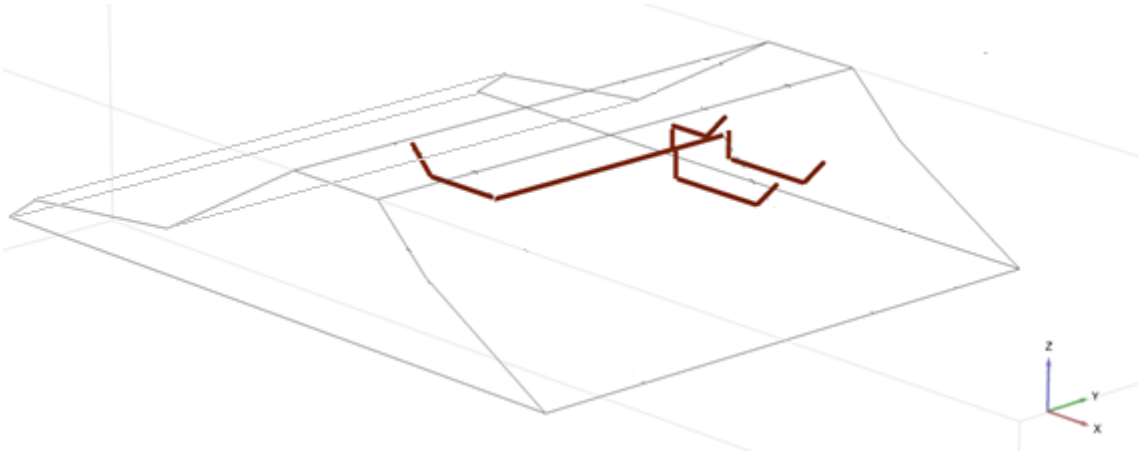

Figure 7.7 Network of animal burrow with the First Scenario implemented in PLAXIS 3D.

The results of the transient flow analysis are analysed for two sections: section A-A crosses the three entrances at the inner slope, while section B-B crosses the entrance at the outer slope, as shown in Figure 7.8.

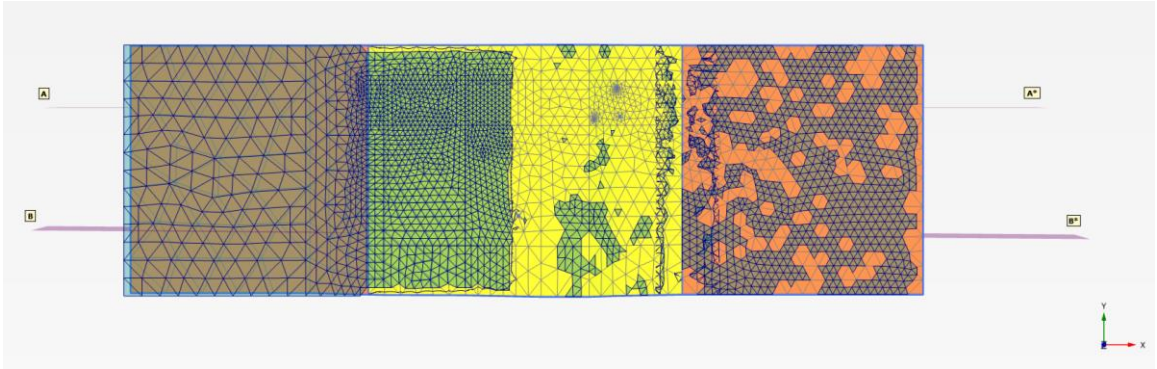

Figure 7.8 Sections analysed in the 3d calculations for the first scenario.

Figure 7.9 reveals the pore pressure distribution at the end of the transient flow calculation for section A-A, which crosses the burrow entrances at the inner slope. The pore pressure distribution is the same than the case without burrows for the same type of analysis (Figure 7.3): the cavities have almost no influence in the results. Also the phreatic line resulting from the steady state analysis (in blue) is not influenced by the animal burrows.

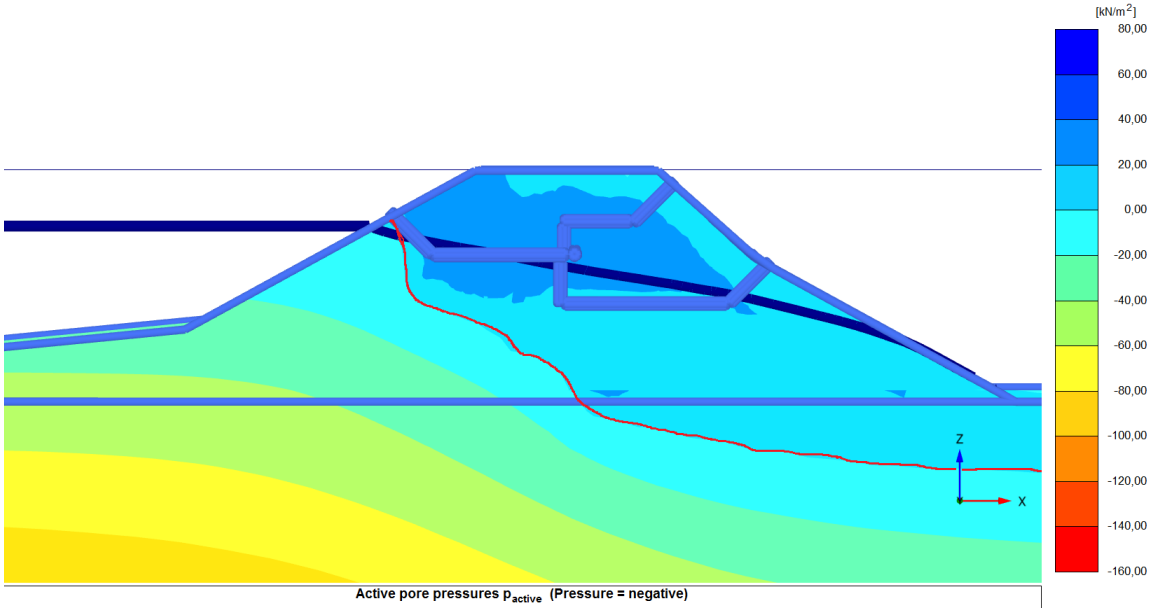

Figure 7.9 Active pore pressure distribution at the end of the transient analysis for the section AA for the first scenario in PLAXIS 3D. The water table at the end of the transient flow analysis is indicated by the red line while the phreatic line for the steady state solution is the blue line.

Figure 7.10 shows the pore pressure distribution at the end of the transient flow analysis for section B-B, which crosses the levee along the burrow entrance at the outer slope.
The phreatic line of the steady state solution (blue line in Figure 7.10) slightly rises in correspondence to the cavity. The influence of the burrow to the phreatic line is not relevant anymore for sections more than 1 meter distance from the burrow entrance.
Instead, the burrow doesn't influence the results for the transient flow analysis: the water table and the pore pressures are the same than the case without cavities.

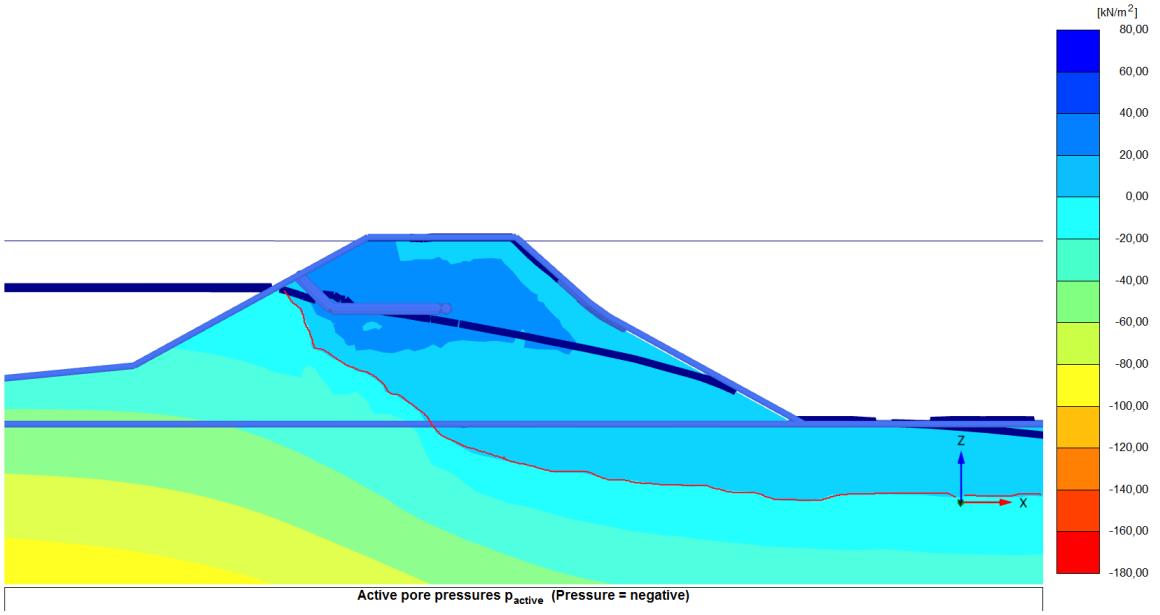

Figure 7.10 Active pore water pressure at the end of the transient flow analysis for section BB for the first scenario in PLAXIS 3D.

7.6.3 Second scenario

The second scenario takes into account the growth of the sett between 2012 and 2014 (paragraph 4.4.4): a new entrance and tunnel are assumed in the analysis. In particular the new cavity (entrance number 5, Figure 7.11) starts at 35.7 m amsl, 1.5 m distant from entrance 1; the burrow starting at entrance 5 continues is connected to the entrances 2,3 and 4 at the inner slope with an additional central tunnel, which is 18.4 meters long.

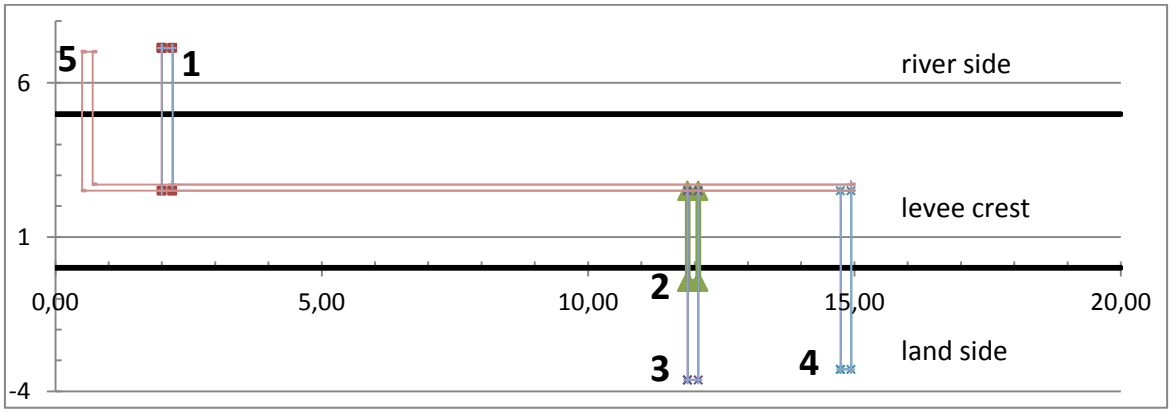

Figure 7.11 Second scenario implemented in the 3d calculation.

Also in this case, the results for a section along entrance 5 show an almost negligible influence of the burrows to the results for the steady state solution, but not for the transient flow analysis. This influence is not present anymore when looking at a section located 1meter far from the entrance, along the longitudinal direction.

7.7 Summary Conclusion

The current chapter has presented the analyses performed with PLAXIS 3D. The same profile of the 2d analyses is here extruded in the longitudinal direction. The dimension of the model is 80x17.5x50 m, that is reduced compared to the 2d analyses in order to minimize the computation time.

First of all, the validation of the model is carried out by comparing the results with those of the two dimensional calculations. The results of the steady state solution correspond to those obtained with PLAXIS 2D, while in the transient flow analysis the infiltration of rain is reduced because of the mesh size: as a consequence, the values of pore pressures are reduced and the water table is lower.

The system of burrows is then implemented in the analysis for two scenarios: the first presents the assumed network with the known entrances in 2012, while the second corresponds to the system taking into account its growth in time between 2012 and 2014.
In the sections crossing the burrow entrances at the outer slope, the phreatic line of the steady state solution is locally influenced by the cavity: the reduced influence of the burrow to the pore pressures is localized in the sections of the entrances and not visible any more for sections more than one meter distant from them. The water table and pore pressures of the transient flow analysis are, instead, almost not affected by it.

7.8 Conclusion

7.8.1 2D versus 3D analysis

The main contribution that the 3D analysis gives for the interpretation of the results, compared to the 2d analysis, is the localized influence of animal burrows to the pore pressure distribution. As a matter of fact, the results of the 3D analyses show a limited and localized influence of the burrows to the pore water pressures for the steady state solution. For sections more than 1meter distance, the presence of animal burrows is negligible for the results.

However, the accuracy of the performed 3D analyses is lower compared to the 2D calculations. The model should be large enough in order to ensure that the results are not affected by the boundaries, but, at the same time, the element size is directly proportional to the model dimension. For this reason, three dimensional models have a mesh which is not highly refined such as the one used in the 2d calculations, so affecting the accuracy of the results. Moreover, refinement of the mesh corresponds to longer computation time, which is already very high for 3d calculations.
In order to find a compromise between element size and computational time, the chosen elements used in the 3d analysis have double size than those of PLAXIS 2D. In such a way, the larger elements decrease the quality of the mesh and rainfall is reduced, since only fine elements allow the infiltration of water. As a consequence, the 3D calculation gives less precise results than the 2D analysis.

The high amount of computational time that the three dimensional calculation requires and the additional time that mesh refinements would need in order to increase the accuracy of the results, suggest to perform 2d calculations. The 2D analysis presents accurate results with highly refined mesh and reduced computation time. However, while analysing the results, it has to be kept in mind that the 2d analysis gives pessimistic results for the scenarios under analysis, since the burrows are assumed with a two dimensional nature and thus infinitely long.

8 Instability of the inner slope

8.1 Introduction

In a deterministic analysis, the factor of safety is the parameter used in the evaluation of the stability of a slope. It is the ratio of available shear strength to the required/mobilized shear strength. Therefore, the slope is unstable for F≤1.0.
LEM (Limit Equilibrium Method) and FEM (Finite Element Method) are the most widespread methods to determine the stability of a slope.

8.2 Limit Equilibrium Method

The Limit Equilibrium Method (LEM) analyses the loads and the resistances at the limit equilibrium stage.

The stability is assessed assuming incipient failure along a potential slip surface and the critical slip surface is the one which gives, after trials, the minimum safety factor for the slope. Usually the factor of safety is simply assumed to be constant all along the failure surface, i.e. it is the average value of F instead of the actual factor of safety which varies along the failure surface. The sliding body is divided into a finite number of slices, usually cut vertically (Figure 8.1). The vertical slices don't need to be equal, while the inclinations of the base of each slide, the slide weight, material properties and pore pressures at the base of each slide are expected to be known before an analysis can be carried out.

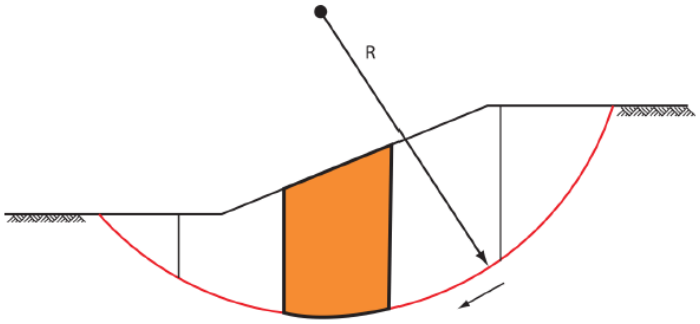

Figure 8.1 Bishop Slip Plane with method of Slices (2014)

Different models are available and their difference lies in thei assumptions of forces and moment equilibrium. The models can be simplified or rigorous: the first satisfy either force or moment equilibrium, while both are satisfied in the latter.

8.2.1 Bishop Model

Bishop model is mostly used when carrying an analysis with the Limit Equilibrium Method. It assumes a circular failure surface and it satisfies vertical force equilibrium for each slice and overall moment equilibrium around the centre of the circular surface. Horizontal forces of each slice are not considered and the inter-slice shear forces are assumed to be zero.
The forces taken into account for each slice are the self-weight of the element W, the shear resistance S, the lateral forces E_n and E_{n+1} acting on the element, the normal forces N acting at the failure surface (Figure 8.2).

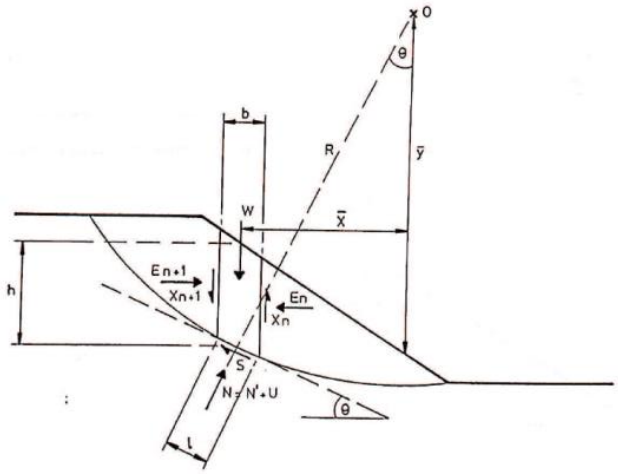

Figure 8.2 Force balance in a finite slope

The Factor of Safety is given by the ratio between the resisting moment and the driving moment:

$$FS = \frac{M_r}{M_s} \tag{8.1}$$

Bishop model is usually preferred among the LEM models because of its simplicity by assuming a circular failure surface and its accurate results with easy calculations.

8.2.2 Introduction of Burrow

The introduction of the burrows in the analysis changes the configuration of the forces involved. In particular, the weight of the soil reduces due to the empty cavities and there is no shear resistance along the sliding circle when intersecting the burrow (section AB). In case the outside water level is higher than the entrances of the burrow, the additional weight of the water inside the cavity needs to be taken into account as well (Armitage, 1999).

Moreover the water acts against the end of the tunnel creating an additional force. After some time, the soil around the cavity changes its moisture content, so that also the shear resistance in the wetting soil is different and the force against the burrow end moves its position.

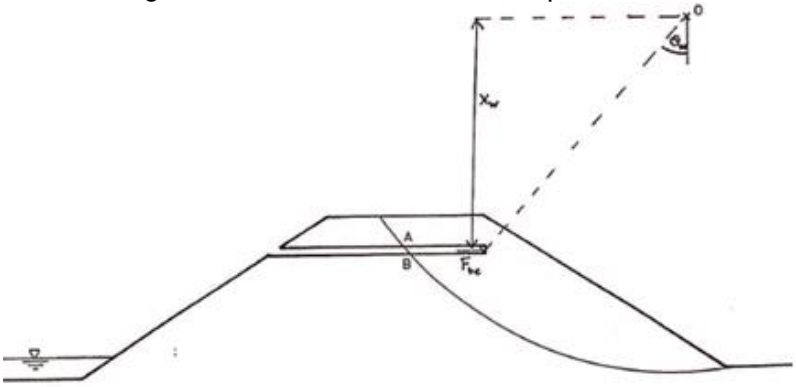

Figure 8.3 Forces considered in the stability analysis with animal burrow: the overall weight of the soil is reduced and there is no shear resistance in the soil between A and B (Armitage, 1999)

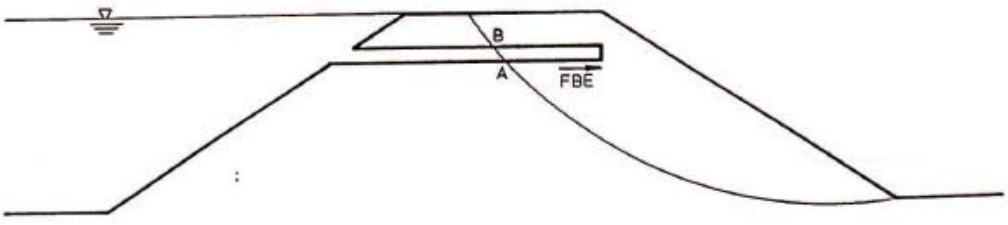

Figure 8.4 Forces considered in the stability analysis with water level above the entrance of animal burrow: the weight of water inside the animal burrow and its additional force FBE acting against the end of burrow (Armitage, 1999)

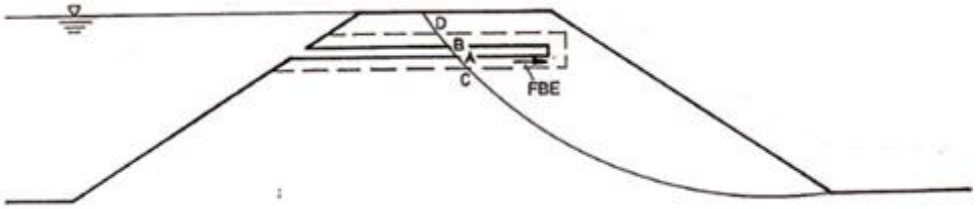

Figure 8.5 Forces considered in the stability analysis with water level above the entrance of animal burrow after the elapsed time t: the wetting profile around the burrow changes the shear resistance between C and D and moves the centroid of the force FBE (Armitage, 1999)

Armitage (1999) performed stability analyses for different configurations of burrows, outside water level and elapsed time, concluding that the factor of safety reduces with the burrows depth, the increase of water level in the river, the number of burrows and the elapsed time.

8.2.3 Limitations

The LEM is relatively simple and few parameters are required for its analysis. However, it presents some limitations, in particular for the case study under analysis:

- 3D analysis is not possible with LEM, which models only two-dimensional failure surfaces.
- LEM consider only static pore pressure field and so it doesn't allow coupled deformation and groundwater flow analysis.

Since 3dimensional and transient flow analyses are required for the case study of the failure of San Matteo, these limitations are overcome by the use of Finite Element Method.

8.3 Finite Element Method

In the Finite Element Method, the continuum is divided into elements, each of whom has a number of nodes. Each node has degrees of freedom corresponding to the unknowns of the problem. The stability of the embankment is estimated through the factor of safety, defined as the ratio of maximum available shear strength over the minimum shear strength required for assuring equilibrium:

$$Safety\ Factor\ = \frac{S_{maximum\ available}}{S_{needed\ for\ equilibrium}} \tag{8.2}$$

According to the Coulomb condition: $\tau = c - \sigma_n \tan\varphi$, where τ is the shear strength, c the cohesion, σ_n the normal stress and φ the friction angle. Thus the Safety Factor can be expressed as:

$$Safety\ Factor\ = \frac{c - \sigma_n \tan\varphi}{c_r - \sigma_n \tan\varphi_r} \tag{8.3}$$

The subscript *r* indicates the reduced strength parameters to ensure equilibrium. Thus the so-called $\varphi - c$ reduction method implemented in PLAXIS reduces the cohesion and the tangent of the friction angle with the same total multiplier ΣMsf :

$$\Sigma Msf = \frac{c}{c_r} = \frac{\tan\varphi}{\tan\varphi_r} \tag{8.4}$$

For every new step in the analysis, the parameter c_r and $\tan\varphi_r$ are increased until failure occurs: the value of ΣMsf at failure is the safety factor (2013a).

8.3.1 Considerations for the analysis

As previously mentioned, in the case under analysis, the failure mechanism was influenced by 3d effects and its time-dependent boundary conditions. Due to the limitations of the LEM, the Finite Element Method is preferred for the stability analysis; the software PLAXIS is then used.

The parameters used in the analysis depends on the used Soil Model. In the current analysis, Mohr-Coulomb model has been chosen. Its simplicity and the need of few input parameters are favourable for the current case.
The soil properties used for the analyses are introduced in paragraph 5.2.1 and their derivation from the data available in the Investigative Evaluation Report is explained in Appendix C.

8.4 Analysis without animal burrows

The stability analysis correlates the deformation of the crest of the levee (node A, Figure 6.7) with the factor of safety.

Case	SF – 2D steady state	SF – 2D transient flow	SF – 3D transient flow
No burrows	1.333	1.812	2.616

Table 8.1 Safety Factors for the analysis performed in Plaxis 2d and 3D without animal burrows (paragraph 6.4 and 6.5).

8.4.1 Steady state

The stability analysis performed after the two dimensional steady state analysis, reveals a factor of safety equal to 1.333: when a constant water load is applied to the levee at 36 m amsl for infinitive time, the dike reveals to be stable (SF>1).

By reducing the properties of the dike body, with the φ-c reduction method, the displacements leading to failure reveals the sliding plane of Figure 8.6. The failure plane is shallow: it starts at the centre of the levee crest and it ends at the inner toe, without intercepting the underlying layer.

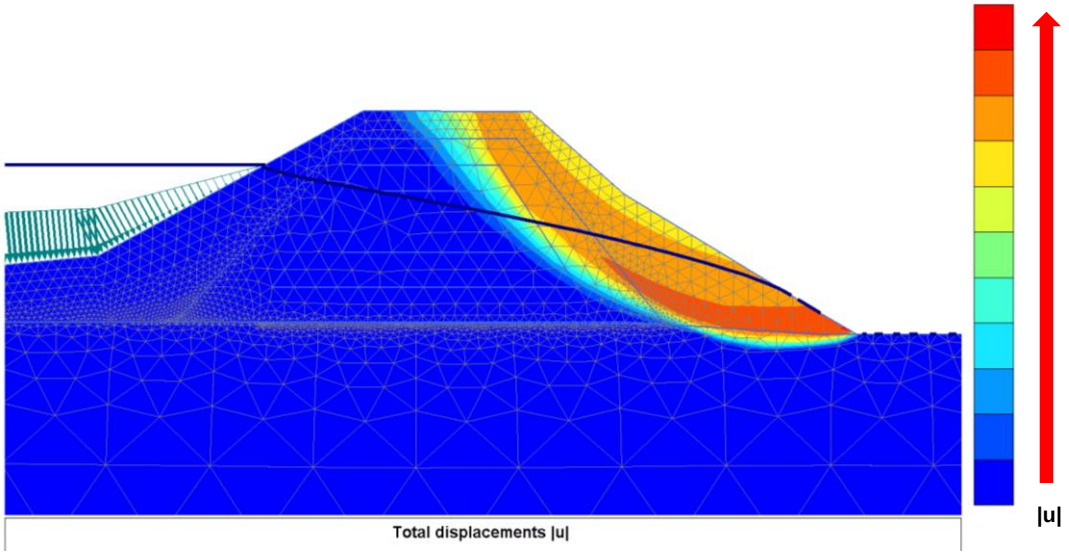

Figure 8.6 Sliding surface after the steady state analysis with water level at the river equal to 36 m amsl (SF=1.333).

8.4.2 Transient Flow

The safety factor for the stability of the dike after the transient flow analysis is equal to 1.812.
It is higher at the end of the transient flow analysis than at the steady state solution. As a matter of fact, the time given to pore pressures to rise during a transient flow analysis is less than for the steady state solution, so that their value is lower (Figure 6.3 and Figure 6.6). As a consequence, the effective stresses and, for Terzaghi's law, the shear stresses are higher, increasing the stability of the embankment. Figure 8.7 shows the failure plane: it is wider than the sliding surface of the steady state solution, it comprises most of the dike body and it penetrates in the layer underneath.

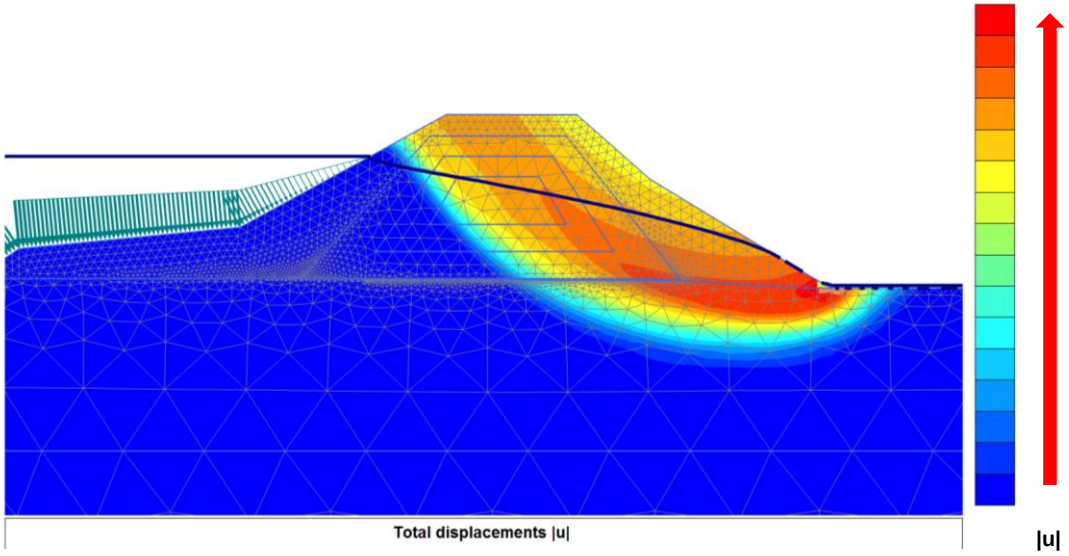

Figure 8.7 Sliding surface obtained with the safety analysis after the transient calculation (SF=1.812).

The influence of rain is visible when comparing the factor of safety at the end of the analyses with and without rain: in the first case SF=1.812 while in the latter case SF=2.157. The development of pore pressures and the reduction of suction due to infiltration of rain contribute to the loss of strength of the levee.

The influence of rain is visible also when looking at the total displacement: the failing soil mass is bigger after it rains (Figure 8.7) compared to the sliding plane without considering it (Figure 8.8), since the increases of saturation and water pressure decrease the overall effective stresses and weaken a larger part of the levee.

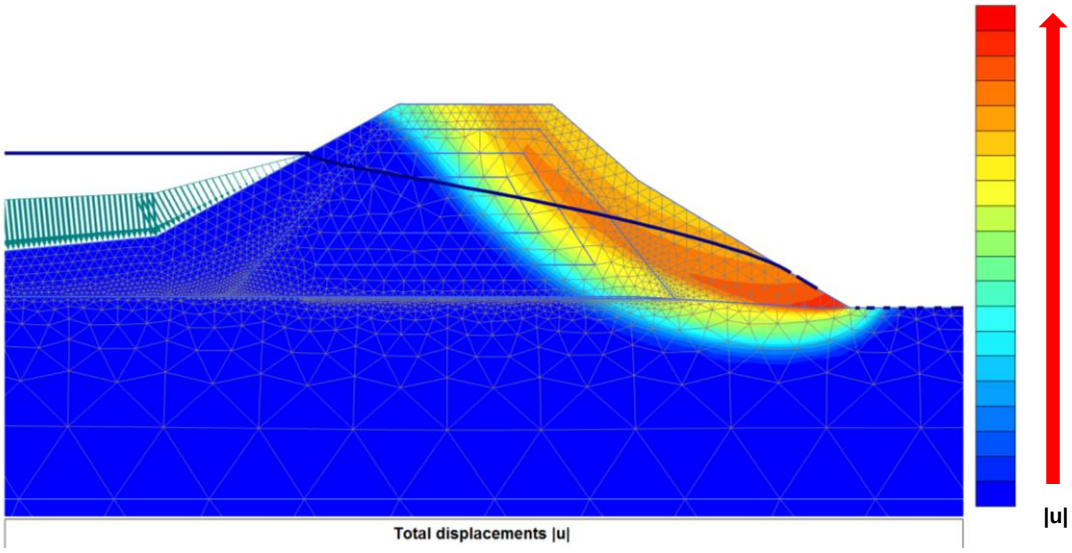

Figure 8.8 Sliding surface after the safety analysis with transient calculation, without rain (SF=2.157).

In conclusion, the performed analyses show that when the animal burrows are not taken into account, the dike proves to be stable with a factor of safety above 1.

8.4.3 Consideration upon the dependency of SF on the time of the simulation

Transient groundwater flow analyses for a short period of simulation time highly depend on the initial conditions. In the current case study, the uncertainty correlated to the initial conditions is high as well, since they are assumed by literature review and not by field measurements. In order to reduce the dependency of the results on the initial conditions, a longer period of time should be used for the simulation. However the computational time increases as well.

The analyses are performed for 3.25 days, which gives accurate results and significantly reduces the time required for the calculations. As a matter of fact, if the analysis is run for a simulation time of 18.25days, during which the water level in the river changes, the safety factor turns equal to S=1.825. In the analysis performed for 3.25 days, instead, the safety factor is equal to 1.812. The chosen simulation period gives very similar and so accurate results for a much reduced computation time.

8.4.4 PLAXIS 3D

Similar analyses are carried out with PLAXIS 3D with the profile used in PLAXIS 2D, extruded in longitudinal direction. Only transient flow analysis is carried out, for which the safety factor is equal to: SF=2.616.

The total displacements at the end of the safety phase for a section in the x-z plane (Figure 8.10) are similar to those obtained with PLAXIS 2D, even if the failure surface is wider and lower.

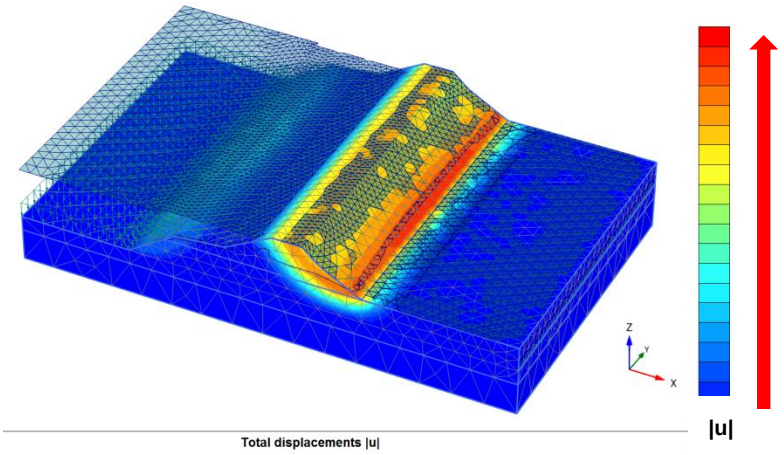

Figure 8.9 Sliding surface obtained with the safety analysis after the transient flow analysis with implementation of rain and water level changing in the river with PLAXIS 3D.

The results are visualized for a section along the x-z plane in Figure 8.10. Since the profile used in the analysis is homogeneous, the results are identical for each section along that plane.

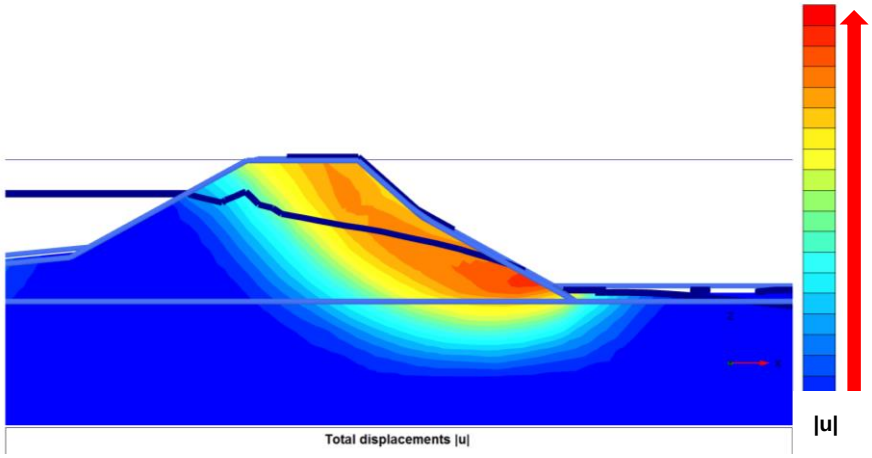

Figure 8.10 Sliding surface for a section along the x-z plane for the transient flow analysis with PLAXIS 3D.

8.4.5 Considerations upon the quality of results with PLAXIS 3D

As described in paragraphs 7.6 and 7.8.1, the 3D calculations are less accurate than the 2D analyses. As a consequence, the resulting safety factor (SF=2.616) differ from the one resulting from the same transient analysis with PLAXIS 2D (SF=1.812).

Three dimensional calculations require high computational time, which increase with the model size and the refinement of the mesh. For this reason, the mesh used in the 3d analysis is wider and so less accurate than that used in PLAXIS 2D. In such a way, the infiltration of rain, which can penetrate only if the mesh is fine enough, is reduced.
Moreover, the implemented initial pore water pressures present higher suction than those used in 2D. The permeability, which depends on the suction head according to the Mualem-Van Genuchten model (paragraph 5.2.2), is also reduced and, as a consequence, the groundwater flow is less.
The resulting less saturation of the soil body in the 3D compared to 2D analysis increases the stability of the dike. Moreover, the final safety factor and slip plane also depend on the mesh used. A finer mesh gives more accurate results, usually lowering the resulting safety factor.

In order to prove the considerations above, a two dimensional analysis which reproduces the performed 3d analysis is carried out. In particular, this 2D analysis has the same initial pore water pressures, refinement of the mesh and model dimension of the 3D calculation. Rain is not implemented, in order to reproduce the almost null infiltration of rain in the 3D analysis.
Finally the results in terms of safety factor and slip plane of the analysis correspond to those obtained with PLAXIS 3D and described in paragraph 8.4.4. This confirms that the initial pore pressures, the refinement of the mesh and the infiltration of rain are the key parameters for which the 3D analysis has a worst quality than the 2D calculation.

8.5 Analysis with animal burrows

The current paragraph presents the results of the 2d and 3d analyses with the implementation of animal burrows. Table 8.2 presents the resulting factors of safety.

Case	SF – 2D steady state	SF –2D transient flow	SF –3D transient flow
No burrows	1.333	1.812	2.616
Burrow at the outer slope	1.258	1.733	-
Burrow at the inner slope	1.390	1.786	-
Burrow in 2014	1.173	1.412	-
System in 2012	-	-	2.565
System in 2014	-	-	2.566

Table 8.2 Safety Factors for the analysis performed in Plaxis 2d with the animal burrows (paragraph 6.6)

8.5.1 Analysis with animal burrows in Plaxis 2d

Table 8.2llustrates the results of Safety Factor obtained for the analyses with the implementation of animal burrows in PLAXIS 2D.

8.5.1.1Burrow at the outer slope

The analysis with the animal burrow placed at the outer slope (paragraph 6.5.2) gives a safety factor equal to 1.258 for the steady state solution and equal to 1.733 for the transient flow analysis. The stability just slightly decreases compared to the case without any burrow: the reason of the slight decrease is caused by the small influence of the burrow to the rise of water table and pore pressure distribution (paragraph 6.5.2).

Also the sliding plane (Figure 8.11) is similar to that obtained without the implementation of burrows (Figure 8.7).

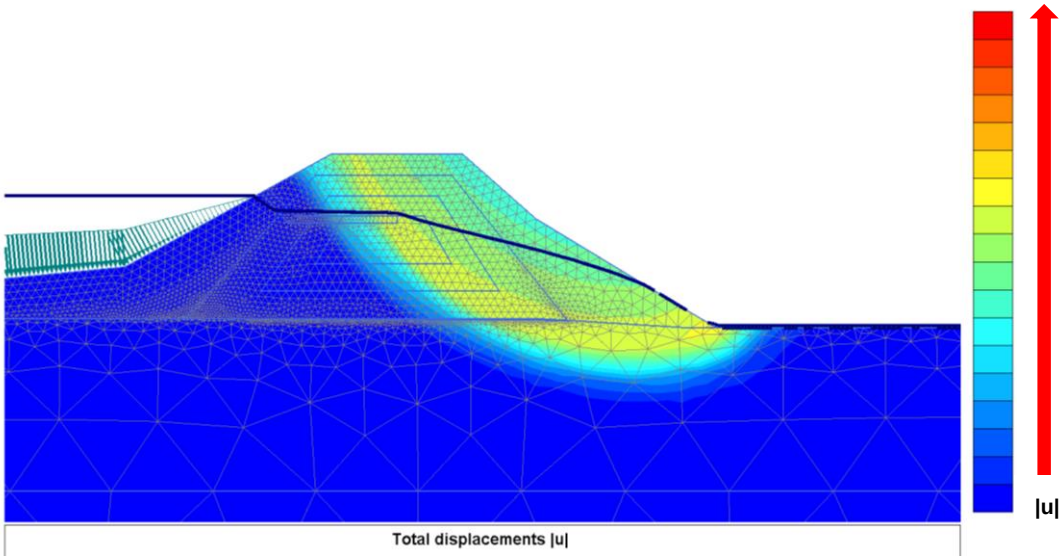

Figure 8.11 Sliding surface after the safety analysis with transient calculation (with changing water level and rain) with burrow at the outer slope.

8.5.1.2 *Burrow at the inner slope*

When the burrow at the inner slope is analysed, the steady state solution presents a safety factor equal to 1.390. This situation is safer than the case without any burrow (SF=1.333). As a matter of fact, the water table is intercepted by the burrow and it decreases rapidly from the entrance point to the centre of the levee where it enters the cavity (Figure 6.15). Due to this rapid decrease, the values of pore pressures in the dike core are lower than the steady state solutions in the analyses without any burrow or with the burrow at the outer slope (Figure 8.12). As a consequence, in that point the effective stresses are higher and so also the resistant shear strength, which is here determinant since the failure surface passes through it (Figure 8.13).

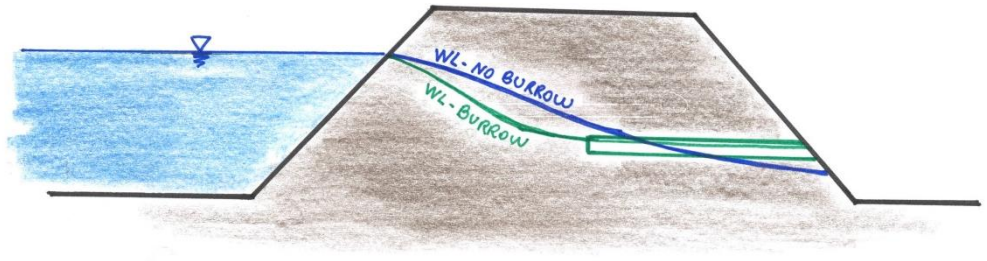

Figure 8.12 Water level for steady steate analysis when no burrow is considered (in blue) and with the burrow ar the inner slope (in green).

Also the transient flow analysis gives a slightly higher safety factor (SF=1.786) similar to the case without burrows (SF=1.812). Here the pore pressure distribution is not influenced by the presence of the burrow at the inner slope (Figure 6.16).

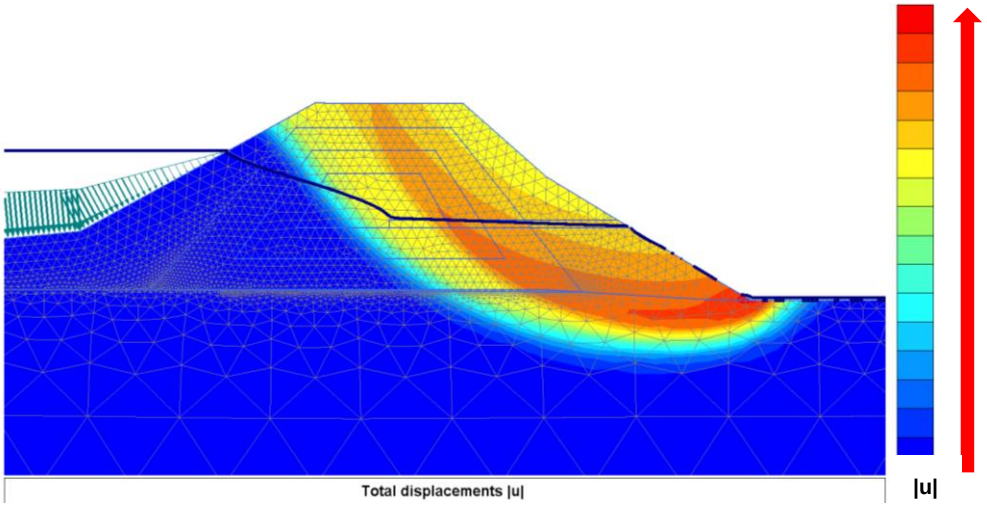

Figure 8.13 Sliding surface after the safety analysis with transient calculation (with changing water level and rain) with burrow at the inner slope

8.5.1.3Burrow at the outer slope in 2014

Finally the burrow with entrance at 35.75 m amsl, assumed for the configuration in 2014, gives the lowest results in terms of safety factor. As described in paragraph 6.5.4, the burrow affects the pore pressure distribution for steady state and transient flow analyses.

In the transient flow analysis, the safety factor decreases from 1.812 obtained with the analysis without burrows to 1.412 when implementing the burrow. Thus the influence to global instability is higher for a burrow placed below groundwater table than above.

The failure plane (Figure 8.14) is shallower compared to the ones previously encountered after the transient flow analysis: it start at the top of the levee and not along the outer slope, and it ends at the inner toe.

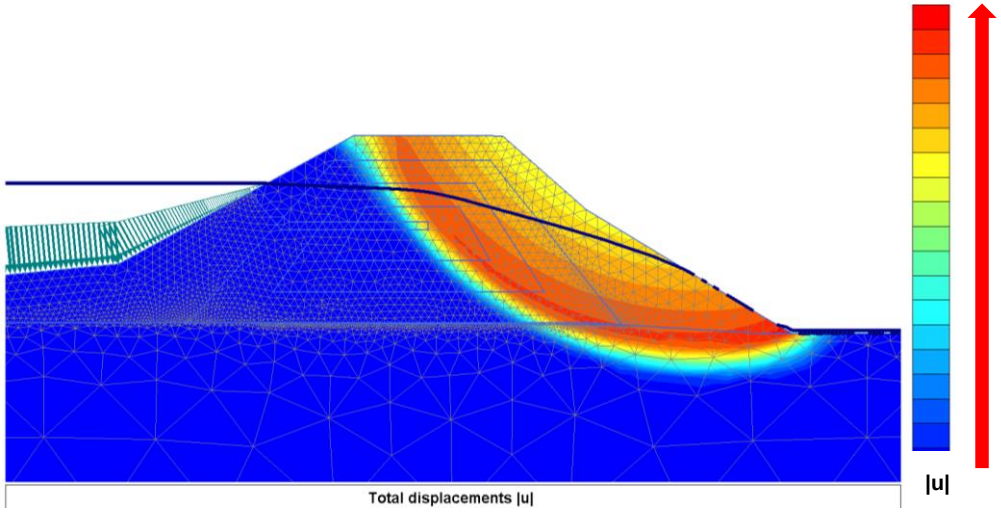

Figure 8.14 Sliding surface after the safety analysis with transient calculation (with changing water level and rain) with burrow at the outer slope assumed in 2014

In conclusion, the safety factors obtained with all of the 2dimensional transient flow analyses presented above are largely above 1. As a consequence, the presence of single burrows is not

sufficient to cause the failure. The interaction and contribution of the burrows is then investigated in the following paragraph.

8.5.2 Analysis with animal burrows in Plaxis 3d

The value of SF when burrows are implemented in the transient flow analyses are just slightly lower than the safety factor obtained when cavities are not taken into account. Moreover, the additional entrance and tunnels present in 2014 compared to the assumed scenario in 2012 doesn't influence the results.

When looking at the failure surface for the system in 2012 (Figure 8.15), high displacements are localized below the entrances at the inner slope. This is the only evident influence of the presence of the cavities to the results.

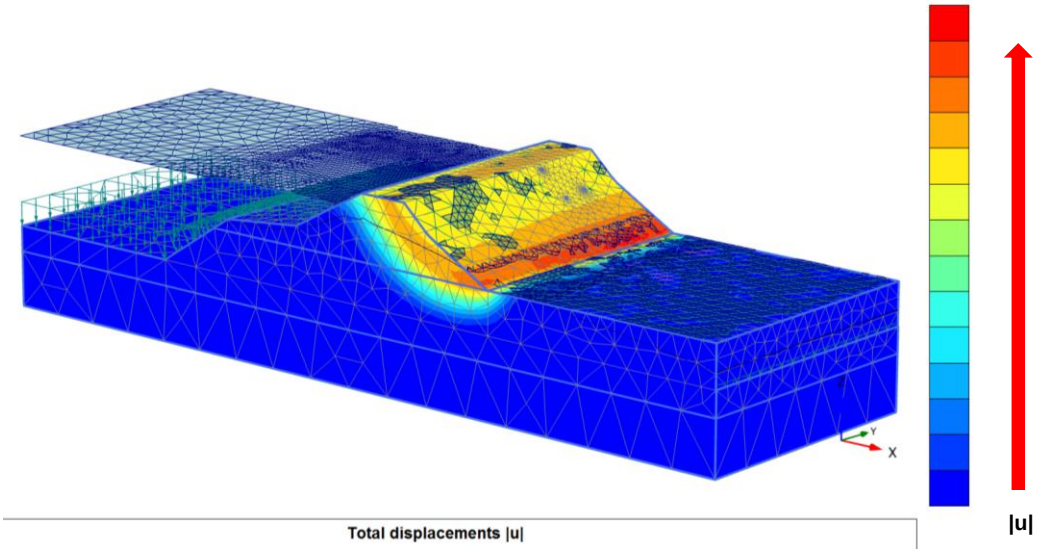

Figure 8.15 Sliding surface in the model for the transient flow analysis with implementation of rain and water level changing in the river with PLAXIS 3D.

The same failure plane and displacements are obtained as result of the analysis for the scenario of animal burrows assumed in 2014.

As a conclusion, animal burrows don't give a significant influence to groundwater flow (paragraph 7.6) and dike stability in three dimensional analyses. In particular, the modification of pore pressures is localized at the burrow entrances and not affected by the geometry and connection of the underground network.
In order to gain a better understanding on the quantity of missing volume due to the cavities and so to its influence to the groundwater flow, a simple calculation is proposed. The analysed volume of the levee is equal to 430m^3, that is the dike body along the 10 meters where the breach happened. The volume excavated by the burrows is equal to 1 m^3 for the scenario in 2012 and to 1.50 m^3 for the one in 2014. As a consequence the missing volume, which has been excavated by the burrow, is negligible compared to the total volume under analysis. The relatively small influence of the burrows to the stability of the dike can be so explained.

8.6 Summary

In order to assess macro-stability of the inner slope, Finite Element Method is preferred to Limit Equilibrium Method: it allows performing three dimensional analyses and coupling deformation and

groundwater flow. In particular, three dimensional analysis are performed since the short width of the breach reflects a three dimensional failure mechanism; moreover, the nature of animal burrows and their network is 3dimensional. Coupled deformation – groundwater flow analysis is also performed: it is a time-dependent analysis that calculates deformation and pore water pressures. The case under analysis depends on varying water level and rainfall which influenced the pore water pressure distribution inside the dike body.
PLAXIS 2D and 3D are the computer programs used for the analyses.

First of all, the analyses are carried out without animal burrows for steady state and groundwater flow solutions. The safety factor obtained with the $\varphi - c$ reduction method is equal to SF=1.333 for the steady state calculation and SF= 1.812 for transient flow analysis. Steady state solution gives lower results than transient flow because of the higher pore water pressures and so the lower effective stresses. Moreover, the rain gives a substantial influence to the results: when it is not considered in the transient flow analysis, the value of safety factor considerably increases to SF=2.157.

Only transient flow analysis in carried out with 3D calculation. When considering both water level changing in the river and rain, the safety factor results SF=2.616. Therefore, the 3dimensional calculation gives higher results than the 2d analysis.

Then, the animal burrows are implemented in the analysis. The results of the 2d calculations for cross sections along the burrow entrances show that the burrows recorded in the Investigative Evaluation Report and located at the outer and inner slope have relatively small influence to the results. Instead, the burrow assumed in the scenario for 2014 and situated along the outer slope below maximum water level, decreases the safety factor to 1.173 for steady state solution and to 1.412 for the transient flow: this burrow gives the biggest impact to the macro-stability of the inner slope.

Finally, the influence of the whole underground network is assessed with three dimensional calculations for the two proposed scenario in 2012 and 2014. However, both of the analyses show no influence of the system to the stability: the safety factor only slightly decreases compared to the case without burrowing.

8.7 Conclusion

8.7.1 Macro-stability for the levee of San Matteo

The dike proves to be safe to macro-instability: the safety factor is largely above one for all the performed analyses (2d and 3d, steady state and transient flow, with and without animal burrowing). Moreover, the sliding surfaces for all the performed analyses have similar trend, going from the crest of the levee till the inner slope, where highest displacements are recorded. The failure planes obtained with macro-instability are larger and lower than the one observed by the witnesses during the event and that led to the breach (paragraph 2.3.1). For this reason, it can be concluded that sliding of the inner slope was unlikely the mechanism leading to the breach.

8.7.2 Influence of animal burrows on macro-stability

The analyses performed with PLAXIS 2D show that animal burrows can influence macro-stability of the inner slope, depending on their position along the outer and inner slope.

Burrows located at the outer slope increase the probability of instability of the inner slope by raising the pore pressures and so decreasing the effective stresses inside the dike body. Their effect increases as their entrance along the outer slope is deeper.
Burrows with entrance along the upper part of the slope do not affect the results (case 1 in Figure 8.16). Lower burrows (case 2) intercept the phreatic line and increase the pore water pressures, so decreasing the effective stresses and the shear resistance. As a consequence, the safety factor SF reduces compared to the case of no burrow. Finally, SF significantly reduces as the entrance is below the reached water level (case 3).

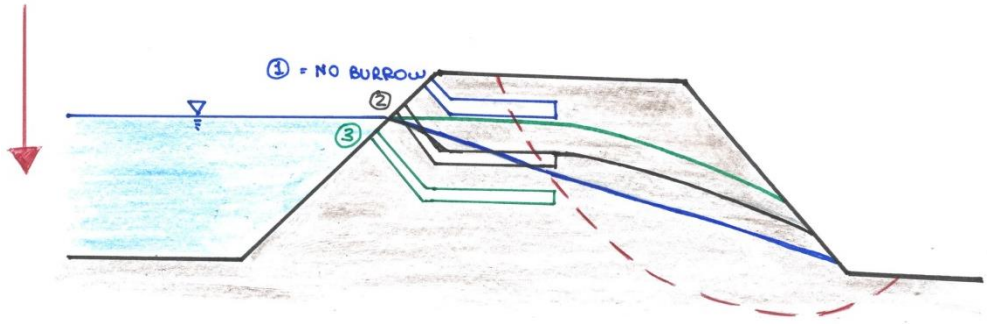

Figure 8.16 Influence of animal burrows with entrance along the outer slope to macro-instability of the inner slope. The sliding surface is indicated by the red dashed line.

The presence of a burrow at the inner slope can have different effects on macro-stability according to its position.
If the entrance is located in the upper part of the inner slope (case 1), the factor of safety is not influenced by the presence of the burrow. If the burrow intercepts the water level and raise the values of pore pressure inside the dike body (case 2), the additional weight of water and the raise of water pressures contribute to the sliding and so decrease the factor of safety.
A burrow with entrance at the lower part of the inner slope (case 3) can increase the SF for macro-stability compared to the case without any burrows or with entrances at the outer slope. As a matter of fact, it acts as a drain, by lowering the water table in the centre of the levee and so reducing the pore pressures. As a consequence the resistance shear strength along the sliding plane (red dashed line in the figure) increases and so also the factor of safety.

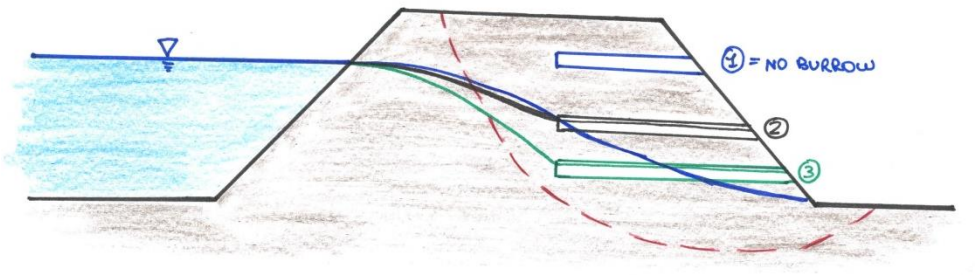

Figure 8.17 Influence of animal burrows with entrance along the inner slope to macro-instability of the inner slope. The sliding surface is indicated by the red dashed line.

The above considerations refer to two-dimensional analyses: the burrows are assumed infinitely long in the longitudinal direction. Parallel systems of burrows with entrances located next to each other

along the slope, which have been recorded in the past, can be described with a two dimensional analysis.

However, the underground networks assumed for the dike of San Matteo and considered in the three analyses hardly affect the macro-stability of the inner slope. As a matter of fact, the amount of excavated volume (1/1.50 m^3) is minimal compared to the total volume under analysis (430m^3, which refers to the failure mass).
In conclusion, underground systems with a large amount of excavated volume in a certain location can there create macro-stability, rather than wide systems with few tunnels and a small digged volume compared to the amount of material of the dike.

8.7.3 3d analysis

As previously described in paragraph 7.8.1, 2d analyses are preferred to 3d because of high amount of the computational time that three dimensional calculations require and the consequent lower quality of the mesh used.
The performed 3d analysis corresponds to a 2d calculation without the implementation of rain and with a bad mesh refinement (paragraph 8.4.5.). As a consequence, the safety factor is much higher than the 2d analysis.

9 Micro-instability and Internal Erosion

9.1 Introduction

In chapter 3, it has been concluded that possible failure mechanisms for the breach of the levee of San Matteo could have been: Sliding of the Inner Slope, Micro-instability or Internal Erosion. After analysing the groundwater flow for 2d and 3d analyses (Chapter 6 and 7), macro-stability analyses have been performed with the $\varphi - c$ reduction method implemented in PLAXIS (chapter 8), concluding the sliding of the inner slope wasn't the failure mechanism leading to the breach of San Matteo.
Consequently, the current chapter investigates what failure mechanism happened between micro-instability and internal erosion.

9.2 Micro-instability

As introduced in Paragraph 3.3, micro-instability occurs when there is a seepage point above the inner toe and the forces created by the flow exceed the resisting shear resistance.

In all the analysed cases, the phreatic level for the steady state solution exits in a point placed 1.5 meter above the toe of the dike (chapter 6 and 7): the seepage could cause micro-instability.

However, it is the transient flow solution which simulates the conditions when failure took place, rather than the steady state analysis. The solution given by the transient calculation presents the water level crossing the dike body, reaching the layer underneath the embankment and finally exiting at the inner toe of the dike (Figure 9.1). The intense rain locally hits the surface, increasing the pore water pressures and so raising the water table at the inner side. However, no real seepage point, which exercises seepage forces against the inner slope, is present and could cause micro-instability.

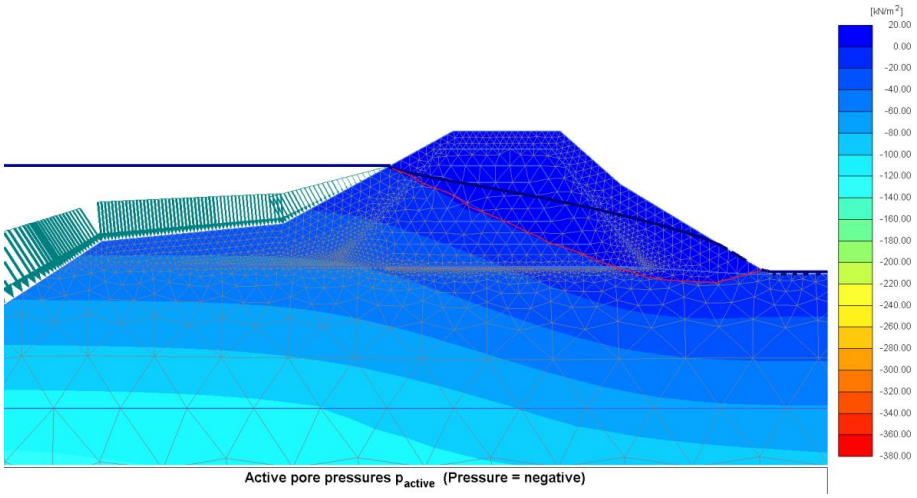

Figure 9.1 Pore water pressure distribution for transient flow analysis with PLAXIS 2D, without animal burrowing. The phreatic of the steady state solution is indicated by the thick blue line and the water table at the end the transient flow analysis is indicated by the red line.

The trend just described is common for all the analyses in 2d/3d and with/without animal burrow, with the only particularity of the water level at the end of the 3d transient flow analysis, which remains below the surface at the inner side.

In conclusion, the water table at the end of the transient flow analysis exits at the inner toe of the dike or it remains below it. No seepage point and forces against the inner slope are present, excluding so micro-instability as failure mechanism for the levee of San Matteo.

9.3 Internal Erosion

The current paragraph investigates the possibility that internal erosion caused the breach of San Matteo. The mechanism would have been facilitated by the presence of animal burrows: water, flowing through the cavities, would have eroded the surfaces and so caused the enlargement of the cavities (paragraph 3.4).

The possibility of internal erosion to have caused the breach of the levee of San Matteo is investigated through the approach derived by the Hole Erosion Test, which is introduced in the following paragraph.

9.3.1 Hole Erosion Test

The failure of the Truckee Canal Embankment (2008) due to a large network of animal burrowing was the incentive for performing Hole Erosion Test (HET) by the U.S. Department of the Interior (Denver, Colorado), in order to gain a better understanding on the influence of animal burrows to piping. The results of these tests present an approach for investigating the growth of a pipe with time due to internal erosion.

The test consists on the analysis of surface erosion on a cylindrical sample of soil with a perforated hole along the longitudinal axis of the cylinder; the hydraulic heads at the inlet and outlet ends are kept constant (Figure 9.2).

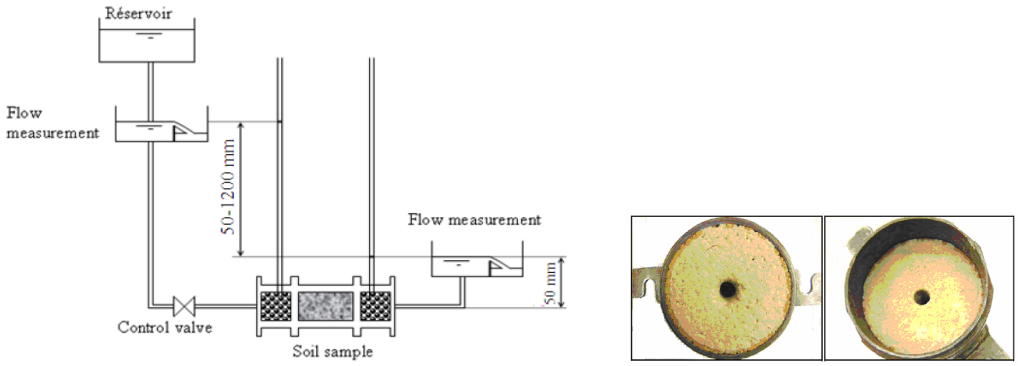

Figure 9.2 Scheme of the experimental setup (left) and soil sample before the tests (right) (Bezzazi et al., 2010)

Bezzazi et al (Bezzazi et al., 2010) have presented a simplified analytical model to the Hole Erosion Test which estimates the evolution of the inner tube radius as a function of time.
Several assumed hypotheses simplify the problem: the surface erosion is considered as a one dimensional phenomenon and the time is the only dependant variable, while all the other quantities are uniform.

Surface erosion starts for $\Delta P \geq \frac{2L\tau_s}{R_0}$, that is when the pressure difference ΔP (Pa), calculated from the hydraulic heads at the inlet and outlet ends, is greater that the critical pressure. R_0 (m) is the initial radius of the tube, L (m) is its length and τ_s (Pa) is the critical shear stress needed to initiate erosion.

The inner tube radius enlarges in time along the cavity according to the following first order linear differential equation:

$$R(t) = \left(R_0 - \frac{2\,L\,\tau_s}{\Delta P} \right) \exp\left(\frac{c_{er}\,\Delta P}{2\rho_d L}\, t \right) + \frac{2L\tau_s}{\Delta P} \qquad (9.1)$$

where c_{er} (s m^{-1}) is a surface erosion coefficient and ρ_d (kg m^{-3}) is the soil density. The surface erosion coefficient, which varies among several orders of magnitude, indicates the ease of the material to erode. Instead, the Erosion Rate Index I_{HET} is expressed with integer numbers ranging from 1 to 6: it is equal to 1 for soils which erode extremely rapidly, while it is 6 if the erosion is extremely slow (Erdogan and Wahl, 2008). The relation between the two parameters is: $I_{HET} = -\log_{10} c_{er}$.

9.3.2 Internal erosion in the levee of San Matteo

The current paragraph applies the approach derived by the Hole Erosion Test for the levee of San Matteo in the conditions that led to the breach.

As previously described, when the water level in the river covers the lower burrow entrance at the outer slope and the burrow is connected to the inner slope, a pressure difference develops between the outer and inner side. If then this pressure difference overcomes the critical shear stress, internal erosion starts and causes the hole to increase.

The scenario used for the analysis of internal erosion corresponds to the network assumed in 2014: a burrow entrance is placed at 35.70 m amsl, under the maximum water level that led to the breach (entrance 5 in Figure 4.10). This burrow is connected to the lower burrow placed at the inner slope (entrance 2 in Figure 4.10) through a central tunnel which longitudinally crosses the levee. The total length of the cavities connecting them is approximately 20meters.

The initial radius R(0) is 0.2 meter, the soil density ρ_d is obtained as ρ_d=Y/g (kg/m^3) and the critical shear stress is τ_s=50 Pa , which is a value found in the literature for similar soil (Bonelli et al., 2006). The soil of the levee is diggable and erodible as proved by the animal burrowing activity, but it also mantains some erosion resistance while standing after the same burrowing activity: it is then assumed I_{HET}=3.8, as suggested in the literature (Erdogan and Wahl, 2008).

R(0) (m)	L (m)	ρ_d (kg/m^3)	τ_s (Pa)	C_{er} (s m^{-1})
0.2	20	1989	50	1.58E-04

Table 9.1 Input parameters for analysis of Internal Erosion.

The pressure loss is equal to 0 until the water level is below the entrance of the tunnel. At 0:00 on 19-01-2014 the water in the river is at the same level of the entrance of the burrow at the outer slope (Figure 9.3); the water level then increases and water enters into the cavity. The pressure difference ΔP (Pa) between the entrances at the outer and inner side increases in the following hours as the water level in the river raises. ΔP is updated at every time step according to:

$$\Delta P = \Delta\psi\, \rho_w g \qquad (9.2)$$

with

$$\psi = \varphi - z \qquad (9.3)$$

Where Δψ is the pressure head between the outer and inner side (m), ρ_w the water density (kg/m^3), g the gravitational acceleration (m/s^2), z the elevation (m) and φ the groundwater head (m).

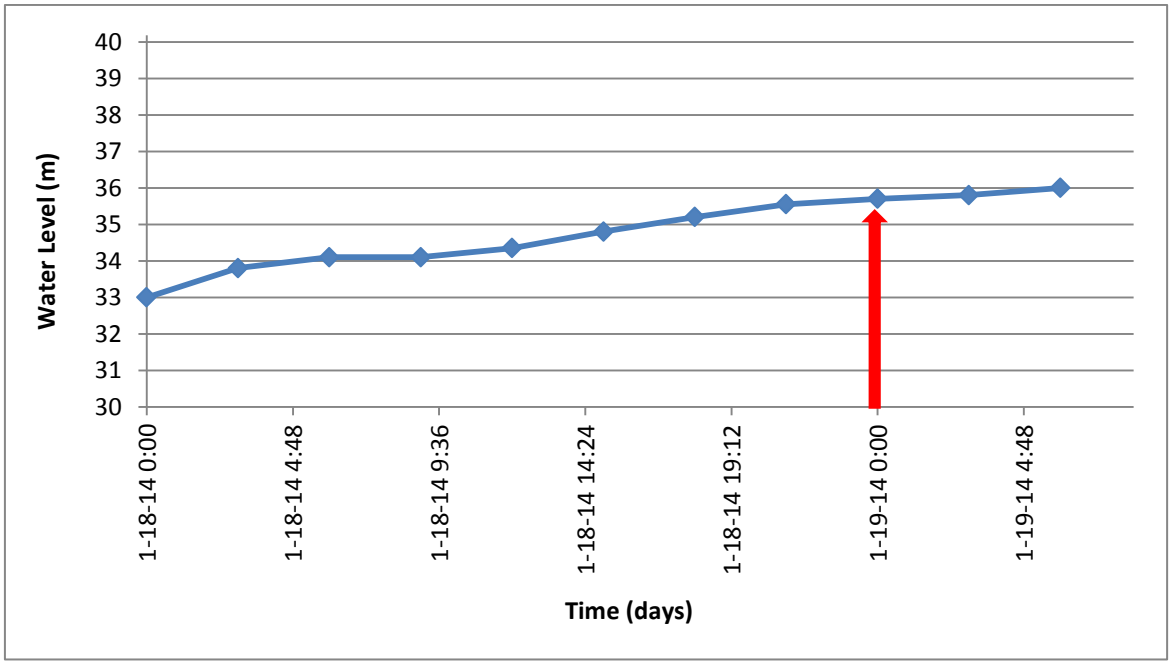

Figure 9.3 Water level in the river before the breach. the red arrows indicates the moment when the water is higher than the entrance of the burrow at the outer slope at 0:00 on 19-01-2014: the water start flowing into the cavity.

Updating Δp at every time step, the radius of the tunnel increases according to equation (9.1). When at 0:00 on 19-01-2014, the water overcomes the entrance of the burrow, erosion starts. The phenomenon develops in time: at 3:00 the radius is equal to 0.60m and it reaches dimension of 1 meter at 04:30 (Figure 9.4).

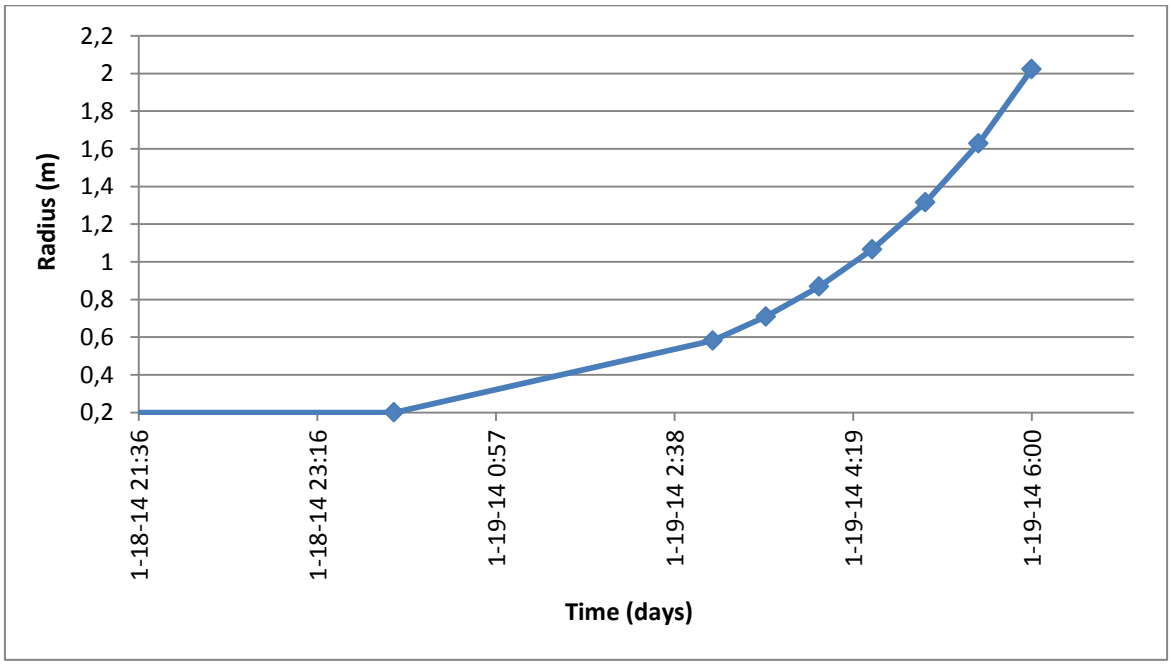

Figure 9.4 Development of Radius with Time due to Internal Erosion, using the approach derived by the Hole Erosion Test.

When the water level in the river is above the entrance of the burrow at the outer slope and once the burrow is filled of water, erosion immediately starts: as a matter of fact, the pore pressure difference ΔP between burrow entrances at the inner and outer slope is five times larger than the critical pore pressure difference equal to $\frac{2L\tau_s}{R_0}$. Later, the erosion develops with time and water level in the river, as shown in Figure 9.4.

In conclusion, the results suggest that internal erosion started when the water level overcame the burrow entrance filling thus the cavity. The enlargement of the burrows would have then caused the breach to develop.

9.3.3 Considerations about the accuracy of the method

The analysis performed in the previous paragraph for the estimation of the evolution of the radius with time depends upon parameters which are not known and so reasonably assumed. For this reason, the results are not considered precise and they depend on the uncertainty related to the input parameters.

Thus the current paragraph aims to evaluate the influence of the input parameters in the results.

First of all, the influence of the Erosion Rate Index on the resulting radius is evaluated in Figure 9.5. High erodible materials (lower I_{HET}) present a final radius which is order of magnitude bigger than those obtained with less erodible soils (higher I_{HET}). The sensitivity of the results on this parameter suggests its calculation beforehand through laboratory tests in order to know its value accurately.

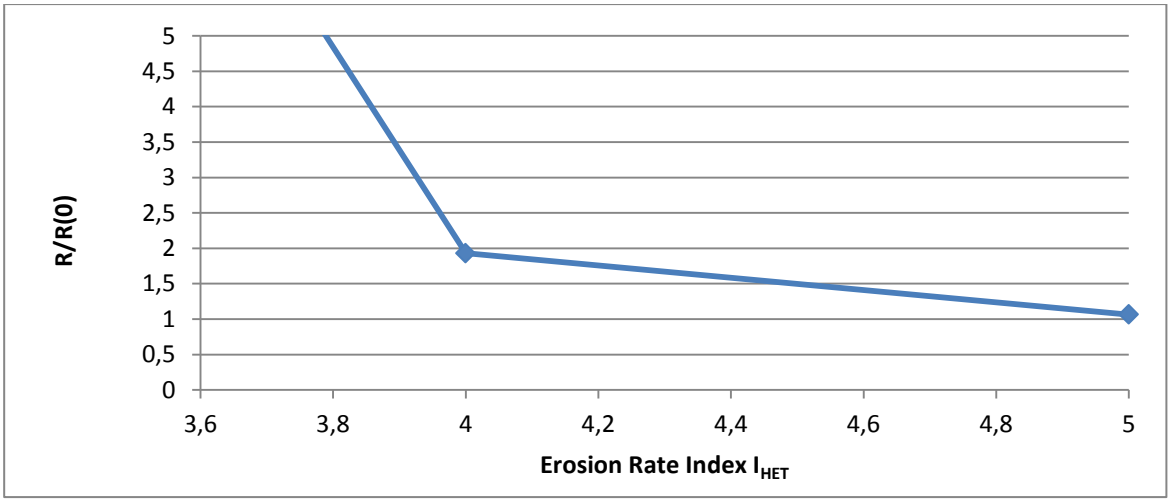

Erosion Rate Index I_{HET}	R/R(0) (m)
1-2-3	>>3
4	1.93
5	1.06

Figure 9.5 Variation of the resulting radius for different Erosion Rate Index used as the input of the analysis. All the other parameters are kept constant. The shear resistance τ_s is 50Pa, the length L is 20m, the initial radius R(0) is 0.20m and the pressure difference is evaluated at 3:00 on 19-01-2014.

The effects of length and initial radius on the results are illustrated in Figure 9.6. Shorter tunnels give faster erosion. In such a way, a burrow connecting the entrance at the outer slope to another entrance located at its opposite site along the inner slope is more dangerous for internal erosion than a widely

extensive network connecting the entrances at the inner and outer slopes. Finally, initial smaller diameters also fastener the erosive process (Figure 9.6).

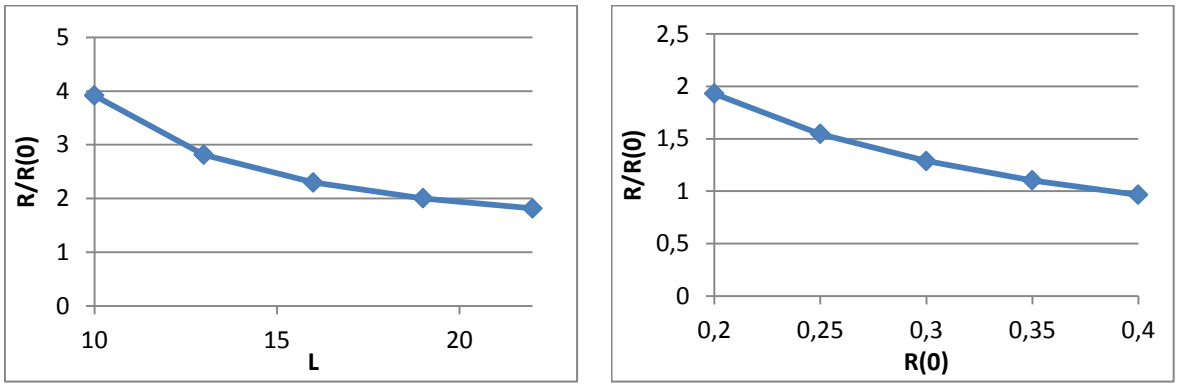

Figure 9.6 Variation in the resulting radius for different length (left) and initial radius (right) used as the input of the analysis. All the other parameters are kept constant. The shear resistance τ_s is 50Pa and the pressure difference is evaluated at 3:00 on 19-01-2014. On the left case the initial radius R(0) is 0.20m while on the right case, the length L is constant and equal to 20m.

Instead, the shear resistance has a limited effect on the results. When considering its range between 0.01 to 100 Pa, the resulting radius after erosion is equal to 2.13 times the initial radius for the less resistant material, while it is equal to 1.72 times R(0) for τ_s equal to 100 Pa. Its influence in the results is less relevant than the other input parameters assumed in the analysis.

As a conclusion, the input parameter that gives the highest effect in term of internal erosion is the Erosion Rate Index, that is the erodibility of the material. Moreover shorter tunnels with a limited diameter are also more prone to erosion, while the shear resistance gives less influence in the development of the hole.

9.4 Summary

After excluding Instability of the Inner Slope as the failure mechanism leading to the breach of San Matteo (chapter 8), the current chapter has investigated Micro-instability and Internal Erosion.

9.4.1 Micro-Instability

Micro-instability for the levee of San Matteo is evaluated by looking at the groundwater flow calculations: the failure mechanism occurs when there is a seepage point exiting above the inner toe and the forces created by the flow exceed the resisting shear resistance.

The results in term of pore pressures at the end of the transient flow analyses performed with PLAXIS 2D and 3D, with and without animal burrowing, present no seepage point along the inner slope. The water flow doesn't exercise forces against the inner slope which could start eroding it. For this reason, micro-instability unlikely occurred.

9.4.2 Internal Erosion

The approach derived by the Hole Erosion Test, which estimates the evolution of the radius of a tube as a function of time, has been used for evaluating if internal erosion caused the failure of San Matteo. This failure mode is initiated in case of a burrow, which connect the outer and inner slopes, is completely filled of water.

The analysis considers the entrance below maximum water level assumed for the network scenario in 2014. On 18th January 2014 at 0:00, the water level in the river exceeds the burrow entrance. According to the model, the pressure difference between the burrow at the outer slope and the lowest burrow with exit at the inner side is five times bigger than the critical pressure difference to initiate internal erosion. The mechanism starts and evolves with time: at 3:00 the radius increases from its initial 0.20m to 0.60m, reaching dimension of 1 meter at 04:30.

The accuracy of the model depends on the uncertainty of the input parameters. In particular, the erodibility of the material gives the highest influence in terms of results. Moreover, erodibility decreases with higher length and dimension of the tunnel.

9.5 Conclusion

9.5.1 The breach of San Matteo

Internal erosion was the likely mechanism leading to failure. The assumed underground network has entrance located at 35.7m amsl and so below the maximum water level reached during the night of the failure: at midnight of the 19 January 2015, the water level overcame its entrance. The tunnel is connected to the inner slope so that water flows into the tube and the hydraulic gradient between the inner and outer slope creates erosive forces acting against the burrows surface.

The approach used, which is derived by the Hole Erosion Tests, shows that internal erosion starts just when the water level is above the burrow entrance and quickly develops increasing the dimension of the burrow.

9.5.2 Influence of animal burrows on Micro-Instability

The presence of burrows can affect Micro-instability. Their influence is evaluated in the current paragraph for steady state condition.

Burrows with entrance along the outer slope can increase the probability of micro-instability to occur. If they are located in the upper part of the dike and they do not intercept the phreatic line (case 1 in Figure 9.7), their influence is null and the probability of micro-instability is equal to the case of no burrow. As the entrance is lower, micro-instability can occur: lower burrows increase the pore water pressures, so that the phreatic line presents higher exit point along the inner slope (case 2 and 3).
Finally, if the phreatic line exits below the inner toe when no burrows are present, the introduction of cavities can lead to an exit point along the inner slope so that micro-instability can occur. As the burrow entrance along the outer slope is lower, the resulting exit point is higher so increasing the risk of micro-instability.

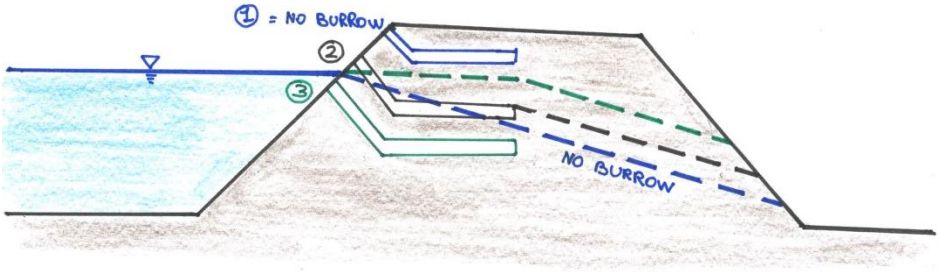

Figure 9.7 Influence of animal burrows with entrance along the outer slope to micro-instability.

Also burrows with entrance along the inner slope can influence micro-instability: erosion starts at the burrow and proceeds backwards towards the outer slope.

If the entrance is located in the upper part and it doesn't have any influence to the water level (case 1 in Figure 9.8), the probability of micro-instability is not affected by the burrows.
As the entrance along the inner slope is placed lower, the slope of the water level inside the dike core is higher, so increasing the seepage forces and the possibility of micro-instability to occur.

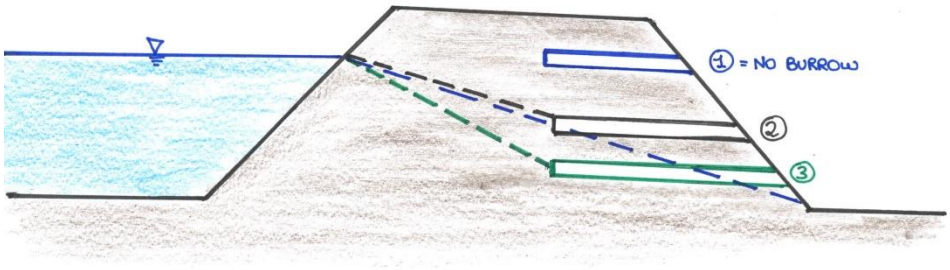

Figure 9.8 Influence of animal burrows with entrance along the inner slope to micro-instability.

9.5.3 Influence of animal burrows on Internal Erosion

The current paragraph presents the conditions for which burrowing networks can cause Internal Erosion.

First of all, as represented by the underground system in Figure 9.9, the entrance of the burrow along the outer slope is placed below the reached water level so that water enters and completely fills the tunnel. Since the development of internal erosion depends on the difference of pressure between the inner and outer side, lower is the burrow at the outer slope and more time it is placed below the water level for transient flow conditions, higher is the risk of internal erosion.

Second, the burrow is connected to the inner slope, so that water flows from the outer to the inner slope, exercising erosive forces along the tunnel surface. Internal Erosion is facilitated by shorter tunnels. For this reason, the most danger is represented by burrows going from the outer directly to the inner slope, with the shortest distance between the entrances.

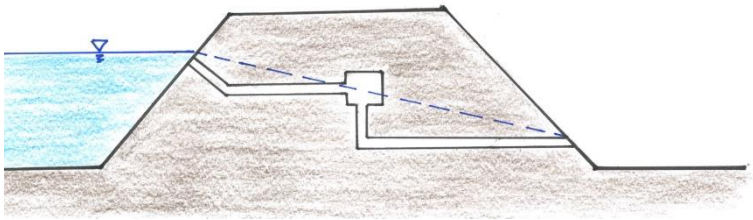

Figure 9.9 Burrowing network which can cause Internal Erosion.

Finally, the most important factor contributing to Internal Erosion is given by the ease to erosion. It can be tested in laboratory and described by erodibility parameters, such as the Surface Erosion Coefficient c_{er} (s m^{-1}) and Erosion Rate Index I_{HET} (-). In particular, animals excavate in erodible and diggable soil, which is so also prone to internal erosion.

10 Conclusions and Recommendations

10.1 Conclusions

The current thesis has analysed the failure of the levee of San Matteo (Italy, 19th January 2014) previously investigated through the Investigative Evaluation Report ("*Relazione tecnico-scientifica sulle cause del collasso dell'argine del fiume Secchia avvenuto il giorno 19 gennaio 2014 presso la frazione San Matteo*") which revealed the possible influence of animal burrowing in the creation of the breach. The study gains a better insight on the influence of animal burrows on groundwater flow and stability analysis for general cases and for the specific failure of San Matteo. The conclusions to the research questions, introduced in paragraph 1.5, are presented below.

10.1.1 Main questions

What was the failure mechanism leading to the breach of the levee of San Matteo?

On 19th January 2014 at 6am a breach happened in a section of the levee of San Matteo along the Secchia river. Considerations lead to exclude some failure mechanisms among the ones that could have caused the breach.

First of all, the water level in Secchia river was at 36 m amsl while the dike crest is at 37.30m amsl, so that overflow can be excluded. Second, before the breach, the river presented ripples without crests: waves were negligible and so not significantly high to cause overtopping. Third, sliding along the base of the dike body is excluded for type of soil and testimonies about the dimension and characteristics of the breach. Moreover, the water level in the river was rising until its peak, so no sudden draw-down could have caused sliding of the outer slope. Finally, other mechanisms, such as erosion at the outer slope, foreshore erosion, settlement, drifting ice and collision by vessels are not significant for the case under analysis;

For this reasons, the possible failure mechanisms that could have taken place and have been analysed in the current study are: Instability of the Inner Slope, Micro-Instability and Internal Erosion.

In the Investigative Evaluation Report, entrances of animal burrows along the section that failed on 19th January 2014 are illustrated. They belong to European badger, Foxes and Crested porcupine. The entrances, located along the inner and outer slope, have maximum distance of 10meters: it is likely that they form a unique connected system with the function of a main sett of reduced dimension. Moreover, the Investigative Evaluation Report presents the burrow entrances deduced by aerial photos of the levee in 2010 and 2012; when the breach took place, in 2014, the system was likely more developed with a new entrance located below the maximum water level at the outer slope and connected to the main sett.
Consideration about the breach characteristics lead to assume the possible influence of animal burrowing on the failure of the levee of San Matteo. First of all, the breach was approximately 10 meters long and localized at the same location of the burrows entrances and so also of the underground system digged by the animals. Moreover, the weakness of that specific spot is confirmed by the fact that, after the breach, the water level in the river reached its peak but there were no breaches in other locations of the levee. Finally, the depth of the breach according to witnesses corresponds to the depth of the assumed realistic burrow network.

The analyses performed in the current study consider the possibility of Instability of the Inner Slope, Micro-Instability and Internal Erosion to occur, with and without animal burrowing.

First, the dike proves to be safe to macro-instability: the safety factor is largely above one, with and without animal burrowing. Moreover, the obtained sliding surfaces for all the performed analyses, which go from the crest of the levee till the inner slope, are larger and lower than the one observed by the witnesses during the event and that led to the breach. For this reason, it can be concluded that sliding of the inner slope was unlikely the mechanism leading to the breach.
Second, in all the performed transient groundwater flow analyses, with water level changing in the river and rainfall which happened before the event, the water level presents no seepage point exiting above the inner toe. Also when implementing the animal burrows, the water flow doesn't exercise forces against the inner slope which could start eroding it. For this reason, micro-instability unlikely occurred.

Finally, internal erosion was the likely mechanism leading to failure. The connected underground system with burrows running from the outer to the inner slope and the entrance of a burrow located below maximum water level gave the conditions for water to fill the burrow and erode the tunnels in the whole connected network.

How do preferential paths due to animal burrows influence the resulting water pressure distribution?

The burrows are preferential flow paths which intercept the phreatic line and the resulting pore pressure distribution. The position of the cavities in the levee determines how they influence it. Figure 10.1 illustrates their effect to the groundwater flow for steady state solution.

Burrows located at the highest part of the dike do not influence the pore water pressures. If instead their entrance is located along the outer slope, they raise the pore pressures as they are deeper. In particular, in case of burrows with entrance below the water level, the results of the transient flow analysis present water pressures and water table approaching the steady state solution.

If the burrows have entrance along the inner slope, their negative or positive depends on their position. If the burrow is located near the inner toe, the steady state analysis revels that it can act as a drain so decreasing the values of pore pressures inside the dike body (positive influence). A higher entrance above the toe can instead have a negative influence, intercepting the water table at the end of the burrow in the centre of the levee body and so raising the values of pore pressures. However, is case of transient flow analyses, the burrow may not be intercepted by the water level and so have no influence in the results.

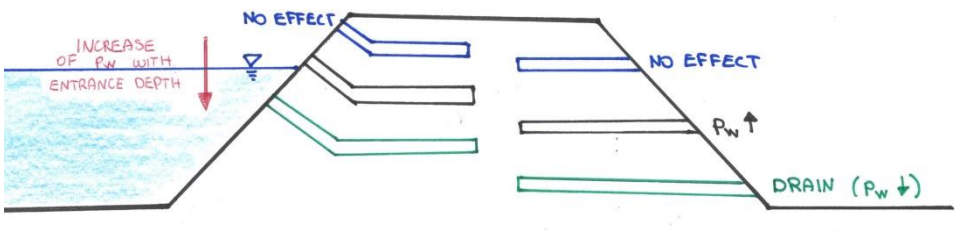

Figure 10.1 Influence of burrows withe entrance along the outer and inner slope to the groundwatre flow for steady state solution.

How can animal burrows influence dike safety?

Animal burrows introduce preferential flow paths and they represent heterogeneities of the dike body. For this reason, they also influence the failure mechanisms of a levee. The current study has

investigated the influence of animal burrowing in Sliding of the Inner Slope, Micro-instability or Internal Erosion, since these failure mechanisms were analysed for the breach of San Matteo. These mechanisms and the influence of the animal burrows are here introduced.

First, the presence of animal burrows can cause macro-instability. The heterogeneity that they introduce alter the phreatic surface: if it rises, the increase of water pressures causes the decrease of effective stresses. The shearing resistance is consequently reduced and, if the actual shear stress exceeds it, macro-instability of the inner slope occurs.
Second, the presence of animal burrows at the inner or outer slope can increase the phreatic line so that it exits at a point above the inner toe. If seepage flow develops and forces created by the flow exceed the resisting shear resistance, particles are flushed away from the soil matrix and erosion develops backwards. Therefore, micro-instability occurs.
Third, if the water level in the river overcomes the entrance of a cavity placed along the outer slope, water flows into the entrance tunnel and fills it. If then this tunnel is connected to the inner slope, a pressure difference develops between the outer and inner exits. The seepage forces which act along the surface can erode the particles and remove the subsurface soil, so developing the mechanism of "internal erosion as evolution of defects".

The development of Sliding of the Inner Slope, Micro-instability or Internal Erosion depends on the position of the burrows and so their entrances along the slopes.
First, burrows placed at the highest part of the dike give no influence to the safety, since they do not affect the water level and the reduction of weight that they introduce is negligible.
Second, burrows located at the outer slope give a bigger effect to the three failure mechanisms as they are lower. They raise the water level and pore water pressures inside the dike body: they can lead to macro-instability, for the consequent decrease of effective stresses, and micro-instability, if there is an exit point along the inner slope. Internal erosion, instead, develops when the burrow is placed below the water level and water exercises high pressures during the time required for the enlargement of the cavity. For this reason, lower burrows facilitate also internal erosion.
Finally, burrows with entrance located along the inner slope can facilitate different failure mechanisms according to their position. High seepage forces can act against burrows placed near the inner toe, so facilitating micro-instability to occur: the erosion starts at the burrow and proceeds backwards. Low burrows acts as drains, so decreasing the water level and the possibility of macro-instability to occur.
Contrarily, when a higher burrow intercepts the phreatic line, which flows along it, the water pressures rise, so decreasing the effective stresses and adding the water weight inside the sliding plane: macro-instability more likely occurs.
Finally a burrow with exit at the inner slope and linked to the outer slope can cause internal erosion along its cavity.

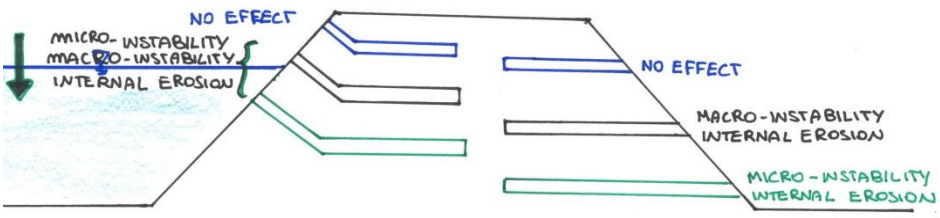

Figure 10.2 Influence of burrows to the failure mechanisms, according to their position along the dike.

10.1.2 Sub-questions

What is the geometry of the burrows under analysis and how can their distribution be defined?

The burrows along the levee of San Matteo were created by European badger (Meles meles) and Crested porcupines (Hystrix cristata) and shared with the Red foxes (Vulpes vulpes).

Their burrows are tunnels with semi-circular (arched) or squashed elliptical form, 0.20 m high and 0.30-0.35 m wide. The entrances are located in the dry part of the levee and the starting tunnel is inclined 40-45° downwards until not more than 1 meter deep underneath the entrance. The tunnels are 5-10 m long; two tunnels intersect at 90° and three tunnels at 120°. At the end of a tunnel or along it, chambers are situated: they can be located in levels of different depths creating a complex 3d structure.

The distribution of the tunnels and chambers can be estimated by knowing the burrow entrances, the excavated volume and the likely geometry of the underground system (Table 10.1).
First of all, the entrances are localized by site investigation or areal photos; the excavated volume can be assumed through the correlation of population dynamics and zoogeomorphic activity (paragraph 4.3.2). Finally the recurrent patterns in the geometry of the underground systems are described in the literature for the animals under analysis.

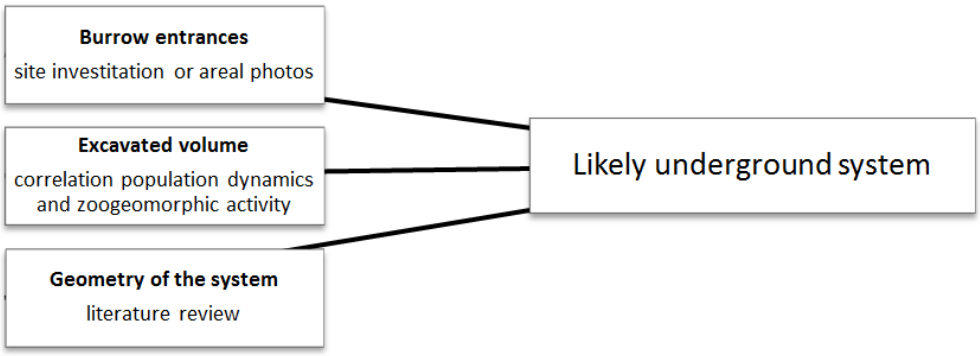

Table 10.1 Estimation of underground system, by knowing burrow entrances, excavated volume and geometry of the system.

What was the critical geometrical distribution of animal burrows for the failure of the case under analysis?

When the breach took place, the burrows in the levee of San Matteo formed a unique connected system with the function of a main sett of reduced dimension.

The Investigative Evaluation Report presents the burrow entrances recorded in 2012. Taking into account the evolution of the underground animal system in time and the correlation between population dynamics and zoogeomorphic activity, the excavated volume in 2014 can be calculated. Likely in 2014 there was an additional entrance at the outer slope, located below the maximum water level and connected to the main sett. In March 2013 a peak of water level in the river was recorded, without leading to any damage to the dike; for this reason, the altitude of the entrance is placed between the peaks in March 2013 and January 2014.

In conclusion, the assumed system is composed by two burrow entrances, placed along the outer slope and connected with two central tunnels (12 and 14m long) to other three entrances along the inner slope. The total excavated volume is 1.582 m^3 and the tunnels length is 50.4 m.

10.2 Recommendations

In order to analyse the risk of dike failure due to animal burrowing in future cases, the following approach of analysis is suggested.

10.2.1 Site investigation and testing

The aim of the field visit is to individuate burrow entrances along the dike and the type of animals responsible for the burrowing activity. It is suggested to perform the site investigation four times during the first year; then, by looking at the recorded data of the four visits, in particular number of entrances and growth rate of the system, the amount and frequency of site investigations needed in the upcoming years is decided.

Before performing the investigation, high vegetation should be removed, in order to ensure good visibility and easily individuate the entrances of the holes. During the site investigator, the inspectors walk along the dike crest and the slopes and individuate the entrances of the burrows. Geophysical methods can also be used in detecting animal burrows (Prinzio et al., 2010).

Once an entrance is recorded, the levee has to be carefully inspected for 150-200meters along the longitudinal direction. In this way, the presence of an underground system can be detected. Moreover, if a burrow entrance is individuated at the outer slope, the opposite inner slope has to be carefully inspected in order to individuate the presence of cavities running from the outer to the inner slope.

In order to recognize the type of animal making the burrows and if these are active or not, it is suggested to the inspector to visit the levee with experts, such as animal scientists or hunters. Particular attention has to be given to the type of vegetation, inclination of the levee slopes and human activity in the area: these factors help in defining the responsible animals. Finally, once the inspector finds an entrance, he/she can estimate the dimensions, direction and depth of the starting tunnel with simple tools such as tape measure and sticks.

In order to perform the following analyses, field and laboratory tests are carried out, giving the required input parameters for the programs. The most important parameter is the permeability of the material, in order to perform groundwater flow analyses. In addition, the internal erosion potential of the material needs to be tested through Hole Erosion Tests (Erdogan and Wahl, 2008).

10.2.2 Desk Study

Animal burrowing network

After the field visit and the definition of the animals responsible of the burrowing activity, the inspector can determine, through literature review, the geometry and patterns of the underground systems that these animals dig.

Second, research helps in defining the population dynamics of the animals in the area, such as the numbers of adults, the age of the system, the sett fecundity and the excavation years. By knowing these factors, it is then possible to estimate the excavated volume, following the procedure illustrated in paragraph 4.3.2.

Finally, the inspector knows the burrow entrances, the likely geometry and pattern of the system and the missing volume: few realistic scenarios for the underground system can be drawn (Table 10.1).

Possible failure mechanisms

Before performing any analysis, the inspector should define the possible failure mechanisms that could take place. A first indication about the possible failure mechanisms is given by the position of the burrow entrances (Figure 10.2).

Internal erosion represents a risk in case of a burrow connecting the outer to the inner slope. The risk increases as the distance between these two entrances is lower and so shorter is the tunnel connecting them. Moreover the results of the performed Hole Erosion Tests give an indication on the potential of the material to internally erode.

If much volume is missing because excavated by the animals, the weakening of whole body represents a problem to the stability of the levee. Particular attention should also be given to entrances located at the outer slope, whose influence increase with the depth. Further indications will be given from the analysis of the groundwater flow and stability with the animal burrows inserted in the dike body.

10.2.3 Analysis

In order to assess the stability of the dike, the burrows can be implemented in the analysis as soil tunnels with same strength of the surrounding material and higher permeability and porosity.

First of all, it is suggested to perform a two dimensional calculation, which over-estimates the influence of the animal burrowing activity, for its simplicity and reduced computational time of the analysis. If then there are several burrow entrances located at the same altitude and close together, the 2dimensional analysis represent a realistic representation of the reality.

The first performed analysis is with steady state condition, considering the maximum water level recorded in the chosen time period (e.g. T=100years) that is required for the safety of the levee. If the animal burrows do not influence the groundwater flow, it can be concluded that they are not dangerous for the dike. If instead they influence the pore water pressures, it is suggested to perform transient flow analysis with scenarios of changing water level in the river and rainfall obtained from historical data in the defined time period (e.g. T=100years). If the animal burrows prove to influence the groundwater flow inside the dike body, it is suggested to intervene and repair the dike.

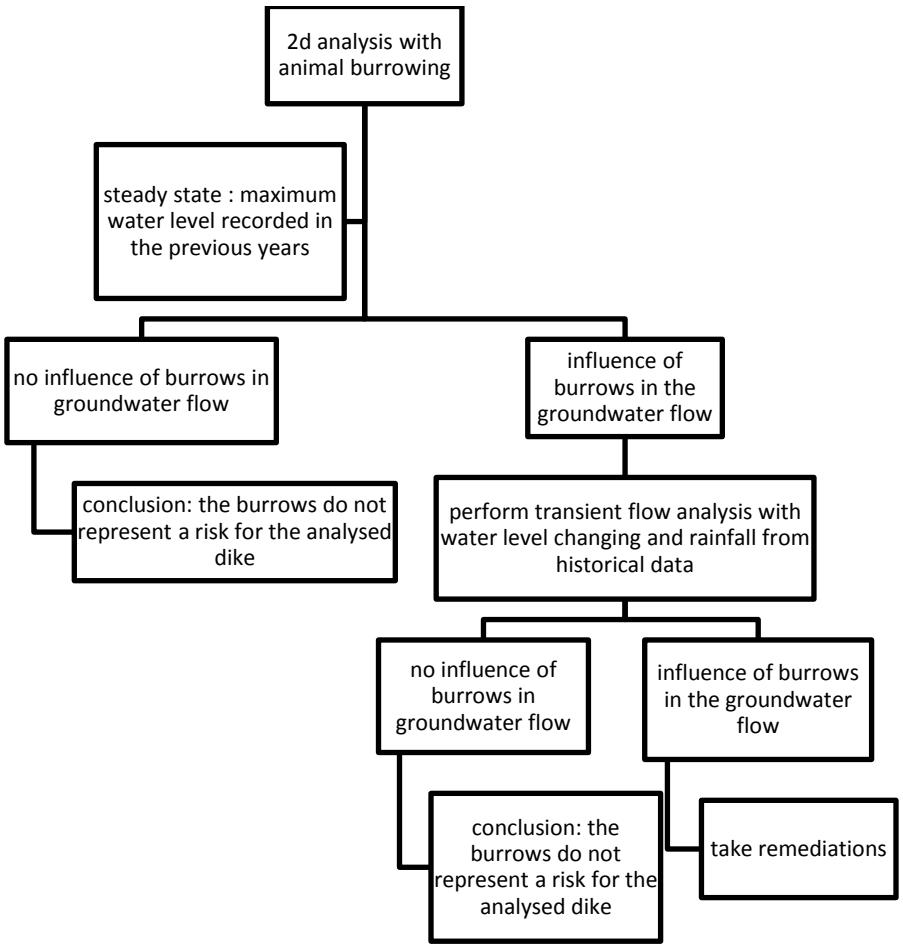

Table 10.2 Scheme flow suggested for the analysis of influence of animal burrows to the groundwater flow inside a dike.

10.2.4 Remediation

If the groundwater flow analyses show the influence of certain animal burrows to the pore pressure distribution, intervention for their reparation is suggested. If, instead, analyses are not performed, it is suggested to give priority in repairing the burrows with lowest entrance along the outer slope or with entrance within two meters from the toe at the inner side. As a matter of fact, they present the highest risk for the safety of the dike under transient conditions.

In order to reduce the influence of animal burrowing to dike stability, soil can be placed on top of the burrow, after a shallow excavation, and then a net above it. However, the risk that animals return in the same location and create a hole near the old ones, in order to have access to the tunnels, is high. Animals can be captured with traps and then moved to places suitable for their survival, while the animals that are not protected species can be hunted.
However, since practical remediation techniques have not been investigated in the current study, the consultation of the International Levee Handbook (Finsbury et al., 2013), which gives indication for the operation and maintenance, is suggested to the reader.

References

1999. *Carta Geologica di pianura dell'Emilia-Romagna - scala 1:250.000* [Online]. Available: http://mappegis.regione.emilia-romagna.it/gstatico/documenti/Schemi_Geo/Schema_Geologico_sintesi.htm.

2005. Technical Manual for Dam Owners, Impacts of Animals on Earthen Dams. FEMA.

2012. Diagnosis of urban flood embankment performance. Deltares.

2013a. *PLAXIS 3D | Tutorial Manual 2013*.

2013b. *Reference Manual | PLAXIS 3D 2013*.

2014. *D-Geo Stability, User Manual*.

ARMITAGE, J. M. 1999. *The initiation of breaching in flood defence embankments due to animal burrowing.* Oxford Brookes University.

BEZZAZI, M., KHAMLICHI, A., VERA, M. P., RUBIO, M. D. C. & OLEGARIO, C. L. 2010. A Simplified Analytical Modeling of the Hole Erosion Test. *American J. of Engineering and Applied Sciences,* 4**,** 765-768.

BONELLI, S. 2006. Interpreting Hole Erosion Tests with a constant flow rate.

BONELLI, S., BENAHMED, N. & BRIVOIS, O. 2006. On Modelling of the Hole Erosion Test. *ICSE, 3rd International Conference on Scour and Erosion.* Amsterdam.

BYRNE, A. W., SLEEMAN, D. P., O'KEEFFE, J. & DAVENPORT, J. 2012. The Ecology Of The European Badger (Meles Meles) In Ireland: A Review, Biology and environment: proceedings of the royal irish academy. *Royal Irish Academy* 112.

CARROL, P. H. 1949. *Soil piping in south-eastern Arizona*. United States Department of Agriculture Soil Conservation Service, Region 6, Albuquerque, New Mexico.

CHLAIB, H. K., MAHDI, H., AL-SHUKRI, H., M.SU, M. & CATAKLI, A. 2014. Using ground penetrating radar in levee assessment to detect small scale animal burrows. *Journal of Applied Geophysics,* 103**,** 121-131.

CLAUß, U. 2013. *Flood-induced interaction between beavers and flood embankments along rivers.* TU Dresden.

COOMBES, M. A. & VILES, H. A. 2015. Population-level zoogeomorphology: the case of the Eurasian badger (Meles Meles L.). *Taylor & Francis*.

D'ALPAOS, L., BRATH, A., FIORAVANTE, V., GOTTARDI, G., MIGNOSA, P. & ORLANDINI, S. 2014. Investigative Evaluation Report. *Relazione tecnico-scientifica sulle cause del collasso dell'argine del fiume Secchia avvenuto il giorno 19 gennaio 2014 presso la frazione San Matteo.* Bologna, Italy.

ERDOGAN, Z. & WAHL, T. 2008. Results of Laboratory Physical Properties and Hole Erosion Tests, Truckee Canal Embankment Breach, Newlands Project, Nevada. *In:* RECLAMATION, B. O. (ed.). Technical Service Center, Denver, Colorado.

FEDERAL EMERGENCY MANAGEMENT AGENCY 2000. Plant and Animal Impacts on Earthen Dams. Lexington, Kentucky.

FINSBURY, R. H. L. S. O., STOCKTON, S. L. & LOUDIERE, D. 2013. *The International Levee Handbook,* London.

HEPTNER, V. G. & SLUDSKII, A. A. 1988. *Mammals of the Soviet Union. Vol. II, part 1b, Carnivores (Mustelidae and Procyonidae),* Washington, D.C., Washington, D.C. : Smithsonian Institution Libraries and National Science Foundation.

J.W.FRANCE & MOLER, B. 2008. Truckee Canal Failure on 5 January 2008.

JONKMAN, S. N. & SCHWECKENDIEK, T. 2015. FLOOD DEFENCES, Lecture Notes CIE5314. *Department of Hydraulic Engineering, Faculty of Civil Engineering and Geosciences.* Delft University of Technology.

KRUUK, H. 1978. Spatial organization and territorial behaviou of the European badger (Meles Meles). *J. Zool.,* 184**,** 1-19.

LU, N. & LIKOS, W. J. 2004. *Unsaturated Soil Mechanics*.

MASANNAT, Y. M. 1980. Development of piping erosion conditions in the Benson area, Arizona, U.S.A. *Q. J. eng. Geol. London,* 13**,** 53-61.

NICHOL, D., LENHAM, J. W. & REYNOLDS, J. M. 2003. Application of ground-penetrating radar to investigate the effect of badger setts on slope stability at St Asaph Bypass, North Wales. *Quarterly Journal of Engineering Geology and Hydrogeology,* 36.

PAUL, D. & SLAVEN, C. 2009. Potential failure modes of the truckee canal failure at Fernley, Nevada. *Managing Our Water Retention System.* Nashville, Tennessee.

PINDER, G. F. & CELIA, M. A. 2006. *Subsurface Hydrology*.

PLAXIS 2014. Reference Manual | PLAXIS 2D | Anniversary Edition. *In:* PLAXIS (ed.).

PO, A. D. B. D. F. Linee generali di assetto idrogeologico e quadro degli interventi Bacino del Secchia.

PRINZIO, M. D., BITTELLI, M., CASTELLARIN, A. & PISA, P. R. 2010. Application of GPR to the monitoring of river embankments. *Journal of Applied Geophysics,* 71**,** 53-61.

REDDI, L. N. 2003. *Seepage in Soils*.

REDDI, N., ETHERINGTON, T. R., WILSON, G. & R.A & MONTGOMERY, W. I. 2008. Badger Survey of Northen Ireland 2007/2008. *Report prepared by Quercus and Central Science Laboratory for the Department of Agriculture & Rural Development (DARD)* Northern Ireland, UK.

RICHARDS, K. S. & REDDY, K. R. 2007. Critical appraisal of piping phenomena in earth dam. *Bullettin of Engineering Geology and the Environment,* 66 381-402.

ROPER, T. J. 2010. *Badger*.

SORENSEN, R. M. 1993. *Basic Wave Mechanis : for coastal and ocean engineers*.

STADLER, L., HINKELMANN, R. & HELMIG, R. 2011. Modeling Macroporous Soils with a Two-Phase Dual-Permeability Model.

STADLER, L., HINKELMANN, R. & ZEHE, E. 2009. Two-phase flow simulation of water infiltration into layererd natural slopes inducing soil deformation.

TONGIORGI, P., SALA, L., FONTANA, R., SPAMPANATO, A., LANZI, A. & GIANAROLI, M. 1998. La nutria in provincia di Modena (Myocastor coypus). Distribuzione, aspetti ecologici e gestionali. *Habitat* 81**,** 54-61.

VOROGUSHYN, S., MERZ, B. & APEL, H. 2009. Development of dike fragility curves for piping and micro-instability breach mechanisms. *Natural Hazards and Earth System Sciences,* 9**,** 1383-1401.

A Field and laboratory tests in the Investigative Evaluation Report

In order to define the stratigraphy and the properties of the soil on the section under analysis, a number of field and laboratory tests have been performed.

A.1 Location of the sections

The three sections are represented in Figure 10.3:

- The first section is on the right riverside, around 900 meters upstream of the breach
- The second section is on the left side, in the opposite side of the breach
- The third section is on the right riverside, just downstream of the breach

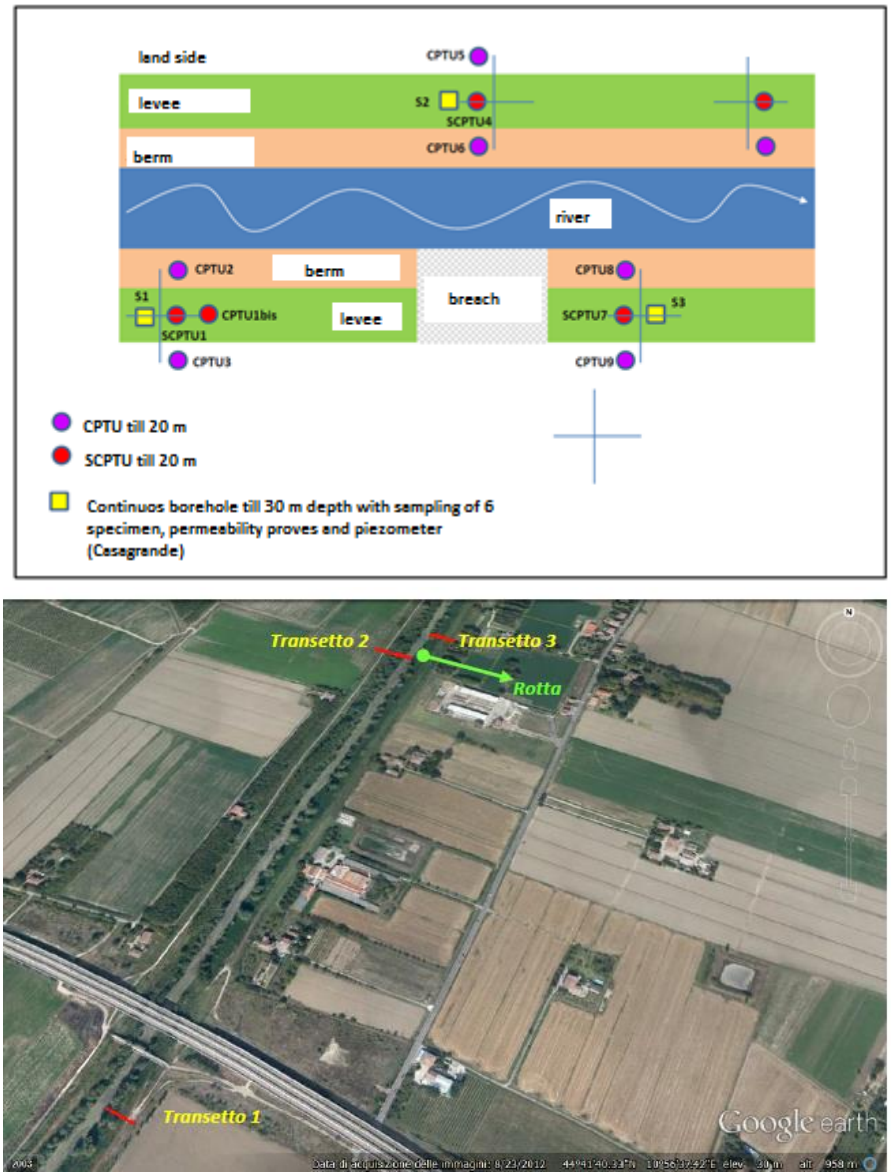

Figure 10.3 Position of geotechnical proves: scheme above and areal photo below.

A.2 In-situ tests

In-situ tests consist on CPTU and SCPTU until 20meters depth, while the samples have been taken with continuous borehole till 30 meters depth.
In particular, Cone Penetration Test CPTU gives the values for the q_c (tip resistance), the f_s (lateral friction), the pore pressure u and the penetration tilt angle. SCPTU (Seismic cone penetration testing) gives, in addition, the value of the shear and compressional wave velocities.
The results of the in-situ tests are presented below

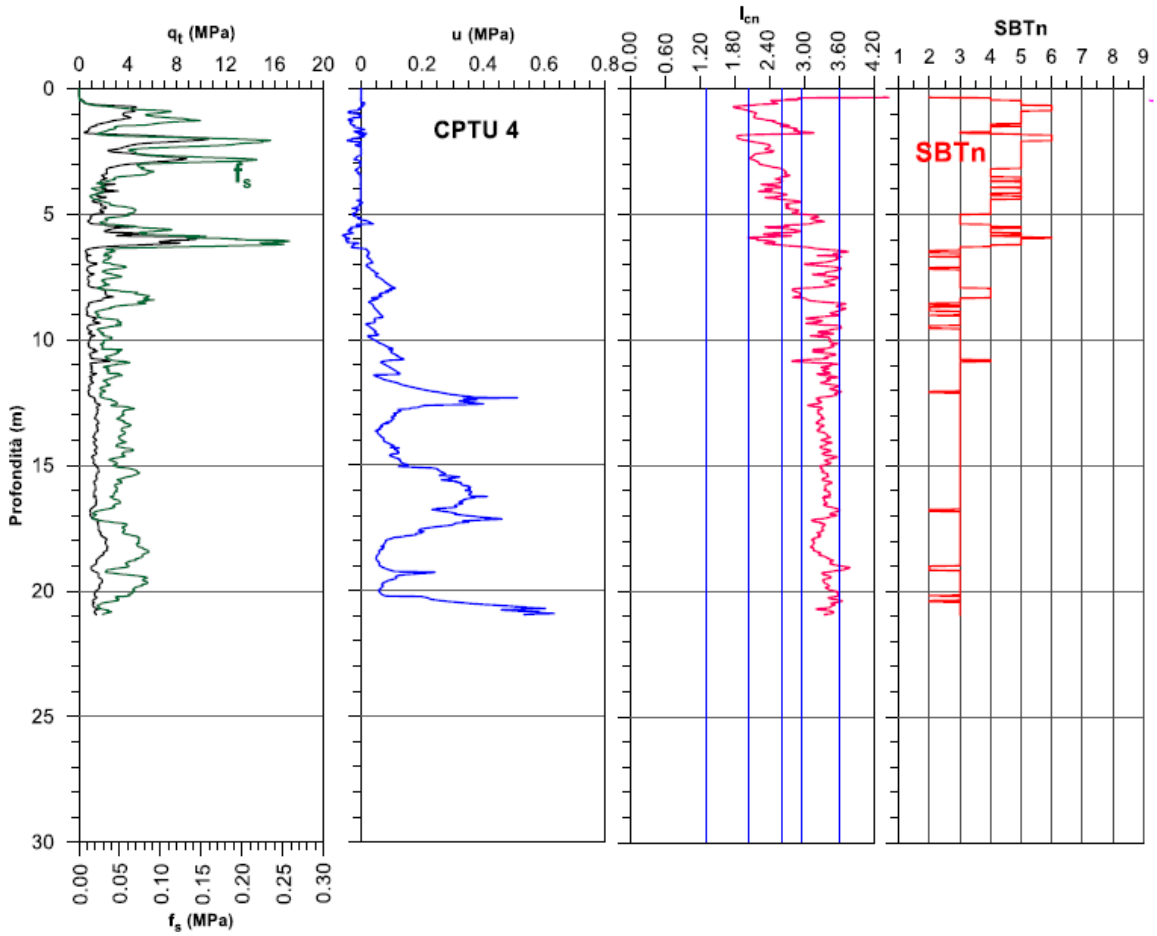

Figure 10.4 Graph of test CPTU4, representing the tip resistance q_c ,the porewater pressure u , the Soil Behaviour Type index I_{cn} and the Soil Behaviours type SBT_n.

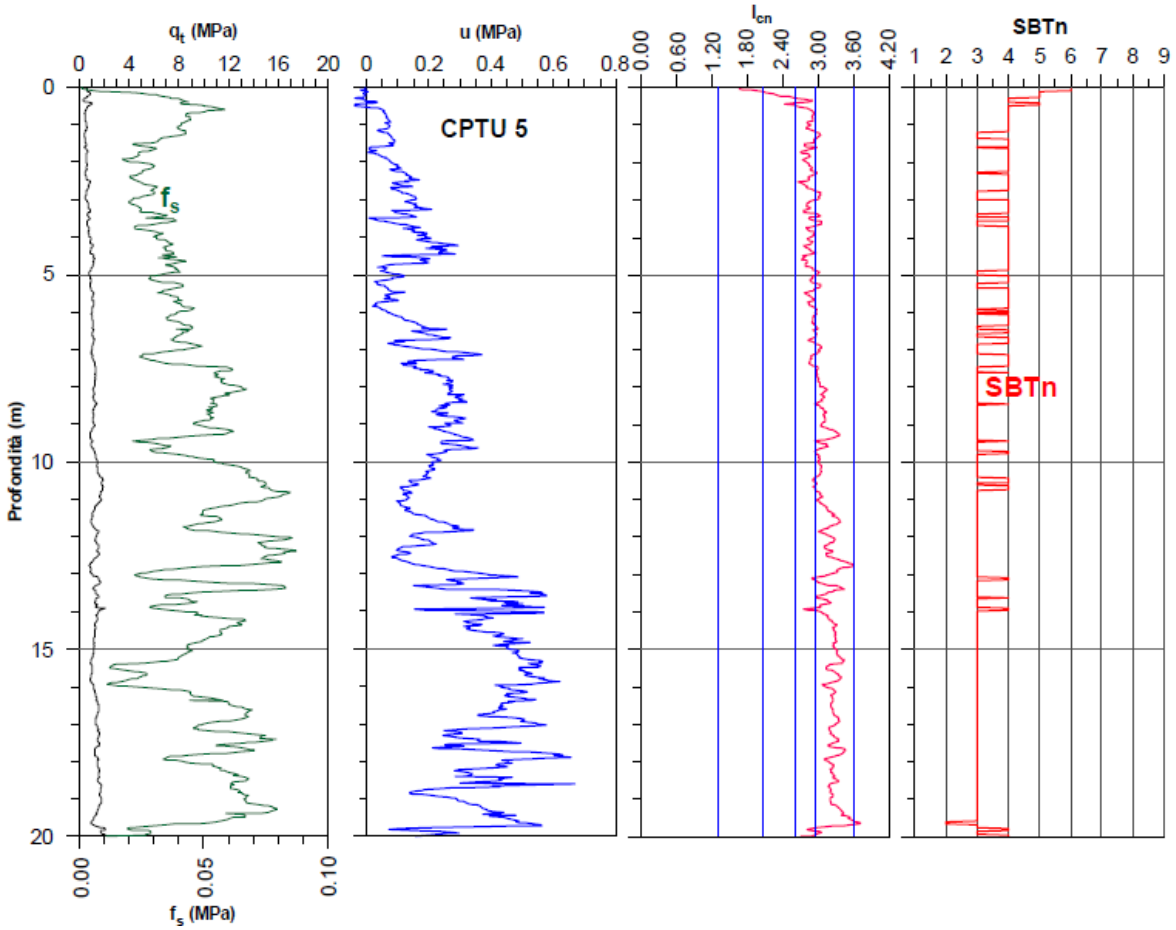

Figure 10.5 Graph of test CPTU5, representing the tip resistance q_c ,the porewater pressure u , the Soil Behaviour Type index I_{cn} and the Soil Behaviours type SBT_n..

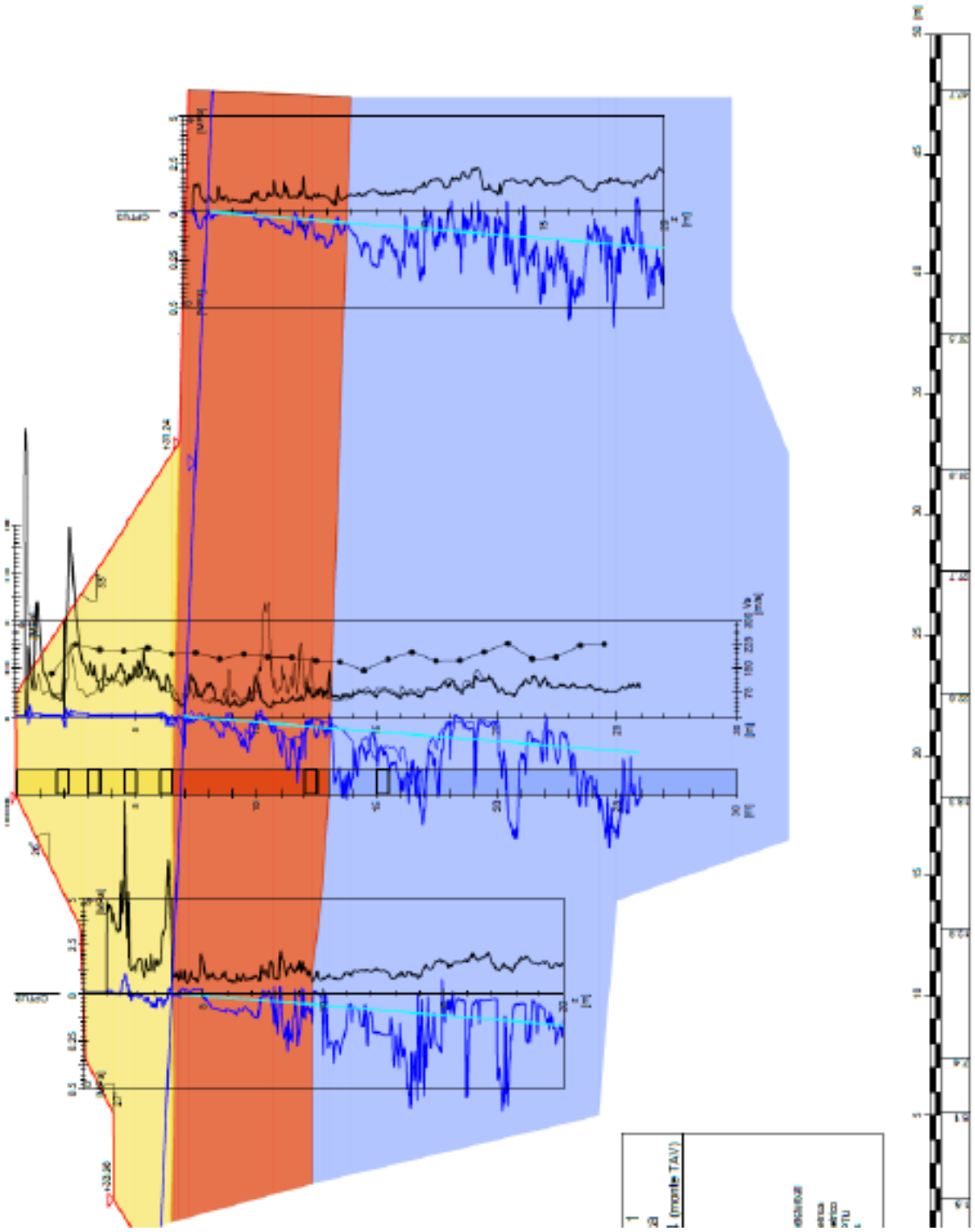

Figure 10.6 Section 1: lithostratigraphic sequence. From the top, Unit AR (yellow), Unit B (orange) and Unit C (blue), with the profiles of the tip resistance q_c(black) and the porewater pressure u (blue) in three locations. (D'Alpaos et al., 2014)

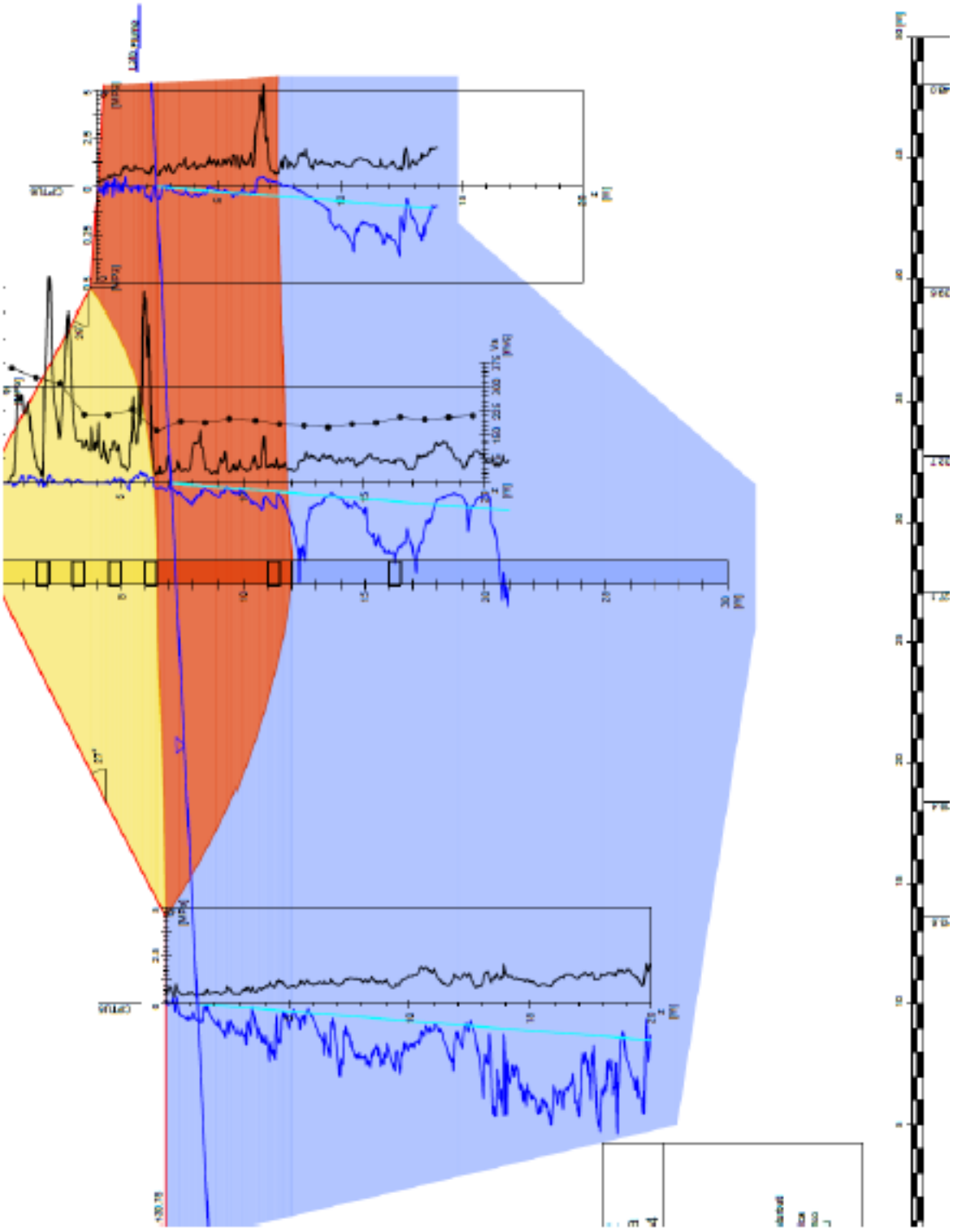

Figure 10.7 Section 2: lithostratigraphic sequence. From the top, Unit AR (yellow), Unit B (orange) and Unit C (blue), with the profiles of the tip resistance q_c(black) and the porewater pressure u (blue) in three locations. (D'Alpaos et al., 2014)

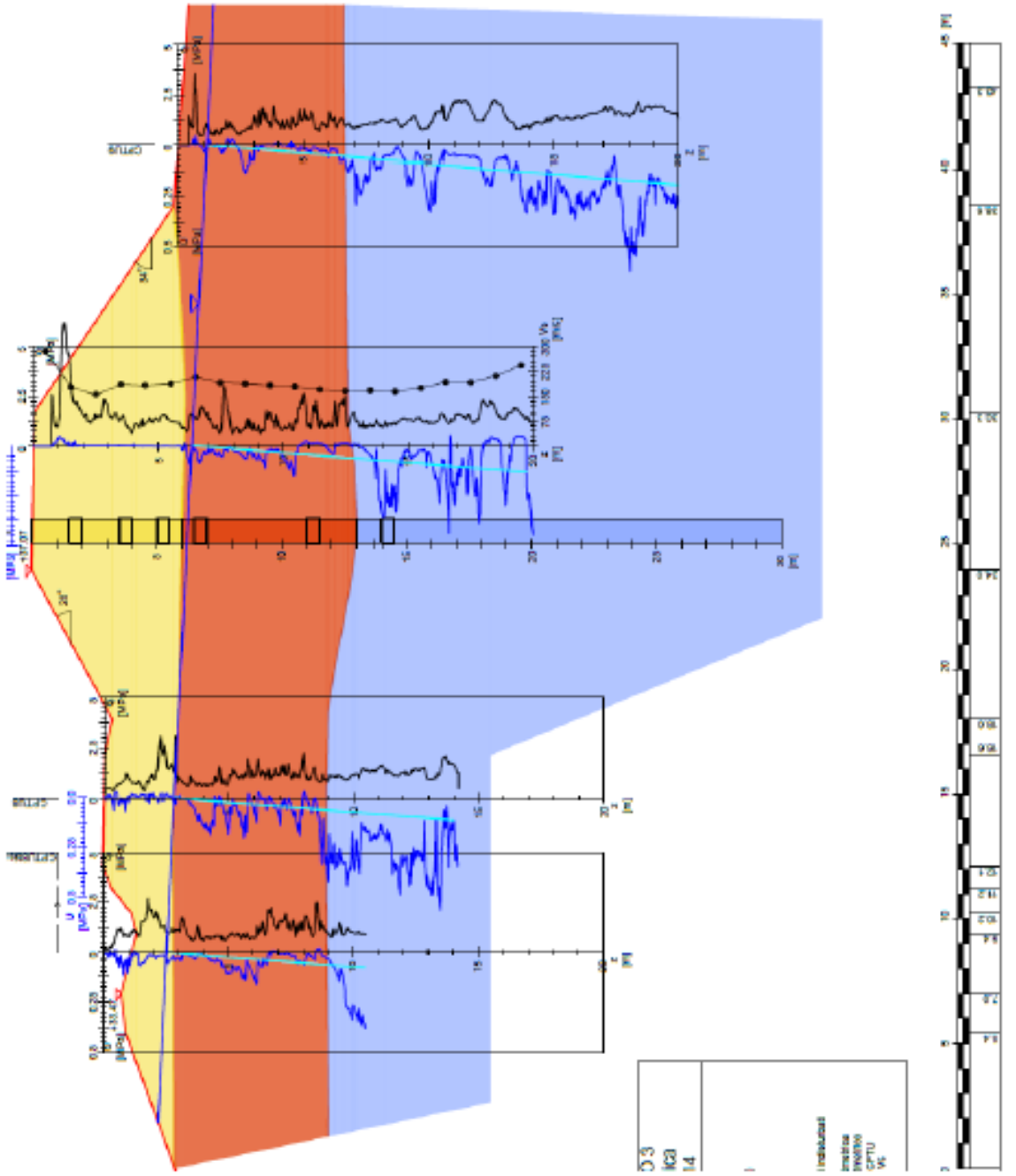

Figure 10.8 Section 3: lithostratigraphic sequence. From the top, Unit AR (yellow), Unit B (orange) and Unit C (blue), with the profiles of the tip resistance q_c(black) and the porewater pressure u (blue) in three locations. (D'Alpaos et al., 2014)

A.3 Laboratory tests

The laboratory tests performed on the core samples from the three locations are the followings:

- Particle size analysis: Hydrometer and Sieve Analysis
- Determination of $CaCO_3$(calcium carbonate) content

- Determination of organic content
- Measure of unit weight γ
- Measure of water content w
- Measure of Specific Gravity Gs
- Measure of liquid and plastic limits
- Edometric test
- Isotropic consolidated-drained triaxial test
- Isotropic consolidated-undrained triaxial test
- Direct Shear Test

The results available in the Investigative Evaluation Report are illustrated below.

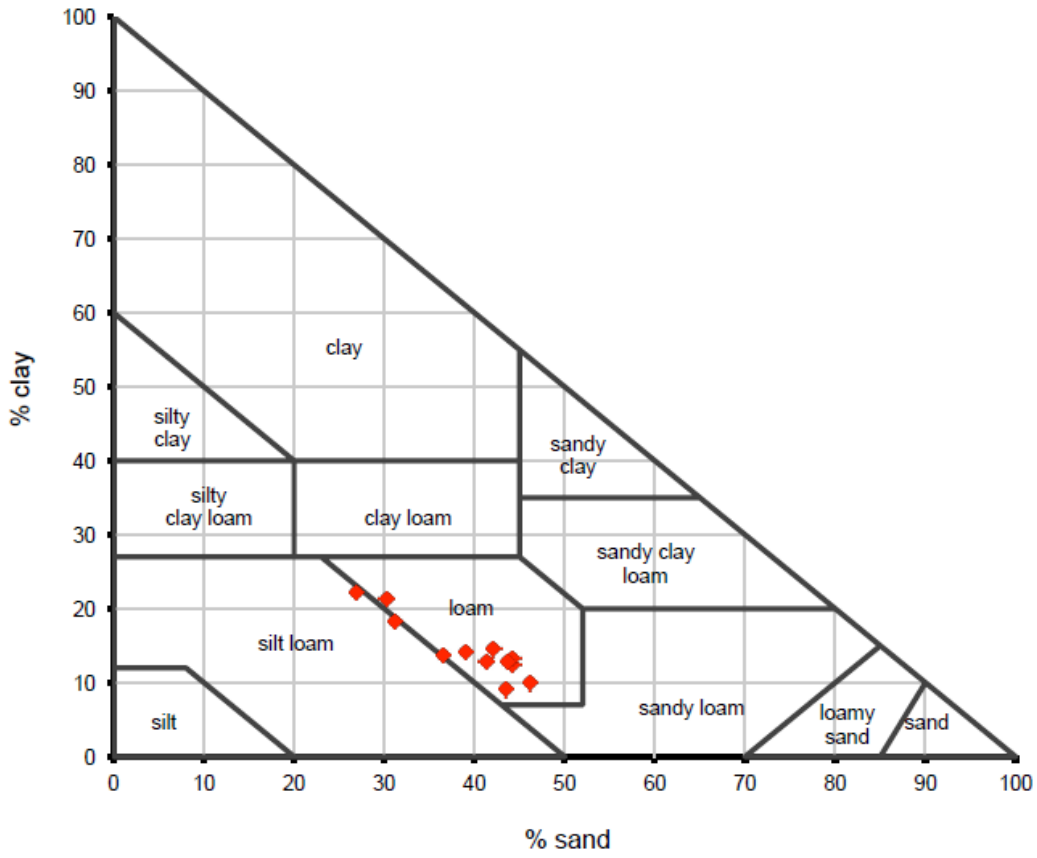

Figure 10.9 Granulometric analyses for the 12 samples.

S	CI	da m	a m	z_m m	unità -	S %	L %	A %	Descrizione	D_{60} mm	D_{50} mm	U_C -	w_n %	γ_n kN/m^3	LL %	LP %	IP %	IC -	G_S -	$CaCO_3$ %	SO %
S1	A	1.7	2.2	1.95	AR	29.63	64.35	6.02	L,S(A)	0.041	0.025	8.07	17.7	16.28	30	23	7	1.8		21	2.5
S1	B	3	3.5	3.25	AR	44.57			S,L(A)-LS	0.085			7.4	16.02	22	16	6	2.4	2.707		
S1	C	4.5	5	4.75	AR	30.97			L,S(A)				10.3	16.06	25	14	11	1.3	2.695		
S1	D	6	6.5	6.25	AR	27.05			L,S(A)				18	18.71	26	16	9	0.9			
S1	E	12	12.5	12.25	B	23.65	70.97	5.38	L(S,A)	0.05	0.039	8.31	29.7	18.82	38	22	16	0.5	2.625		
S1	F	15	15.5	15.25	C	1.15			AL				38.7	18.25	81	31	50	0.8		7	4
S2	A	1.7	2.2	1.95	AR	51.61			S,L(A)	0.152	0.085		8.2	20.55	23	19	4	3.7			
S2	B	3	3.5	3.25	AR	20.75			L(S,A)				9	19.18	28	20	8	2.4	2.634		
S2	C	4.5	5	4.75	AR	21.23			L(S,A)				18.4	19.47	27	21	6	1.4	2.644		
S2	D	6	6.5	6.25	AR	19.96	70.36	9.95	L(S,A)	0.036	0.025	15.6	19.3	16.24	33	16	7	2.0	2.658	18	1.2
S2	E	11	11.5	11.25	B	23.07	66.99	9.94	L(S,A)	0.037	0.025	16.4	33.3		26	16	13	-0.6		19	0.9
S2	F	15	15.5	15.25	C	0.37			AL				34.2	19.55	68	26	41	0.8			
S3	A	1.7	2.2	1.95	AR	31.68			L,S(A)				9		25	19	6	2.7		18	0.8
S3	B	3.5	4	3.75	AR	36.3	58.32	5.38	L,S(A)	0.064	0.041	15.13	16.6		27	17	9	1.2	2.636		
S3	C	5	5.5	5.25	AR	37.39			L,S(A)				22.5		26	20	6	0.6		18	1
S3	D	6.5	6.7	6.6	AR	33.63			L,S(A)				23.9	19.51	32	22	10	0.8			
S3	E	11	11.5	11.25	B	31.85			L,S(A)				30.4		25	22	3	-1.8	2.656		
S3	F	14	14.5	14.25	C																

Table 10.3 Results of classification tests on undisturbed samples

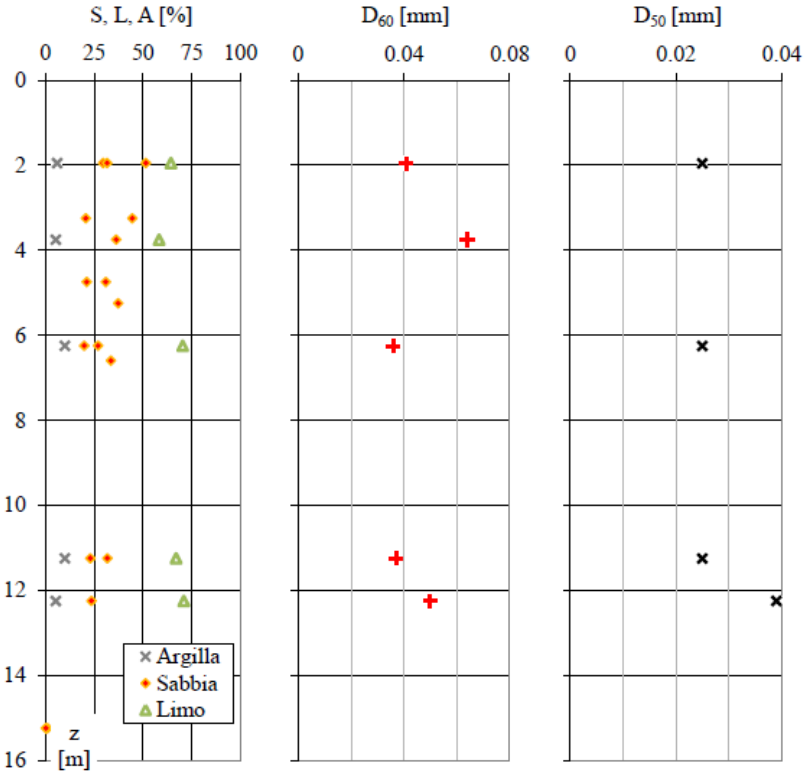

Figure 10.10 Granulometry characterization of undisturbed samples.

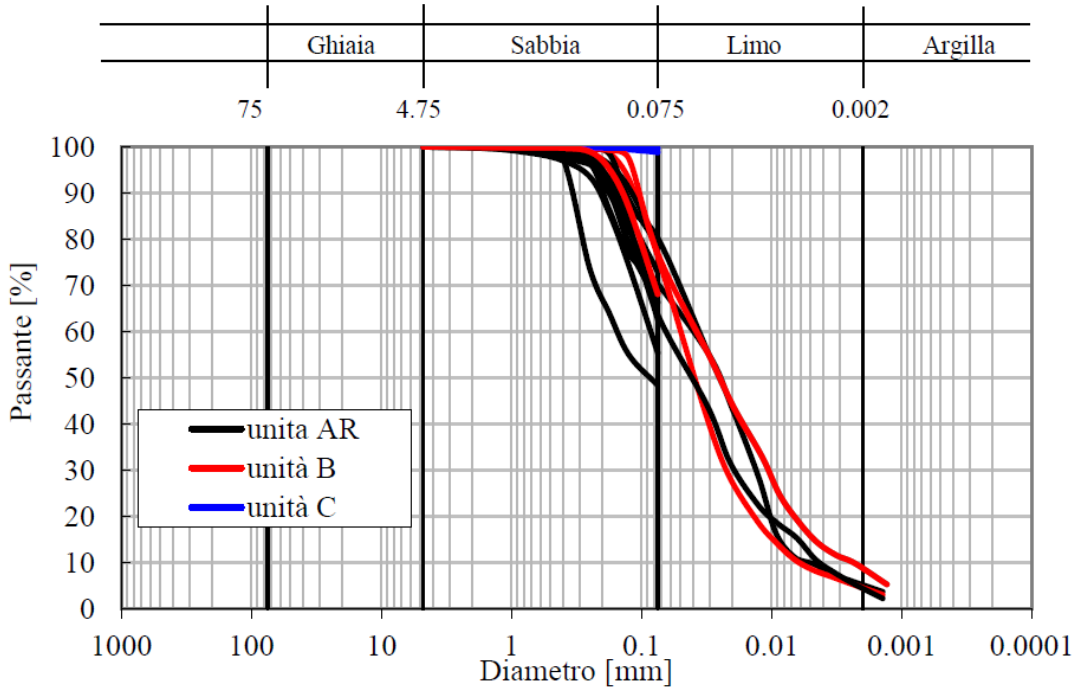

Figure 10.11 Granulometry curves of undisurbed samples

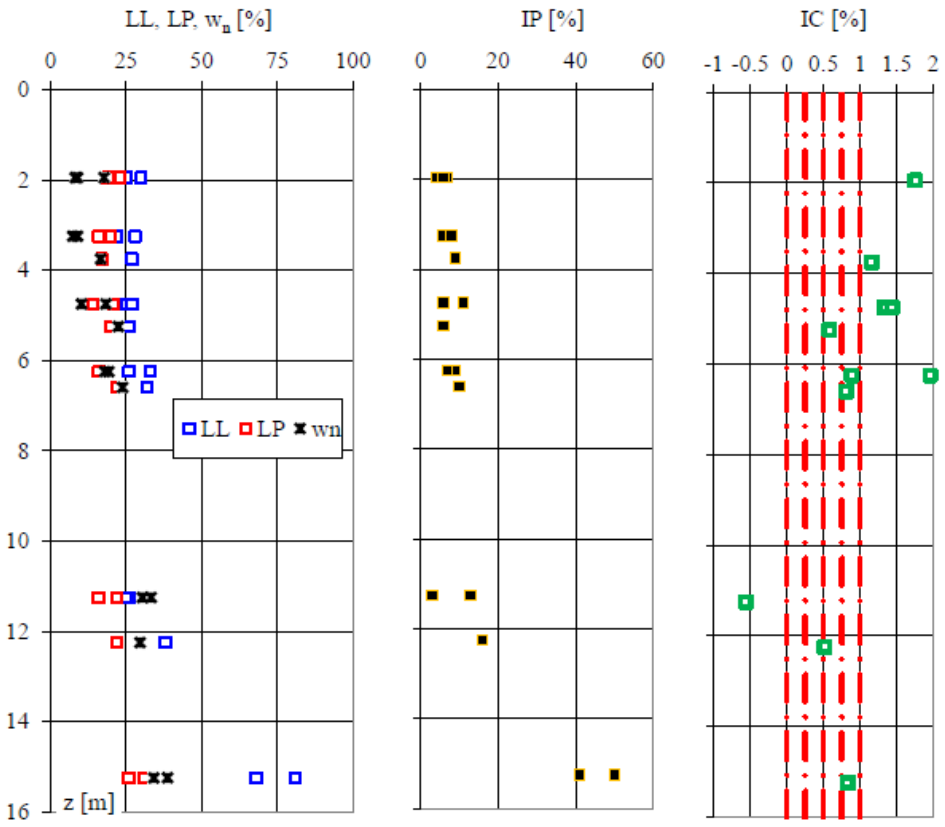

Figure 10.12 Index properties of undisturbed samples.

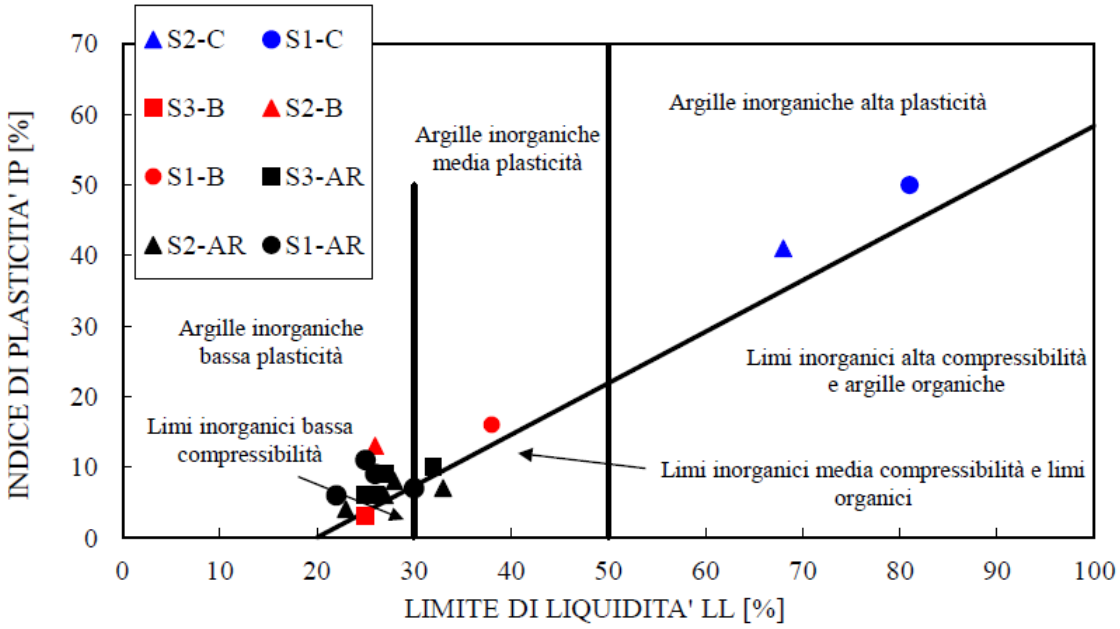

Figure 10.13 Classification chart by Casagrande.

B Analysis in the Investigative Evaluation Report

B.1 Introduction

The analyses performed by the Investigative Evaluation Committee try to reproduce the groundwater flow inside the dike body with a 2d model. The profile used is a simplification of the stratigraphic profile of section 3 and the hydraulic properties obtained are illustrated in Figure 10.14. The profile used has no cavities. The simulation time is between 22-12-2013 at 0:00 an 03-02-2014 at 23:50 with the hydraulic boundary conditions illustrated in paragraph 2.4. The initial phreatic level is equal to 29.50 m amsl.

Parametro medio	Valore Medio
α (cm^{-1})	0.0154
n (adimensionale)	1.4938
m (= $1-1/n$, adimensionale)	0.3306
θ_r (adimensionale)	0.0785
θ_s (adimensionale)	0.4037
K_s ($cm\ h^{-1}$)	0.6771

Figure 10.14 Average values of the input parameters for the Van Genuchten-Mualem equations.

The stability analyses are carried out with the software SEEP and they have been performed with the method of Morgenstern&Price and failure model of Mohr-Coulomb. Steady state and the transient flow analyses have been performed.

Figure 10.14and Figure 10.15 illustrate water content and pore pressures in the section of the breach for three times under analysis on19/01/2014

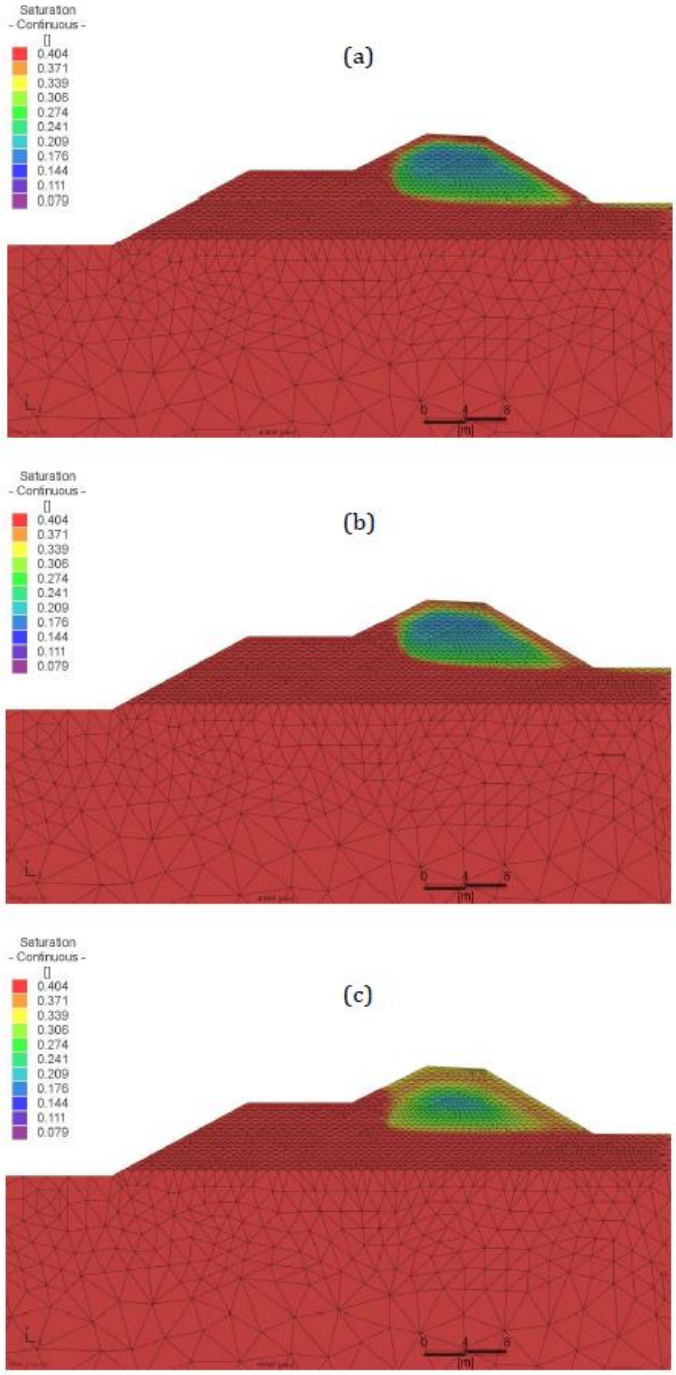

Figure 10.15 Water content in the section of the breach at 2:00 (a), 6:00 (b) and 12:00 (c) on 19/01/2014, considering silty soil with parameters of Van Genuchten.

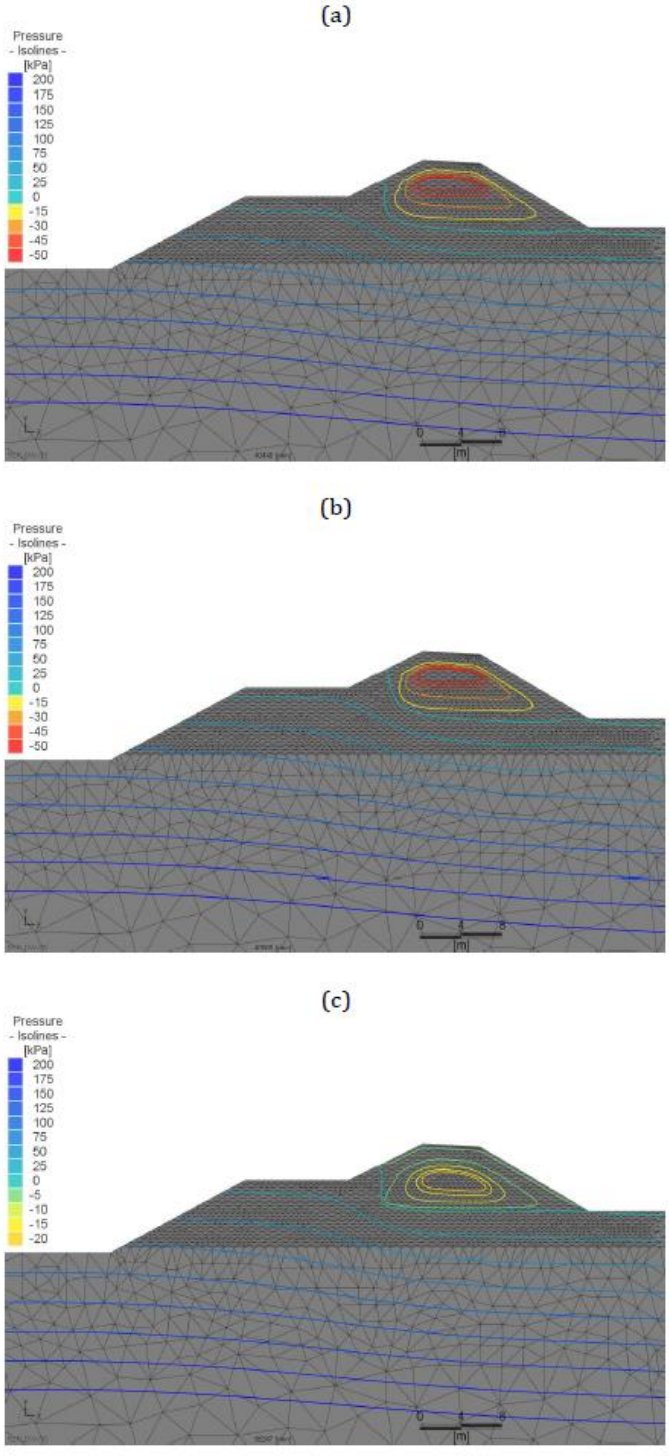

Figure 10.16 Pore water pressure in the section of the breach at 2:00 (a), a:00 (b) and 12:00 (c) on 19/01/2014, considering silt with parameters of Van Genuchten.

B.2 Steady state analysis

The aim of the steady state analysis performed by the Investigative Evaluation Committee is to evaluate the safety of the levee with the design values.

At the inner side the phreatic line corresponds to the surface level, while the several simulation takes into account different water levels in the river.
In order to take into account the uncertainty correlated to the spatial variability, Monte-Carlo simulations have been performed. The normal distribution of the shear strength is illustrated in Figure 10.17.

Unità	Parametro	μ	σ
AR	ϕ' (°)	32	1.94
B	ϕ' (°)	28.8	3.2
C	ϕ' (°)	24.9	2.4

Figure 10.17 Parameters for the normal distribution of shear strength used in the Monte-Carlo simulations form the steady state analyses.

The first slip surface analysed is shallow: it starts from the inner top of the crest and it reaches the inner toe. Figure 10.18 shows the stability analyses and Figure 10.19 reports the fragility curves, showing the probability of failure for the different water levels.

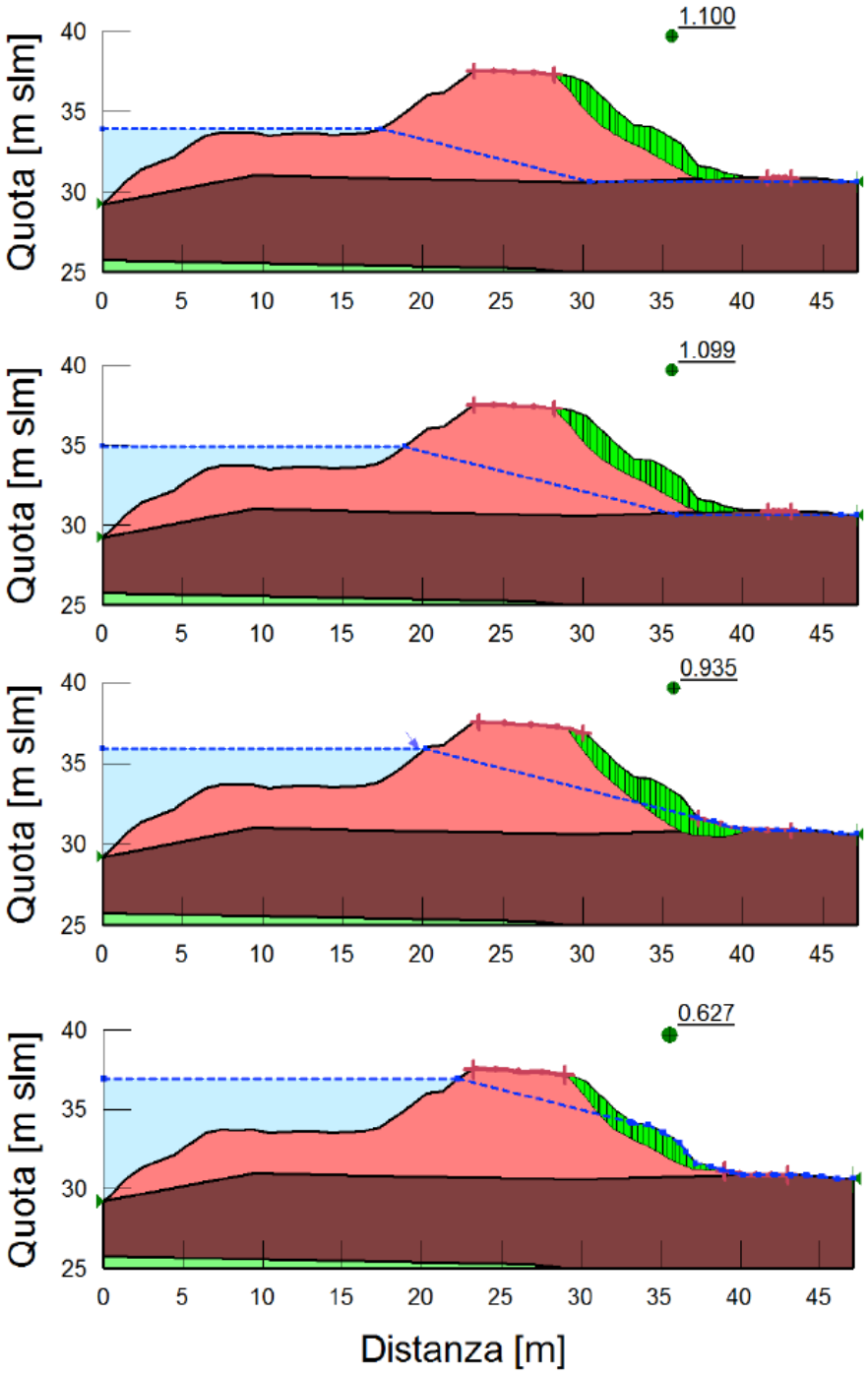

Figure 10.18 Steady state analysis for different water levels and shallow slip plane.

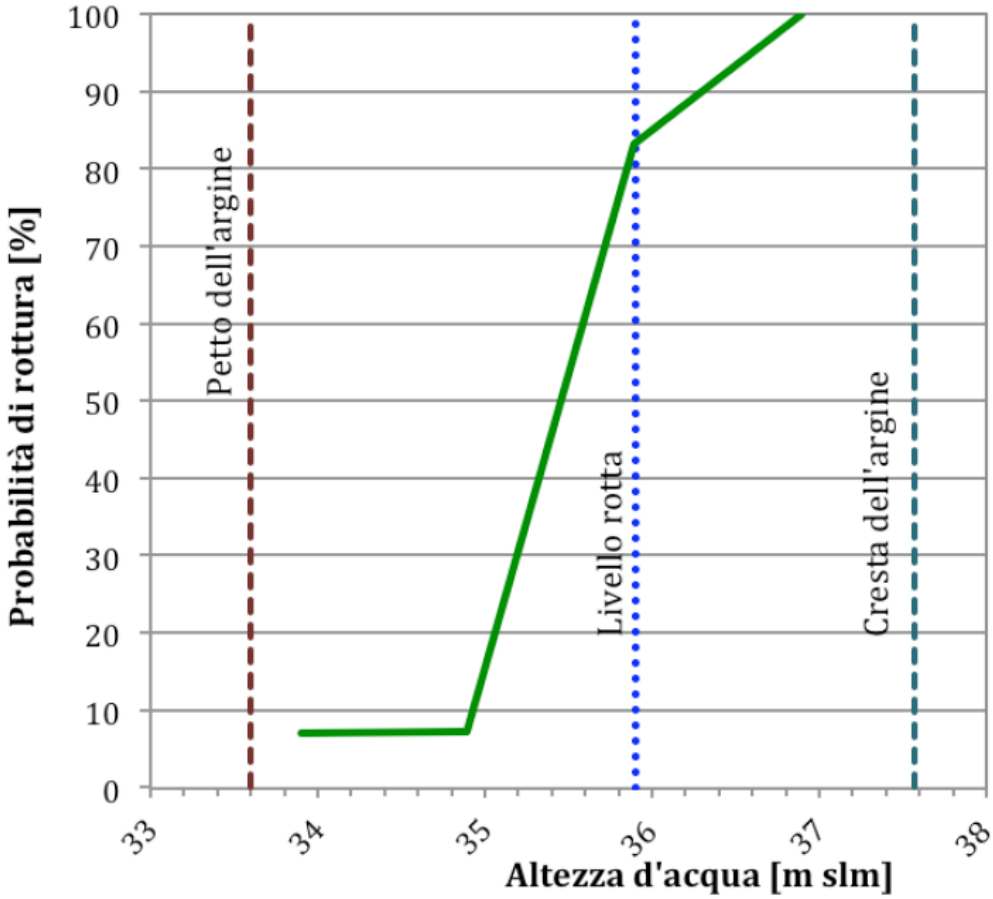

Figure 10.19 Fragility curves for the shallow slip plane varying the water level: probability of failure (y-axis) versus water level (x-axis). The dashed blue line indicates the water level at the moment of the breach at 36 m amsl and the green dashed line the top of the levee.

Second, a deeper failure surface is analysed. It covers the all dike crest, starting from the outer top, until the inner toe, after having intercepted the layer underneath. The results of the analyses are shown in Figure 10.20 and Figure 10.21.

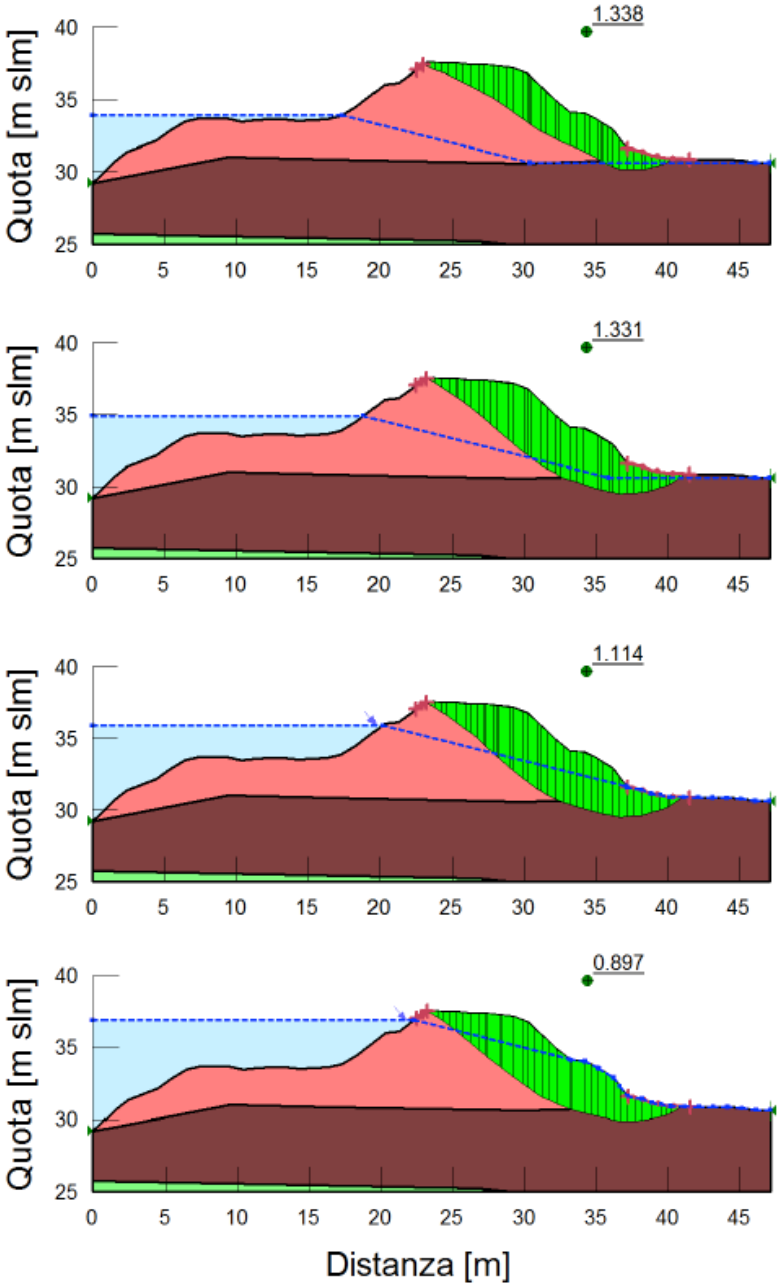

Figure 10.20 Steady state analysis for different water levels and deep slip plane.

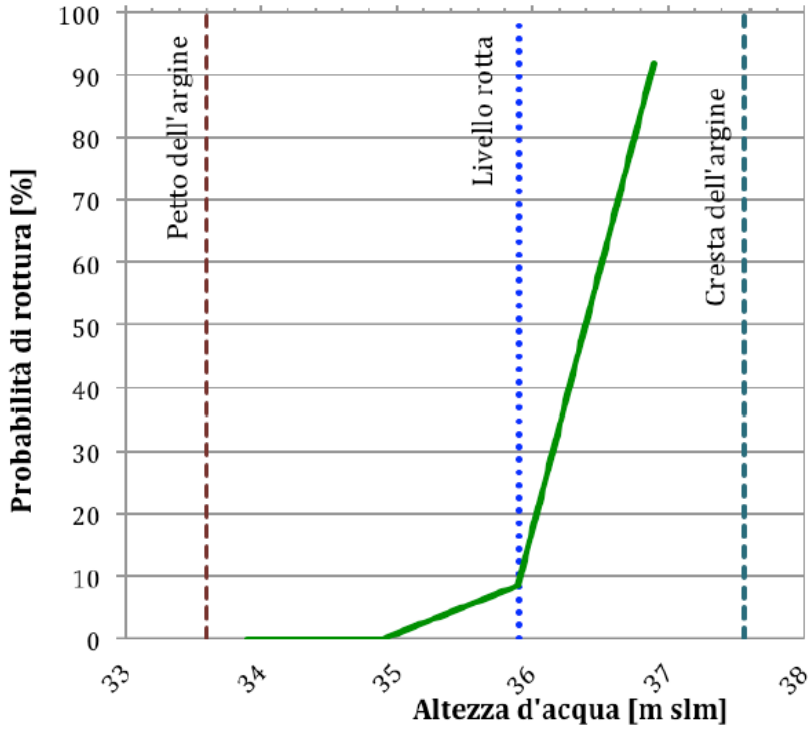

Figure 10.21 Fragility curves for the deep slip plane varying the water level: probability of failure (y-axis) versus water level (x-axis). The dashed blue line indicates the water level at the moment of the breach at 36 m amsl and the green dashed line the top of the levee

B.3 Transient flow analyses

The transient flow analyses aim to reproduce the dike in the conditions of failure. Temporary boundary conditions are applied, while the dike body is assumed partially saturated. The initial pore pressure distribution has suction in the centre of the levee with a minimum of 40kPa (Figure 10.22).

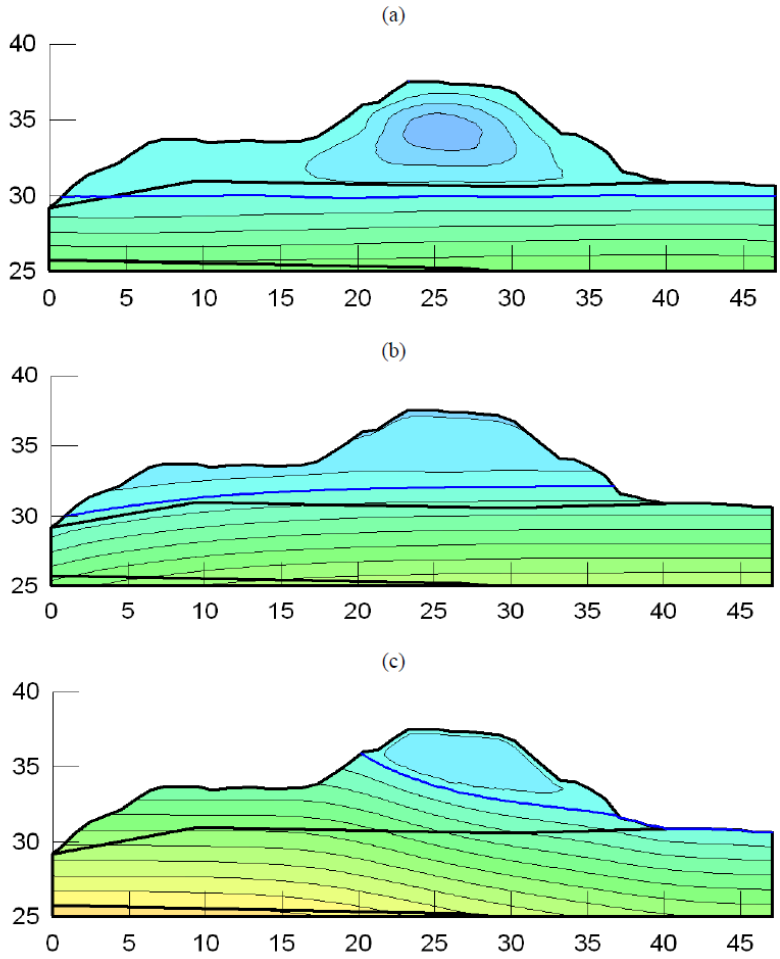

Figure 10.22 Pore water pressure inside the levee at the start of the simulation (a), on 17-01-2014 (b) and at the moment of the breach (c)

Figure 10.23 and Figure 10.24 show the groundwater head and the volumetric water content at the moment of the breach on 19-01-2014 at 6:00.

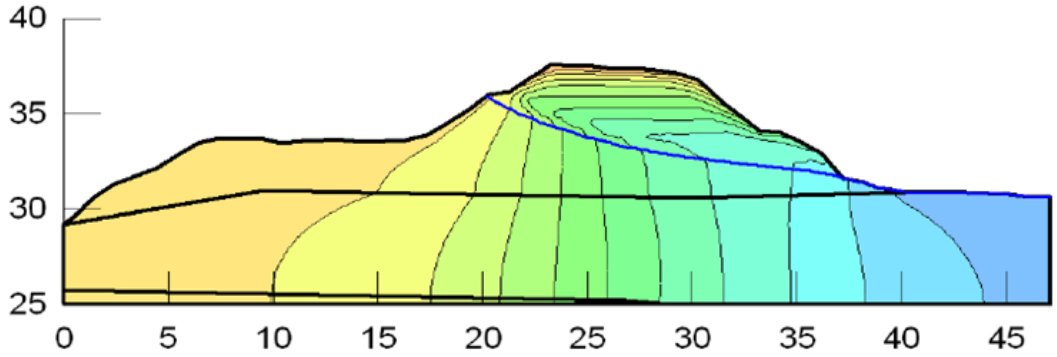

Figure 10.23 Groundwater head at the moment of the breach.

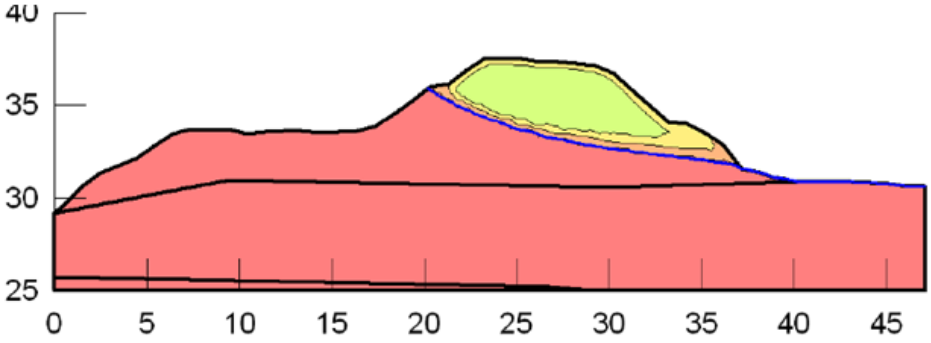

Figure 10.24 Volumetric water content at the moment of the breach.

The results of the analyses have already been illustrated in paragraph 2.8.3.

C Derivation of Input Parameters

The input data used for the analyses with PLAXIS 2D and 3D (Table 5.1) have been derived starting from the data and tests results available in the Investigative Evaluation Report. Table 10.4 lists the tests performed and the available data in the report.

Proves performed	Data available
CPTU and SCPTU Tip resistance q_c , Sleeve friction f_s, Pore pressure u, Shear wave velocity V_s *Core sampling:* Permeability measurements, Piezometric proves, Core samples *Laboratory tests for granulometry and geotechnical properties:* Particle size analysis (Hydrometer and Sieve Analysis), Determination of $CaCO_3$(calcium carbonate) content, Determination of organic content, Measure of unit weight γ, Measure of water content w Measure of Specific Gravity G_s, Measure of liquid and plastic limits, Edometric test, Isotropic consolidated-drained triaxial test , Isotropic consolidated-undrained triaxial test, Direct Shear Test *Laboratory tests for hydraulic properties:* Particle size analysis, Determination of organic content, Water retention curves, Hydraulic conductivity	*CPTU and SCPTU* q_c and u only for SCPTU4 and SCPTU5: q_c , f_s , u , Icn , SBTn *Phreatic line* *Water retention curves* (average of 10 samples and sample #44) *Results of dissipation tests* *Results of classification tests:* Granulometry, D_{60} and D_{50} , Measure of water content w, Measure of unit weight γ, Liquid and plastic limits, Plasticity index and Consistency index, Measure of Specific Gravity G_s, $CaCO_3$ content , SO (organic sostance) content *Geotecnical parameters:* Shear modulus at small deformations G_0 and Shear waves velocities V_s Unit C: s_u and φ'_p (SCPTU4) Unit AR and B: φ'_{cv} and φ'_p

Table 10.4 Tests performed and data made available in the report

Starting from the available data, the needed inputs for Plaxis 2D calculation are derived as explained below.

C.1 Unit weight

The natural unit weight of the soil is available in the report: it can be either γ_{sat} or γ_{unsat} depending on the position of the phreatic line (γ_{unsat} applies above the phreatic line and γ_{sat} below). Thus, $\gamma_n = \gamma_{unsat}$ for unit A and $\gamma_n = \gamma_{sat}$ for units B and C.
It is possible to calculate the unknown unit weights from the formula below.

Unit B and C : $\gamma_{unsat} = \frac{(1+w)\, G_s\, \gamma_w}{1+e}$

Unit A : $S = w\, G_s / e$, $S = 1 \rightarrow e = w\, G_s \rightarrow \gamma_{sat} = \frac{(G_s+e)\, \gamma_w}{1+e}$

However, the void ratio e is not known, so the formula cannot be solved for γ_{unsat} but just reasonably estimated: the values 16 kN/m^3 are assumed for units B and C.

C.2 Young Modulus

The Young Modulus can be estimated by the shear modulus at small deformations:

$$E' \sim 0.8\, G_0 = 0.8\, \rho\, V_s^{\,2}$$

C.3 Poisson Ratio

The values are assumed by literature review.[1]

C.4 Strength Parameters

For Unit A and B the following parameters are required for the analysis:

- c'_{ref} : the cohesion is obtained looking at the correlation found in literature[2] between its values and the soil granulometry according to the Classification USCS:
  - Unit A: CL-ML (Inorganic silts, silty or clayey fine sands, with slight plasticity) → c=7 kPa
  - Unit B: CL-ML (Inorganic silts, silty or clayey fine sands, with slight plasticity) → c=7 kPa
  - Unit C: CH (Inorganic clays of high plasticity - saturated compacted) → c=11 kPa

- φ' : the values are available in the report.

- ψ' : The formula $\Phi_p = \Phi_c + 0.48\psi_p$ for the triaxial compression is used [3], with Φ_c and Φ_p that are available results of the triaxial test.

For Unit B, the only required strength parameter is the undrained shear strength, which is known.

C.5 Soil

The classification USDA, which is used in the report, is also used for Plaxis 2D.

C.6 Flow Parameters

In order to define the hydraulic properties of the dike soil, the report presents the Water Retention Curve and the Hydraulic Conductivity Function. The first correlates the pore water pressure and the volumetric water content and it is derived by the van Genuchten equation, while the second, which gives the value of the hydraulic conductivity, is derived by the Mualem model.

[1] *http://www.sefindia.org/forum/files/appc_soil_properties_718.pdf*

[2] *http://www.geotechdata.info/parameter/cohesion.html*

[3] http://www.civil.utah.edu/~bartlett/CVEEN6920/Mohr-Coulomb%20Model.pdf

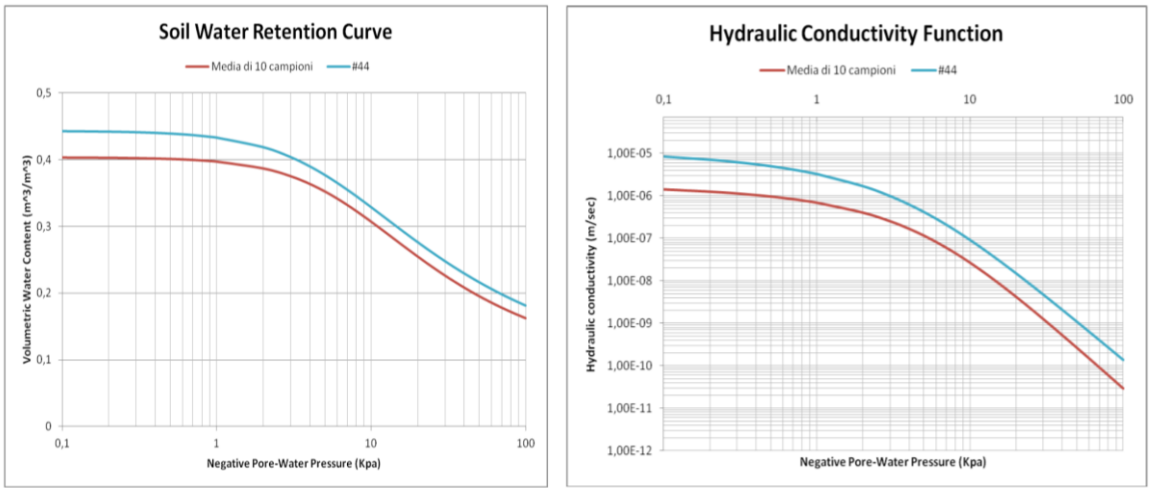

Figure 10.25 Water Retention Curve and the Hydraulic Conductivity Function in the report

The equation proposed by van Genuchten, correlates the water content and the matric potential in order to define the Soil Water Retention Curve:

$$\Theta = \frac{\theta - \theta_r}{\theta_s - \theta_r} = \left[\frac{1}{1 + (\alpha\, \psi_m)^n}\right]^m$$

Where: θ_r is the residual water content, θ_s is the saturated water content, ψ_m is the matric function, while the parameters α, n and m depend on the shape of the curve. These parameters are made available in the report.
Instead PLAXIS implements the following form of the van Genuchten expression:

$$S = S_r + (S_s - S_r)\left[1 + \left(g_a\,|\phi_p|\right)^{g_n}\right]^{g_c}$$

Instead of volumetric water content θ, PLAXIS uses the Saturation. The relation between them is: S = θ/n , where n=porosity. However, the fraction deletes the porosity term.
The relations between the other parameters are: g_a=α , g_n=n , g_c= - m
Thus the final implementation is:

S_r [-]	S_s [-]	g_a [m^{-1}]	g_n [-]	g_c [-]
0.09	0.55	1.948	1.409	-0.290

Table 10.5 Input parameters of the Van-Genuchten-Mualem model for PLAXIS.

C.7 Hydraulic Conductivity

The value used for the saturated hydraulic conductivity for the soil of the dike is the one observed in the Hydraulic Conductivity Function for the sample 44:

$$K_s = 1 \cdot 10^{-5} m/s \cong 1\ m/d$$

The permeability of the other two layers is estimated from CPT with the correlation between permeability and SBTn which is available in literature.

Estimated Permeability (see Lunne et al., 1997)

SBT_n	Permeability (ft/sec)	(m/sec)
1	$3x\ 10^{-8}$	$1x\ 10^{-8}$
2	$3x\ 10^{-7}$	$1x\ 10^{-7}$
3	$1x\ 10^{-9}$	$3x\ 10^{-10}$
4	$3x\ 10^{-8}$	$1x\ 10^{-8}$
5	$3x\ 10^{-6}$	$1x\ 10^{-6}$
6	$3x\ 10^{-4}$	$1x\ 10^{-4}$
7	$3x\ 10^{-2}$	$1x\ 10^{-2}$
8	$3x\ 10^{-6}$	$1x\ 10^{-6}$
9	$1x\ 10^{-8}$	$3x\ 10^{-9}$

Figure 10.26 Correlation between SBTn and permeability.

The use of different values for k_x and k_y depends on stratigraphy : in stratified layers: $k_x >> k_y$. Thus, for the dike body the same values are assumed for the two permeabilities, since the soil is not naturally deposited but artificially placed, while they differ in the soil underneath the embankment. In particular the deeper layer is formed by stratified layers of silt and sand, thus the horizontal permeability largely differs from the vertical.

C.8 Unsaturated zone ψ_{unsat}

By default a very large number (=10^4) is assigned, defining an unlimited unsaturated zone.

C.9 Void Ratio

For unit A (unsaturated soil), the following formula is used: $e = \frac{(1+w)\,G_s\,\gamma_w}{\gamma_{unsat}} - 1$

For units B and C (saturated soil), instead, $e = w\,G_s$.

D Pictures

D.1 The breach on 19th January 2014

Photograph 1 Photo taken at the point of failure. River Secchia on the left, breach on the right side. Photo by R. Ferrari, Protezione Civile di Modena, 19-01-2014.

Photograph 2 Photo taken at the point of failure. River Secchia on the left, breach on the right side and flooded area on the right. Emergency measures are being taken on the top of the levee to close the breach. Photo by R. Ferrari, Protezione Civile di Modena, 19-01-2014.

Photograph 3 Top view of the breach. Photo by R. Ferrari, Protezione Civile di Modena, 19-01-2014.

D.2 The levee of San Matteo – field visit on March 2015

The following photos and observation have been taken during a field visit in March 2015.

On the right side of Secchia river, the levee is covered by grass, while on the opposite side, the vegetation is more abundant. The levee has no inner and outer shoulders, which are only present in the location where the breach occurred and it was later rebuilt. Moreover no pipelines are present.
The soil is muddy very wet: it is not possible to walk along the slope without sliding. When taking a piece of soil, it is easily to roll a thread, indicating that the soil is moderately plastic. Moreover, the hands are left almost cleaned after touching the soil. The soil has no organic content.

Photograph 4 View from the crest of the levee of San Matteo on the field visit during March 2015. Photo by M.L. Taccari, 23-03-2015

Photograph 5 Point of the breach of the levee of San Matteo on the field visit during March 2015. Photo by M.L. Taccari, 23-03-2015

D.3 Presence of animals in the levee - field visit on March 2015

While visiting the levee, many rows of animal footprints are seen at the inner toe, with a frequency of one row every 10 meters. The footprints go from the water towards the dike, suggesting that animals go from the river towards the dike body

Two types of footprints are individuated, but the second type was sighted only once. No burrows are individuated: the difficulty of walking in the toe of the dike or along it prevented me to carefully look for them. Moreover, according to the news, the burrows in this location were repaired just few days ago the field visit.

Photograph 6 Footprints at the outer toe. Photo by M.L. Taccari, 23-03-2015

Photograph 7 Several rows of footprints at the outer toe. Photo by M.L. Taccari, 23-03-2015

Photograph 8 Possible entrance of a burrow at the outer toe. Photo by M.L. Taccari, 23-03-2015

Photograph 9 Rows of footprints going from the river to the levee. They are a different type compared to those in . Photo by M.L. Taccari, 23-03-2015